TRANSCRIPTIONAL AND GENETIC PROFILING OF HUMAN UVEAL MELANOMA FROM AN IMMUNOSUPPRESSED RABBIT MODEL

by

Jean-Claude Marshall, B.Sc., MSc.

Department of Pathology

McGill University

Montreal, Canada

February, 2007

A thesis submitted to the Faculty of Graduate Studies and Research in partial fulfilment of the requirements of the degree of Doctor of Philosophy.

© Jean-Claude Marshall

Library and
Archives Canada

Published Heritage
Branch

395 Wellington Street
Ottawa ON K1A 0N4
Canada

Bibliothèque et
Archives Canada

Direction du
Patrimoine de l'édition

395, rue Wellington
Ottawa ON K1A 0N4
Canada

Your file Votre référence
ISBN: 978-0-494-38615-6
Our file Notre référence
ISBN: 978-0-494-38615-6

NOTICE:
The author has granted a non-exclusive license allowing Library and Archives Canada to reproduce, publish, archive, preserve, conserve, communicate to the public by telecommunication or on the Internet, loan, distribute and sell theses worldwide, for commercial or non-commercial purposes, in microform, paper, electronic and/or any other formats.

The author retains copyright ownership and moral rights in this thesis. Neither the thesis nor substantial extracts from it may be printed or otherwise reproduced without the author's permission.

AVIS:
L'auteur a accordé une licence non exclusive permettant à la Bibliothèque et Archives Canada de reproduire, publier, archiver, sauvegarder, conserver, transmettre au public par télécommunication ou par l'Internet, prêter, distribuer et vendre des thèses partout dans le monde, à des fins commerciales ou autres, sur support microforme, papier, électronique et/ou autres formats.

L'auteur conserve la propriété du droit d'auteur et des droits moraux qui protège cette thèse. Ni la thèse ni des extraits substantiels de celle-ci ne doivent être imprimés ou autrement reproduits sans son autorisation.

In compliance with the Canadian Privacy Act some supporting forms may have been removed from this thesis.

While these forms may be included in the document page count, their removal does not represent any loss of content from the thesis.

Conformément à la loi canadienne sur la protection de la vie privée, quelques formulaires secondaires ont été enlevés de cette thèse.

Bien que ces formulaires aient inclus dans la pagination, il n'y aura aucun contenu manquant.

Canada

McGill University

English Abstract

TRANSCRIPTIONAL AND GENETIC PROFILING OF HUMAN UVEAL MELANOMA FROM AN IMMUNOSUPPRESSED RABBIT MODEL

Jean-Claude Marshall

Abstract: Uveal melanoma is the most common primary intraocular malignant tumour in adults. Despite improvements in the diagnosis and treatment of the primary tumour, patients continue to have the same mortality rate as several decades ago, reflecting our poor understanding of the mechanisms behind the formation of metastases in this disease. The purpose of this study was therefore to characterize an animal model of uveal melanoma and use this model to study the transcriptional changes that cells undergo from culture to intraocular tumour, to circulation and finally to the formation of a metastatic nodule.

Using microarrays we identified 314 changes in transcript abundance between the intraocular tumour and metastatic lesions. Principal Components Analysis was used to cluster these transcripts into four distinct groups. A further 61 gene transcripts showed statistically significant changes between re-cultured cells isolated from the model, with the circulating malignant cells representing an intermediate step between cells isolated from intraocular tumours and metastatic lesions. We have produced a detailed analysis of the molecular changes that take place as human uveal melanoma cells evolve from a primary tumour to metastasis in an animal model, including the decrease in expression of specific melanoma

markers. These changes were verified using quantitative real time polymerase chain reaction and three different functional assays.

In addition we sought to describe the genetic changes that are present in these cells. Using comparative genomic hybridization arrays we were able to successfully describe the deletions and amplifications that are present in genomic DNA extracted from paraffin embedded sections of the primary tumour. This represents the first time that archival tissue has successfully been used for this sort of analysis in uveal melanoma. We identified several genomic amplifications and deletions including an area of amplification of Wnt2, which is involved in beta-catenin regulation and C-Met, which plays a role in tumour cell homing to the liver in patients.

To the best of our knowledge, this is the first time that a detailed genetic analysis has been carried out on the progression of uveal melanoma from intraocular tumour, to circulation, to the formation of metastases.

French Abstract

Le mélanome de l'uvée est la plus fréquente des tumeurs oculaires malignes primitives de l'adulte. Malgré l'amelioration des diagnostics et traitements de la tumeur primaire le taux de mortalité chez les patients affectés demeure constant, ce qui reflète notre piètre compréhension des mécanismes responsables de la formation de métastases liées à cette maladie. Le but de cette étude est donce de caractériser un modèle animal du mélanome de l'uvée et d'utiliser ce modèle pour étudier les changements qui surviennent au niveau de l'expression génique des cellules cancéreuses lorsqu'elles progressent du stade de tumeur primaire au stade métastatique.

Nous avons identifié 314 gènes dont le profile d'expression diffère entre la tumeur intra-oculaire primaire et les lesions métastatiques. Une analyse de compasant principal (PCA) a été utilisée afin de séparer ces gènes en quatre groupes distincts. Un changement significatif au niveau de l'expression de 61 gènes a été detecté entre les cellules de la tumeur primitive en culture et les cellules malignes un processus recapitulant le stade intermédiaire entre les cellules isolees de la tumeur primaire et des lesions metastatiques. Nous avons produit une analyse détaillée des changements moléculaires qui prennent place lorsque les cellules humaines due mélanome du l'uvée évoluent du stade de tumeur primaire au stade métastatique dans un modèle animal, et démontre une diminution substantielle du niveau d'expression de plusieurs marqueurs spécifiques pour le melanome. Ces changements on été confirmés a l'aide de la

méthode de réaction de plymérisation en chaine quantitative et trois autres essai fonctionnels.

A fin de décrire les changements génétiques présent dans ces cellules, nous avons conduit une étude d'hybridation génomique comparative. Nous avons identifié avec succes les deletions et les amplifications présentes dans l'ADN génomique extraite d'échantillons de tissue provenant de tumeur d'une principale. Ceci constitue la premiere démonstration d'utilisation d'échantillons provenant de banque de tissus pour ce type d'analyse du mélanome de l'uvée. Nous avons identifie plusieurs altération genétiques, incluant une région d'amplification dans le gene codant pour Wnt2, qui est impliqué dans la régulation de la béta-catenine et C-Met, qui joue un role dans le homing des cellules tumorales dans des patients.

Au meilleur de notre connaissance, ceci représente la premiere étude fournissant une détaillée de les mécanismes molèculaires impliqués dans la progression du mélanome de l'uvée du stade de tumeur intra-oculaire primitive à la circulation, à la formation de métastases.

ACKNOWLEDGEMENTS

There are many different people who have helped me to reach this point in my life and I wish I could list each one individually here. To any of you who I don't have the room to include in this area, please forgive me for omitting you.

I would like to start out by thanking Dr. Miguel Burnier Jr., who has been my mentor, advisor and friend over the past five years. Neither this project nor any of my past research investigations would have been possible without his continued support and guidance. I will forever be thankful to him for all that he has done for me throughout the years. It is my hope that someday I can become an equally great teacher and mentor to students, although that is a lofty ambition.

Throughout this time there have been two other people who have advised me on my project and the opportunities that lay ahead for me. Dr. Phil Gold has been one of my advisors since I entered the Master's program in 2001. It has been my great pleasure and honour to have one of the finest minds in cancer research available to help guide me through my PhD. Dr. Alessandra Duncan has also been one of my advisors since I began the Master's program. Her advice and guidance have always been sound and supportive. I feel blessed to have both Dr. Gold and Dr. Duncan as my advisors throughout my graduate training.

My fellow researchers and students in the Henry C. Witelson Ocular Pathology Laboratory have become an extended family over the course of my PhD research. I will never forget any of you and I hope that we shall always remain in touch. You are all among the most brilliant people I know, and your kindness, laughter, and humility will stay with me forever.

Last, but not least I would like to thank my family and fiancée, Angela, for their support throughout the past several years. They have always encouraged me to strive for my goals, no matter the problems that lay ahead. Without them I could never have completed this journey.

Co-Author Contributions

I certify that I am the primary author of all manuscripts originating from this thesis and that the research presented in this thesis represents original work in the field of uveal melanoma research. This is the first time in uveal melanoma that transcriptional analysis has been used to see the changes that tumour cells undergo as they progress from intraocular to circulation and finally the formation of metastases. In addition I have described a method for the extraction of genomic DNA from paraffin embedded archival material for the identification of chromosomal abnormalities that have occurred in our tumour sections using comparative genomic hybridization arrays.

Published Papers:

1. Di Cesare, S., J.C. Marshall, P. Logan, E. Antecka, D. Faingold, S. Maloney, M.N. Burnier, Jr. *Expression and migratory analysis of 5 human uveal melanoma cell liens for CXCL12, CXCL8, CXCL1 and HGF.* Journal of Carcinogenesis, 2007. 6:2
2. Fernandes, B.F., J.C. Marshall, and M.N. Burnier, Jr., *Blue light exposure and uveal melanoma.* Ophthalmology, 2006. **113**(6): p. 1062 e1; author reply 1062.
3. de Souza Filho, J.P., Z.M. Correa, J.C. Marshall, E. Anteka, A.B. Coutinho, M.C. Martins, et al., *The effect of a selective cyclooxygenase-2 (COX-2) inhibitor on the proliferation rate of retinoblastoma cell lines.* Eye, 2006. **20**(5): p. 598-601.
4. Marshall, J.C., K.D. Gordon, C.S. McCauley, J.P. de Souza Filho, and M.N. Burnier, *The effect of blue light exposure and use of intraocular lenses on human uveal melanoma cell lines.* Melanoma Res, 2006. **16**(6): p. 537-41.
5. Pereira, P.R., A.N. Odashiro, J.C. Marshall, Z.M. Correa, R. Belfort, Jr., and M.N. Burnier, Jr., *The role of c-kit and imatinib mesylate in uveal melanoma.* J Carcinog, 2005. **4**: p. 19.
6. Cools-Lartigue, J., J.C. Marshall, A.L. Caissie, V.S. Saraiva, and M.N. Burnier, Jr., *Secretion of hepatocyte growth factor and vascular endothelial growth factor during uveal melanoma-monocyte in vitro interactions.* Melanoma Res, 2005. **15**(3): p. 141-5.
7. Blanco, P.L., J.C. Marshall, E. Antecka, S.A. Callejo, J.P. Souza Filho, V. Saraiva, et al., *Characterization of ocular and metastatic uveal melanoma in an animal model.* Invest Ophthalmol Vis Sci, 2005. **46**(12): p. 4376-82.
8. Saraiva, V.S., J.C. Marshall, J. Cools-Lartigue, and M.N. Burnier, Jr., *Cytotoxic effects of violacein in human uveal melanoma cell lines.* Melanoma Res, 2004. **14**(5): p. 421-4.
9. Marshall, J.C., A.L. Caissie, S.A. Callejo, E. Antecka, and M.N. Burnier Jr, *Cell proliferation profile of five human uveal melanoma cell lines of different metastatic potential.* Pathobiology, 2004. **71**(5): p. 241-5.
10. Marshall, J.C., A.L. Caissie, and M.N. Burnier, Jr., *How in vitro techniques have increased our understanding of uveal melanoma cellular biology.* Can J Ophthalmol, 2004. **39**(4): p. 428-32.
11. Cools-Lartigue, J., J.C. Marshall, A.L. Caissie, V.S. Saraiva, and M.N. Burnier, Jr., *Secretion of interleukin-6 and prostaglandin E2 during uveal melanoma-monocyte in vitro interactions.* Exp Eye Res, 2004. **79**(4): p. 451-4.
12. Callejo, S.A., J.C. Marshall, J. Cools-Lartigue, V.S. Saraiva, and M.N. Burnier, Jr., *Macrophage-derived soluble factor enhances melanoma*

inhibitory activity expression by uveal melanoma cells in vitro. Melanoma Res, 2004. **14**(2): p. 91-5.

Papers In Press and Under Review:

1. Jean-Claude Marshall, Andre Nantel, Paula Blanco, Josee Ash, Stephanie R.Cruess, Miguel N Burnier Jr. Transcriptional profiling of the evolution of uveal melanoma from cell lines to intraocular tumours to metastases. Clinical Can Res. Under Review.
2. Jean-Claude Marshall, Amanda L. Caissie, Stephanie R. Cruess, Jonathan Cools-Lartigue, Vinicius S. Saraiva, Miguel N. Burnier Jr. The effects of a cyclooxygenase-2 (COX-2) expression and inhibion on human uveal melanoma cell lines and macrophage nitric oxide production. Ophthalmic Res. In Press.
3. Jean Claude A. Marshall, Bruno Fernandez, Shawn Maloney, Patrick Logan, Sebastian DiCesare, Miguel N. Burnier Jr. The use of a cyclooxygenase-2 inhibitor (Nepafenac) in an ocular and metastatic animal model of uveal melanoma. Under Review

Association for Research in Vision and Ophthalmology (ARVO) peer reviewed abstracts and American Association for Research in Cancer (AACR) Presentations as first author:

1. J.-C.A. Marshall, S. Di Cesare, S. Maloney, B. Fernandes, E. Antecka, M.N. Burnier, Jr. Comparative genomic hybridization array of paraffin embedded tissue from an animal model of uveal melanoma. ARVO 2007
2. J.-C.A. Marshall, A.Nantel, P.L. Blanco, J.Ash, M.N. Burnier, Jr. Transcriptional Profiling of Circulating Malignant Cells Isolated From an Animal Model of Uveal Melanoma. ARVO 2006
3. J.-C. A. Marshall, Andre Nantel, Paula Blanco, Josee Ash, Miguel N. Burnier Jr. Transcriptional profiling of circulating malignant cells isolated from an animal model of uveal melanoma. AACR 2006
4. J.-C.A. Marshall, A. Nantel, P. Blanco, J. Ash, S.R.Cruess, E. Achenson, M. N Burnier Jr. Transcriptional profiling of the evolution of uveal melanoma from cell lines to intraocular tumours to metastasis. ARVO, 2005.
5. J.-C.A. Marshall, Andre Nantel, Paula Blanco, Josee Ash, Stephanie R.Cruess, Elise Achenson, Miguel N Burnier Jr. Transcriptional profiling of the evolution of uveal melanoma from cell lines to intraocular tumours to metastasis. AACR 2005
6. J.-C. A. Marshall, A. L. Caissie, V.S. Saraiva, S. A. Callejo, J.P. Souza Filho, M.N. Burnier Jr.: Inhibition of uveal melanoma cell proliferation by nepafenac, a selective cyclooxygenase-2 (COX-2) inhibitor. ARVO, 2004.

7. J.-C. A. Marshall, A. L. Caissie, V.S. Saraiva, P. L. Blanco, M.N. Burnier Jr.: The in vitro expression of cyclooxygenase-2 (COX-2) and its effect on the proliferation of uveal melanoma cells. AACR, 2004.
8. J.-C.A. Marshall, A.L. Caissie, J.J. Cools-Lartigue, S.A. Callejo, M.N. Burnier: The Invasive Properties of Uveal Malanoma Cell Lines and Their Response to Interleukin-6 (IL-6) and Vascular Endothelial Growth Factor. ARVO, (64), 2003.
9. J.-C.A. Marshall, M. Pardo, A.L. Caissie, S.A. Callejo, M.N. Burnier: Cell proliferation Profile of Five Human Uveal Melanoma Cell Lines of Different Metastatic Potential. ARVO, 2002.

Invited Speaker:

1. UNIFESP Ophthalmology Symposium, Research Course, March 2007, Three Lectures.
2. ARVO 2007 Meeting, Ocular Tumours: Emerging Scientific Concepts. May 2007.

ARVO peer reviewed abstracts as an author:

1. *J.J. Cools-Lartigue, C.S. McCauley, F.J. Gregoire, J.-C.A. Marshall, C.Edelstein, M.N. Burnier, Jr.* Immunomagnetic Isolation From Blood of Five Human Uveal Melanoma Cell Lines. ARVO 2006
2. *M.N. Burnier, Jr., J.-C.A. Marshall, F.J. Gregoire, S.Di Cesare, P.Logan, A.Al-Kandari.* The Effect of a Cox-2 Inhibitor on an Ocular Melanoma Animal Model. ARVO 2006
3. *S.Di Cesare, P.Logan, J.C. Marshall, F.J. Gregoire, D.Faingold, M.N. Burnier, Jr.* Migratory and Immunohistochemical Analysis of 5 Human Uveal Melanoma Cell Lines Towards CXCL-12, CXCL-8, CXCL-1, and HGF. ARVO 2006
4. *P.Logan, J.-C.A. Marshall, B.F. Fernandes, S.Maloney, V.Saraiva, M.N. Burnier, Jr. In vivo* Imaging of Fluorescently Labelled Human Uveal Melanoma Cells in Nude Mice. ARVO 2006
5. *S.Bakalian, J.C. Marshal, D.Faingold, P.Logan, A.C. Frota, M.N. Burnier, Jr.* The Effect of Curcumin on the Proliferation Rate of Human Uveal Melanoma Cell Lines. ARVO 2006
6. *D.Faingold, J.-C.Marshall, S.Bakalian, A.Al-Kandari, C.Edelstein, M.N. Burnier, Jr.* Immune Expression and Inhibition of Hsp90 in Human Uveal Melanoma. ARVO 2006
7. *C.S. McCauley, D.Faingold, J.-C.A. Marshall, S.Di Cesare, S.Bakalian, M.N. Burnier, Jr.* Expression and Inhibition of P-Glycoprotein in Retinoblastoma Cell Lines. ARVO 2006
8. F.J. Gregoire, B.F. Fernandes, J.-C.A. Marshall, S.Di Cesare, E.Antecka, M.N. Burnier, Jr. In vitro Characterization of Vascular Loops in Four Uveal Melanoma Cell Lines. ARVO 2006

9. D. Faingold, J.-C. A. Marshall, S. Bakalian, S.R. Cruess, E. Antecka, O. Kasner, M.N. Burnier Jr. The effect of lens proteins on proliferation in uveal melanoma cell lines. ARVO, 2005.
10. A.N. Odashiro, P.L. Blanco, J.-C.A. Marshall, J.P. Souza Filho, V.S. Saraiva M.N. Burnier Jr. Intraocular inoculation of cutaneous melanoma cells in an uveal melanoma animal model. ARVO, 2005.
11. J.P. Souza Filho, Z.M. Correa, J-C. A. Marshall, A.B. Coutinho, M.C.Martins, M.N.Burnier Jr. The effect of a selective cyclooxygenase-2 (COX-2) inhibitor on the proliferative rate of retinoblastoma cell lines. ARVO, 2005.
12. J.J. Cools-Lartigue, E.Antecka, J.-C.A. Marshall, V. Saraiva, C. McCauley, M.N. Burnier Jr. Immune-expression of Hypoxia-Inducible Factor -1α in an Animal Model of Uveal Melanoma. ARVO, 2005.
13. C. McCauley, J.-C. Marshall, S.R. Cruess, L. Kaysabi , S.A. Callejo, M.N. Burnier Jr. The Effect of Blue Light Exposure and use of Intraocular Lenses on Human Uveal Melanoma Cell Lines. ARVO, 2005.
14. A.L.Caissie, C.Esmerado, J.C.Marshall, P.L.Blanco, S.Callejo, M.N. Burnier Jr. Expression of cytokines in the vitreous of a uveal melanoma animal model. ARVO, 2005.
15. S. Bakalian, J.P. Souza Filho, Z.M. Correa, J.C. Marshall, A.B. Coutinho, M.N. Burnier Jr. The Effect of Blue Light Exposure on the proliferation rate of Human Retinoblastoma Cell Lines. ARVO, 2005.
16. M.S. Lowen, P.R. Pereira, A.N. Odashiro, J.-C.A. Marshall, D. Faingold, J.V. Burnier, M.N. Burnier Jr. Determination of Melanoma Inhibitory Activity (MIA) levels in an animal model of uveal and cutaneous melanoma. ARVO, 2005.
17. S.R. Cruess, E. Antecka, J-C. Marshall, P.L. Blanco, S.A. Callejo, M.N. Burnier Jr. Disseminated Melanoma Cells in Bone Marrow from an Immuno-Suppressed Rabbit Model. ARVO, 2005.
18. A.L. Caissie, J.-C.A. Marshall, A.N. Odashiro, P.R.Pereira, D. Faingold, M.N. Burnier Jr. The cyclooxygenase-2 inhibitor Nepafenac improves the function of macrophages suppressed by uveal melanoma conditioned medium. ARVO, 2005.
19. J.J. Cools-Lartigue, J.-C.A. Marshall, P.L. Blanco, V.S. Saraiva, M.N. Burnier Jr., E. Antecka: Changes in the proliferation behaviour of a human uveal melanoma cell line from different steps in the metastatic cascade. ARVO, 2004.
20. A.L. Caissie, V.S. Saraiva, J.-C.A. Marshall, J.P. Souza Filho, L. Segal, M.N. Burnier Jr.: Phospho-Akt in uveal melanoma. ARVO, 2004.
21. J.-C. A. Marshall, A. L. Caissie, V.S. Saraiva, S. A. Callejo, J.P. Souza Filho, M.N. Burnier Jr.: Inhibition of uveal melanoma cell proliferation by nepafenac, a selective cyclooxygenase-2 (COX-2) inhibitor. ARVO, 2004.
22. P.L. Blanco, S.A. Callejo, J.-C.A. Marshall, E. Antecka, J.P. Souza Filho, M. Mansour, M.N. Burnier Jr.: Uveal melanoma progression in an animal model. ARVO, 2004

23. S.A. Callejo, E. Antecka, J.-C.A. Marshall, R. Connolly, M.N. Burnier: Detection of Spiked Uveal Melanoma Cells in Peripheral Blood of Healthy Volunteers. ARVO (64), 2003.9.
24. A.L. Caissie, J.-C.A. Marshall, E. Antecka, I. Zundane, M.N. Burnier: The Effect of Conditioned Medium from COX-2 Expressing Macrophage on the In Vitro Proliferation of Uveal Melanoma Cell Lines. ARVO (64), 2003.
25. M.M. Valenca Cordeiro Barbosa, A.L. Caissie, J.-C.A. Marshall, P.L. Blanco, M.N. Burnier: The Effect of In Vitro Macrophage-Tumour Cell Interaction on the Production of Migration Inhibitory Factor (MIF). ARVO, (64), 2003.
26. J.J. Cools-Lartigue, E. Lewandowski, T.S. Chernin, J.-C.A. Marshall, E. Antecka, M.N. Burnier: The Expression of Prostaglandin E2 (PGE2) and Interleukin 6 (IL-6) in Macrophage and Uveal Melanoma Conditioned Media. ARVO, (64), 2003.
27. S.R. Cruess, T.S. Chernin, S.A. Callejo, J.-C.A. Marshall, M.N. Burnier: The Effects of Melanoma Inhibitory Activity (MIA) on the Invasive Properties of Uveal Melanoma Cell Lines. ARVO, (64), 2003.
28. K.M. Oliver, G.S. Lima, A.L. Caissie, J.-C.A Marshall, J. Deschenes, M.N. Burnier: Cyclooxygenase (COX-2) Expression in Primary Acquired Melanosis. ARVO, 2002.
29. J.-C.A. Marshall, M. Pardo, A.L. Caissie, S.A. Callejo, M.N. Burnier: Cell proliferation Profile of Five Human Uveal Melanoma Cell Lines of Different Metastatic Potential. ARVO, 2002.
30. Morilla-Grasa, M.C. Mendez, A.L. Caissie, J.-C.A. Marshall, R. Lopez, M.N. Burnier: The Expression of Cyclooxygenase-2 (COX-2) in an Animal Mode of Primary and Metastatic Human Uveal Melanoma. ARVO, 2002.
31. M. Pardo, J.-C.A. Marshall, A.L. Caissie, S.A. Callejo, M.N. Burnier, G. Pinard: Cyclooxygenase-2 (COX-2) Expression in Uveal Melanoma and Macrophage Cell Lines. ARVO, 2002.
32. S. Al-Khalifa, J. Burnier, A.L. Caissie, S.A. Callejo, J.-C.A. Marshall, M.N. Burnier: Second Non- Ocular PrimaryTumours in Uveal Melanoma Patients. ARVO, 2002.

Table of Contents

Table of Contents

Chapter 1

INTRODUCTION

1. Uveal Melanoma

1.1 Overview of Uveal Melanoma

The first published histopathological classification of uveal melanoma was carried out by Major George R. Callender in 1931 at the Armed Forces Institute of Pathology [1]. Since that time these tumours of the eye have had several different names, *melanosarcoma*, *melanocarcinoma*, *leukosarcoma*, *angiosarcoma,* and *giant cell sarcoma* [2]. These terms were subsequently covered by the title of uveal malignant melanoma, which is the recommended term by the World Health Organization.

Uveal melanoma (UM) is the most common intraocular malignant tumour in adults [2]. It accounts for approximately 5 percent of all reported melanomas [3] and has an incidence of six to seven individuals per million people in North America [4]. These tumours arise from melanocytes that are present in the uveal tract of the eye. This tract is comprised of the iris, ciliary body and choroid.

1.1.2 Risk Factors

Several different risk factors have been studied including, age, race, sex, genetic factors, predisposing lesions and exposure to sunlight. The average age at diagnosis is 55 years old and fewer than 1.6 percent of cases are in patients under the age of 20 [2]. The incidence of this tumour increases with age [5]. A person of Caucasian descent is 8.5 times more likely to develop uveal melanoma than a

person of African descent [6]. It is believed that one of the reasons that may lead to this predisposition is the, on average, lighter coloured iris in people of Caucasian descent [7]. There is also a slight increase in the number of men compared to women who are diagnosed with uveal melanoma, although the reasons for this are currently unclear [2]. Unlike Retinoblastoma, the most common intraocular malignant tumour in children, there has been no clearly defined genetic component for uveal melanoma. There have only been a handful of familial uveal melanomas that have been reported in world literature [8-13]. Until now no definitive link in any genetic abnormality has been associated with these familial cases.

There are two lesions that have been well documented as raising an individual's risk for developing uveal melanoma, congenital melanosis and nevi. The exact mechanisms involved in these transformations from benign lesions to malignant uveal melanoma are unclear although exposure to environmental factors may play a role. The presence of nevi in the choroid is asymptomatic; therefore the majority of the population is unaware of their existence. From autopsy studies, 5 to 10 percent of the population is estimated to have at least one choroidal nevus. The exact percentage of those nevi that may lead to uveal melanoma is unknown. Most nevi are flat lesions that are less than 5 mm in diameter, although they can attain sizes as large as 10 mm in diameter and 1.5 mm in thickness. Large nevi can be difficult to differentiate from small uveal melanomas.

The exposure to UV radiation has long been suspected to play a role in the malignant transformation of nevi, although there have been contradictory epidemiological studies surrounding this issue [7, 14]. Recently our laboratory has investigated the possible effects of blue light exposure on the transformation of uveal melanocytes into a more malignant phenotype [15, 16]. These experiments have demonstrated that sufficient blue light exposure can lead to a malignant transformation in these melanocytes. Further epidemiological experiments are necessary to investigate the effect that this exposure may have on the general population.

1.1.3 Anatomy of the Eye

The human eye is composed of several distinct and morphologically unique tissues. In the posterior part of the globe are several layers that are essential for vision. Light enters through the cornea into the anterior chamber, which is filled with a transparent liquid called aqueous. Light continues through the opening in the iris called the pupil, passes through the lens whose shape is controlled by the muscles of the ciliary body, and enters the posterior compartment of the eye [17]. The compartment is filled with a thick, transparent, viscous substance known as vitreous, which aids in giving the eye its shape and form. The first tissue layer that light will encounter is the retina, posterior to which is the choroid, and finally the sclera. The retina includes specialized nerve cells known as rods or cones, which allow for actual sight. The choroid, immediately posterior to the retina, is a vascular layer that provides nourishment for the retina. The sclera is a tough fibrous layer that serves as the protective outer

coat for the eye. Ocular melanomas arise from one of three locations in the eye, collectively named the uveal tract. The uveal tract is composed of the iris, choroid and ciliary body as shown in Figure 1.1. Each of these three locations contain melanocytes and are therefore capable of giving rise to what is commonly known as uveal melanoma. Over 90 percent of uveal melanomas arise from the choroid, while the majority of the remaining 10 percent are melanomas of the iris [2].

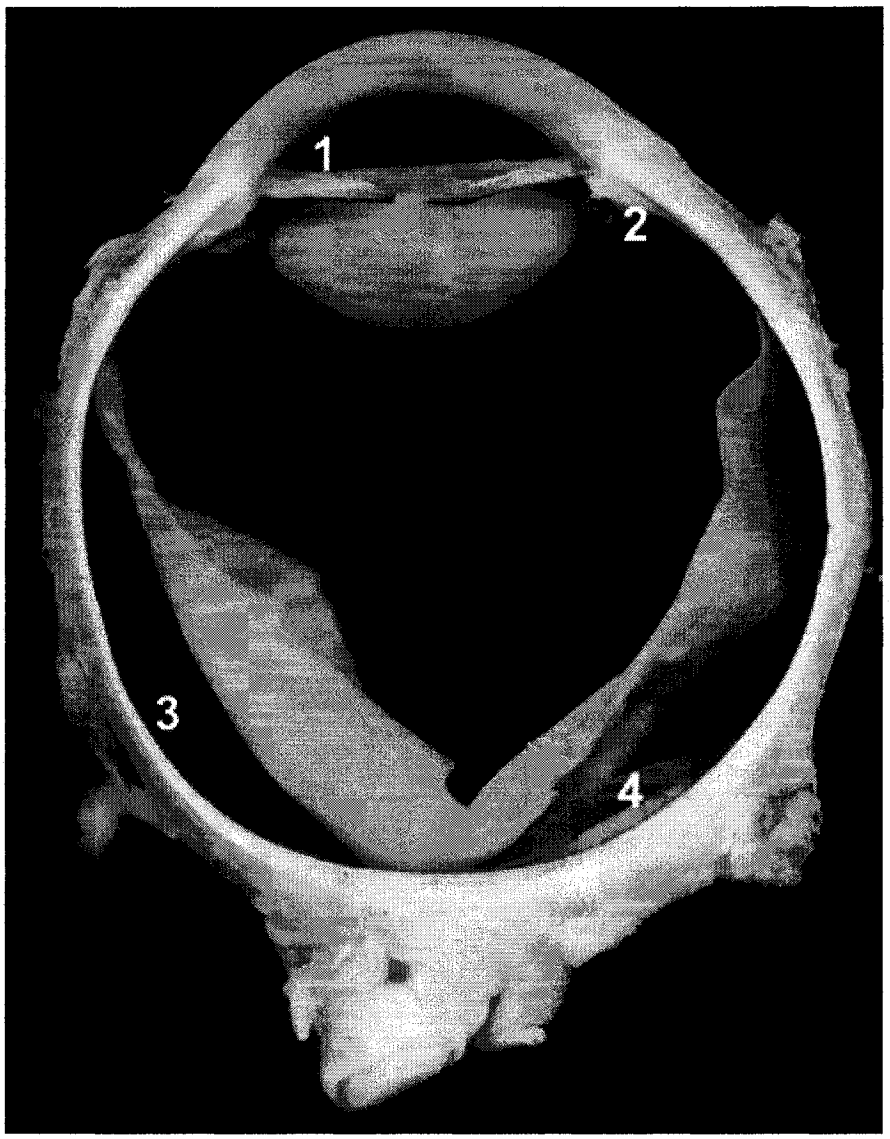

Figure 1.1) Gross Pathology Section of the Human Eye

Photograph of a pupil to optic nerve section of an eye with a small discoid uveal melanoma from a patient (x5). The different parts of the uveal tract or labelled 1) Iris, 2) Ciliary body, 3) Choroid, with 4) a small uveal melanoma shown in the posterior of the eye.

1.1.4 Clinical Diagnosis

The clinical manifestations of UM depend on its location. As described previously, UM arises from the melanocytes in the eye of the patient. These melanocytes are located within the uveal tract, which is comprised of the iris, ciliary body and the choroid.

Melanomas arising from the iris represent five percent to eight percent of all UM and are also called anterior melanomas. They usually present as a dark elevated mass within the iris. Signs associated with iris melanomas include hyphema, glaucoma and cataracts [18-20].

Melanomas of the ciliary body and choroid are predominantly posterior melanomas. Ciliary body melanomas represent seven percent of UMs and given the lack of signs and symptoms due to its location out of the field of view, are not usually diagnosed until the tumour has grown to a considerable size.

Choroidal melanomas are the most common types of UM. They are typically asymptomatic and the tumour is usually diagnosed during routine examinations. Patients with large tumours may present with visual field deficits. The initial lesions often appear as an elevated well-circumscribed, sub-retinal, pigmented mass upon fundus exam as shown in Figure 1.2. Larger lesions usually rupture through Bruch's membrane, a basement membrane located between the choroids and the retina, and grow towards the subretinal space, assuming a typical mushroom shape [19, 21].

Tumours located in the iris seem to be less aggressive than the ones located in the ciliary body. Choroidal melanomas carry an intermediate prognosis

[22]. Tumour size is directly correlated with the prognosis of the patient and is the most important clinical prognostic factor. Extraocular extension is another clinical characteristic that correlates with high mortality rates due to metastasis [23].

The ability of ophthalmologists to diagnose uveal melanomas has increased from an average accuracy of 87.5 percent in 1980 [24] to approximately 99.5 percent in 1990 [25]. This increase in diagnostic accuracy reflects better training of ophthalmologists as well as increased awareness of the disease and its indications by ophthalmologists. One of the major technological advances that has contributed to this increase in diagnostic accuracy was the introduction of A and B scan ultrasound [26]. This allowed for the imaging of the intraocular tumour as well as accurate measurements of tumour diameter and maximum height from the base of the choroid.

Based on these measurements the tumours are divided into three different groups, small if the largest tumour dimension is 10 mm or less, medium if it is between 10 to 15 mm, and large if the largest tumour dimension exceeds 15 mm. The tumour is prevented from expanding through the sclera by the tough fibrous nature of this layer. The tumour therefore expands internally through Bruch's membrane, which is relatively weak. Small tumours are usually discoid in shape and are confined to the choroid. As the tumour grows larger, it ruptures through Bruch's membrane and into the subretinal space. The growth in this space is usually greater than the growth that was present in the choroid. As the tumour continues to grow it adopts the typical mushroom shape as seen in Figure 1.3. As this occurs, the retina that is overlaying the tumour becomes detached and patients

often have subretinal haemorrhage associated with the tumour formation. These tumours can continue to grow destroying tissues in the eye and eventually filling the entire globe.

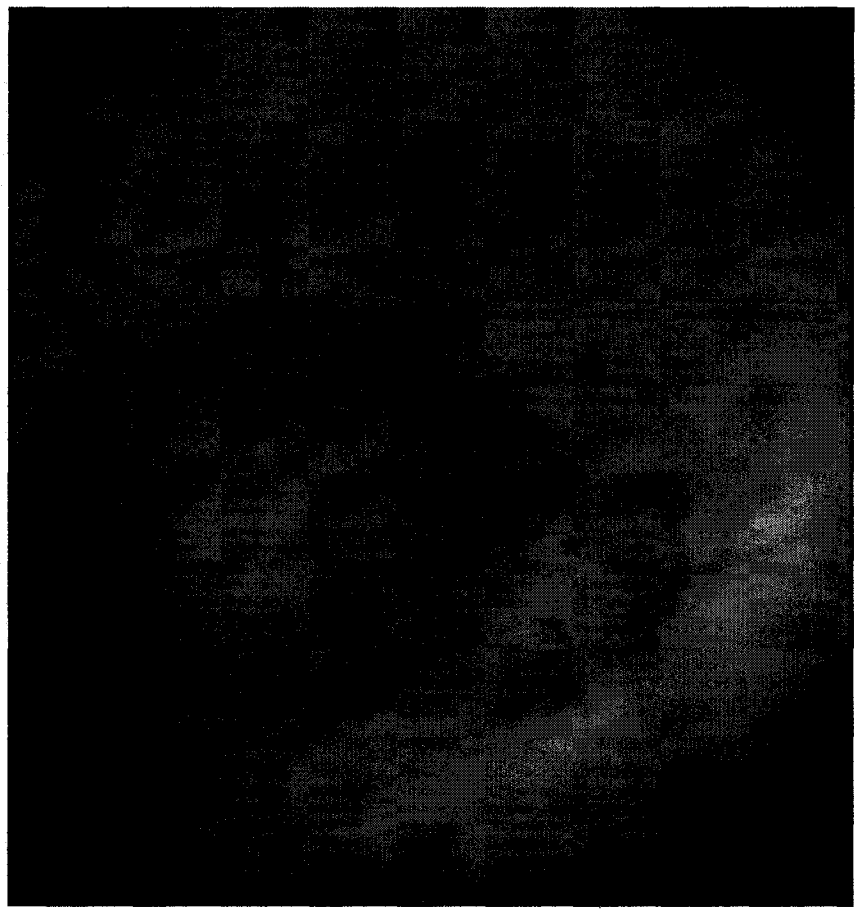

Figure 1.2) Fundus Picture of a Uveal Melanoma

Fundus exam of a patient with uveal melanoma showing a well circumscribed elevated mass (arrow) with the retina overlaying it as can be seen by the retinal vessels going over the tumour. An associated retinal detachment can be seen (star) next to the tumour.

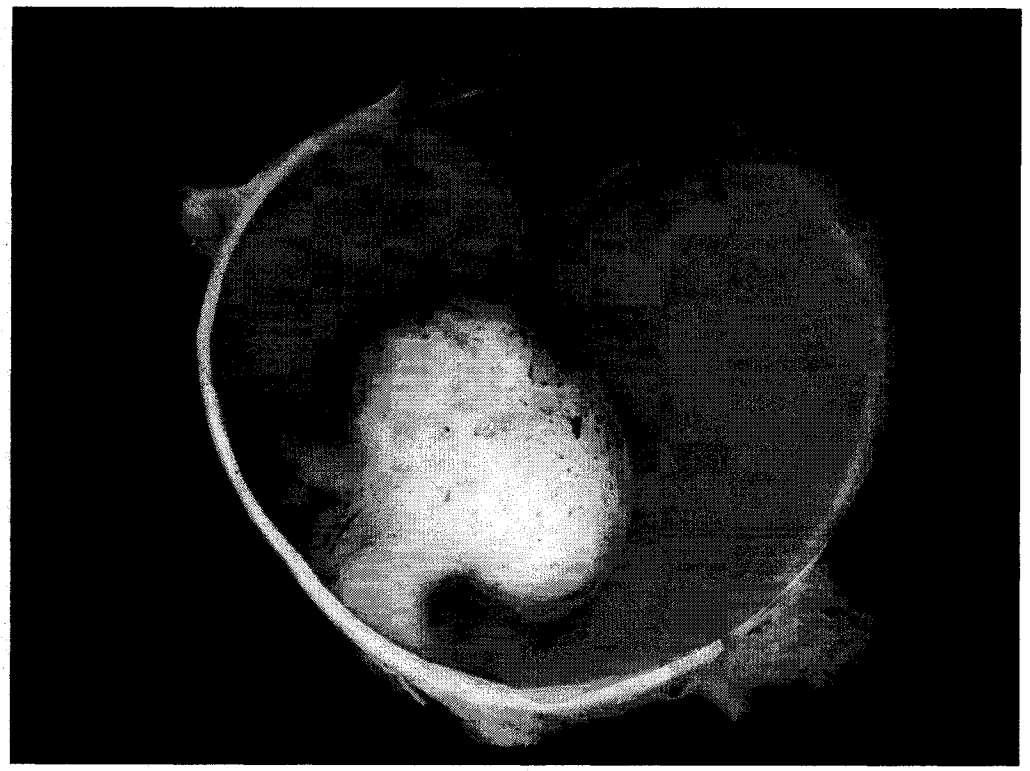

Figure 1.3) Large Uveal Melanoma

Gross pathology picture of a large uveal melanoma, greater than 15 mm in tumour diameter, displaying a typical mushroom shape appearance (x5).

1.1.5 Treatment of the Primary Tumour

The traditional treatment for the primary tumour has been the removal of the affected eye, or enucleation. This technique was succeeded by the development of plaque radiotherapy where a plaque with I-125 is surgically placed in the socket of the eye, opposite the location of the intraocular tumour [27]. The treatment is limited to tumours with a maximum height from the choroid of 9 mm. Tumours that are larger than this are generally considered unacceptable for plaque radiotherapy. Since the introduction of this alternative therapy several studies have sought to investigate differences in patient mortality rates depending on the treatment of the primary tumour. The largest of these

studies was the Collaborative Ocular Melanoma Study (COMS) which investigated the survival of patients randomized between plaque radiotherapy and enucleation [28]. After 12 years of follow up they concluded that there was no significant difference in mortality rate depending on which form of treatment was used for the primary tumour.

Several other treatment options have now become available although none of these have decreased the mortality rate of patients. Transscleral resection of the tumour has been tried, although this technique may leave behind viable cells; therefore, adjuvant brachytherapy is recommended. Proton beam therapy can be used as an external source of radiation, although the outcomes are not significantly different than with the more traditional plaque radiotherapy. Transpupillary thermotherapy has also been tested but proved to be successful only in select circumstances. Long-term results with this method have shown poor local control of the tumour with no significant increase in visual acuity of the patient following treatment as compared to plaque radiotherapy.

1.1.6 Mortality Rates

Unfortunately even with these advancements in diagnosis and local treatment of the tumours, the ten-year mortality rate for patients diagnosed with uveal melanoma has remained relatively stable at approximately 50 percent [29].

Clinically, the best prognostic indicator is tumour size [30]. Small tumours, those that have a largest tumour diameter of less than 10 mm, have a 16 percent mortality rate over five years. Tumours with a diameter between 10 and 15 mm lead to a 32 percent mortality rate over five years. Those tumours with a diameter

of over 15 mm at the time of diagnosis carry with them a 53 percent mortality rate over 5 years. No differences in mortality rates have been shown using any of the therapies that have been used to control the primary intraocular tumour [28].

1.2 Histopathological Prognostic Factors

Ocular pathologists have established several well documented histopathological prognostic factors based on enucleated eyes and patient follow up after treatment. A wide variety has been described in the literature. The most commonly accepted prognostic factors are: cell type, number of mitotic figures, presence of tumour infiltrating lymphocytes, and vascular loops [31].

Ever since the days of Major George Callender, cell type has been recognized as a prognostic indicator in uveal melanoma and is recognized as the single most predictive indicator of outcome along with tumour size [32]. The original classification that was described by Major George Callender was based on cytologic and histopathologic features that he and his coworkers at the Armed Forces Institute of Pathology described. They classified uveal melanoma into six groups based on the cell type and patterns seen within the tumours. Since then this classification has been simplified and the malignancy can be divided into three groups based on cell type: epithelioid, spindle, and mixed [33].

Spindle cells are generally smaller, fusiform, well stratified cells. Epithelioid cells are large, non-stratified and poorly coherent with surrounding cells. Tumours composed of spindle shaped cells have the best prognosis, and those composed of epithelioid cells have the worse prognosis. These cell types can also be correlated with tumour size [34], with small tumours almost

exclusively composed of spindle shaped cells, and large tumours classified as being composed of either mixed cell type or epithelioid cells.

The number of mitotic figures present in an average of 10 high-powered fields has been shown to be a prognostic indicator [31]. The number of mitotic figures seen in the section is thought to directly correlate with the proliferation rate of the tumour [35]. The mean size of the 10 largest nucleoli in a field of view has also been correlated with prognosis and relates to the larger size of the epithelioid cell type [36].

Presence of tumour infiltrating lymphocytes (TIL) was described in the early 1990s [37]. The poor prognosis associated with the presence of these TILs was a surprise, as their presence in cutaneous melanoma is associated with a better prognosis for the patient [38]. Although the reason for this is still not clear, there have been several interesting hypotheses put forward. The one that has best fit the results so far revolves around the fact that the eye is an immunopriviliged site. These TIL must therefore be called from the rest of the body to invade into the primary tumour. This may reflect the presence of circulating malignant cells or even micrometastasis, which would alert the immune system to the presence of the primary tumour. Therefore the poor prognosis associated with these TILs would be a reflection of the already disseminated uveal melanoma cells in the body of the patient.

The final classical histopathological prognostic indicator is the presence of vascular loops in the primary tumour [39, 40]. These patterns are seen as vascular loops that stain positive for factor VIII related antigen. The loops that are seen in

the histopathological analysis represent three-dimensional vascular structures that provide nutrients to the tumour. There has been considerable debate regarding the composition of these loops, such as if they are formed by endothelial cells under the influence of the primary tumour through angiogenesis or if they are composed of fibrous sheets of material produced by the tumour cells [41-43].

1.3 New Histopathological Prognostic Indicators

Despite these well-established prognostic indicators there has been no significant decrease in the mortality rate of patients with this tumour in the past several decades. There has therefore been considerable effort made in the past several years to find new prognostic markers, with the hope that these may provide new therapeutic targets to improve patient mortality rates.

1.3.1 Cell Surface Molecules

Several different cell surface molecules have been studied for their potential use as therapeutic target. CD95 (Fas) and the CD95 ligand (FasL) have been shown to be expressed in approximately 90 percent of studied UM tumours [44]. Neither of these was considered to be an independent prognostic indicator for the development of metastasis. A more promising target is CD117, or C-KIT, which is a transmembrane tyrosine kinase that can be targeted with the drug Gleevec. It has been shown to be correlated with patient survival and the drug was shown to decrease proliferation and invasion rates of uveal melanoma cells [45]. Similarly, the expression of insulin-like growth factor 1 receptor (IGF1-R) by the primary tumours has been shown to be correlated with a decrease in survival [46].

The inhibition of this receptor led to decreased cellular proliferation in culture and caused tumour regression in a xenograft animal model [47].

1.3.2 Cytoplasmic Proteins

Several different cytoplasmic proteins have been actively studied. Akt is a protein kinase in the phosphatidylinositol-3 kinase-signalling pathway, which when activated controls a vast array of cellular functions including proliferation, migration and invasion. The expression of high levels of phospho-Akt, the active form, was associated with worse prognosis and current testing of inhibitors for the activation of Akt are underway [48].

Cylooxygenase-2 is an inducible prostaglandin synthase that we have studied extensively in the laboratory and associated with worse prognosis when present in the intraocular tumours [49]. The inhibition of COX-2 with a topical anti-COX-2 drug has shown promise *in vitro* and in a rabbit model of uveal melanoma [50, 51]. These COX-2 inhibitors have decreased the metastatic burden in our rabbit model and have decreased the proliferative ability of UM cell lines *in vitro*.

The change in the expression of intermediate filaments was first described in breast cancer and then explored in uveal melanoma [52]. The transition of cells from expressing vimentin, a mesenchymal cell marker, to the expression of keratins, markers of epithelial cells, is believed to be involved in the change of cells from a spindle type to an epithelioid cell type. This change of expression pattern was associated with worse prognosis [53]. Another indicator of worse prognosis is the increased production of matrix metalloproteinases (MMPs),

which are involved in tumour cell invasion. The expression of MMP-2 and MMP-9 by these tumours has been associated with worse prognosis [54].

1.3.3 Nuclear Proteins

Cyclin D1 is a cell cycle protein that is a crucial regulator of the progression from G1 to S phase. It has been shown that a high expression of Cyclin D1 significantly correlates with prognosis in UM patients [55]. The expression of two other markers of cellular proliferation, Ki-67 and proliferating cell nuclear antigen (PCNA) has also been correlated with worse prognosis [56, 57].

1.4 Metastasis

In the majority of cancers, malignant cells can escape through the lymphatics. Therefore lymph nodes are used to stage the disease, with breast cancer serving as one of the best-known example of this. The interior of the eye has no lymphatics and is an immunopriviliged site. Due to the lack of lymphatics, it is impossible to do traditional staging of the progression of the disease. In addition, due to the lack of lymphatics, uveal melanoma cells must escape the eye hematogeneously in order to reach metastatic sites. Unlike retinoblastoma, the most common intraocular tumour in the eye of children, the occurrence of metastasis is not significantly related to extraocular extension. For retinoblastoma, the presence of extraocular extension is the most important prognostic indicator. In uveal melanoma the presence of extraocular extension is most significantly linked to large tumour size, and it is the large tumour size that is correlated with poor prognosis.

It has long been documented that the preferred site of primary metastasis in UM patients is the liver. The liver has been documented as the first site of metastasis in 60 to 95 percent of patients [58, 4]. This large range appears to be a result of the methods used to detect the presence of liver metastasis. North American centres rely upon liver function tests and chest X-rays for the detection of metastases in asymptomatic patients. The majority of European centres prefer the use of liver ultrasounds [59]. The specificity of liver function tests was shown to be 14.7 percent in a continuation of the COMS study [60]. The specificity and positive predictive values were better at 92.3 and 45.7 percent respectively.

A study from Memorial Sloan-Kettering Cancer Centre recently documented the locations of the first detectable metastatic lesion in a series of 119 patients. They confirmed that liver was the primary site of metastasis in approximately 61 percent of patients. In the remaining patients the lung was the location of the first metastatic nodule in 24.4 percent. Skin and soft tissue was found to be the first site in 10.9 percent and 8.4 percent had the first metastatic lesions in their bones, with the remaining patients presenting with metastases to their brain.

The average survival rate of patients after diagnosis with liver metastasis from uveal melanoma is 15 months [61]. There is no standardized treatment available for patients once they have detectable metastatic lesions. Resection of single nodules in the liver has been shown to increase survival rate by a small margin [62, 63]. This has proven to be of limited use when there are multiple

metastatic nodules present. Intra-arterial catheter for direct delivery of chemotherapeutics to the liver has also been used with mixed results [64].

1.5 Aims and Objectives

It is clear from this that further understanding of the biology behind the formation of metastases in UM patients is required. Our treatments of the primary tumour are sufficient to control the local tumour in the eye. New techniques have offered ophthalmologists the ability to spare the globe and even to retain some vision in patients. None of these treatments, however, has led to a change in the mortality rate since the 1960s. It is therefore apparent that we must develop a better understanding of those factors that allow cells to form metastasis in patients. Since the metastatic process in patients can take up to 10 years, we chose to model this system using immunosuppressed animals and human-derived uveal melanoma cell lines. It was our aim to use tissue isolated from the intraocular tumours, circulating malignant cells and metastasis to transcriptionally profile the changes that occur in cells as they go from *in vitro* to intraocular tumours, to circulation, to metastases. We were also interested in profiling the genomic changes that these cells had accumulated using array comparative genomic hybridization.

Chapter 2

LITERATURE REVIEW

2.1 Uveal Melanoma Cell Lines

The establishment of uveal melanoma cell lines from the primary tumours of patients has allowed for a wide variety of studies that would have otherwise been impossible. With a decline in the use of enucleations and thus the availability of fresh tissue from patient tumours, these cell lines have become an even more important source of information.

2.1.2 Functional Assays

A range of functional assays is available to study our uveal melanoma cell lines. Our laboratory has explored several different proliferation assays and has characterized the proliferative ability of the five human uveal melanoma cell lines that were available for our use, including the cell line that was used for the animal model [65]. In addition to these assays we have the ability to measure the invasive rate of our cells to pass through an artificial basement membrane.

2.1.3 Proliferation Rates

Studies of uveal melanoma proliferation rates have historically used monoclonal antibodies to cell cycle markers such as Ki67 and Proliferating Cell Nuclear Antigen (PCNA)[56]. A higher fraction of cells expressing PCNA in uveal melanoma samples has previously been correlated with poor patient prognosis. These methods, while adequate for studying pathological specimens, are not ideal for the rapid screening of potential therapeutic treatments in *in vitro*

systems. The traditional method of counting cells under high power fields has its limitations with regard to the quantitative accuracy of the method from laboratory to laboratory, and also to the time required. Several rapid and sensitive tests for *in vitro* cellular proliferation rates have been developed with the aim of improving techniques used to screen potential anti-cancer agents.

Radioactive methods, such as pulse labelling with tritiated thymidine, have lessened the quantitative problems, although they introduced the new problem of dealing with radioactive materials. Pulse labelling with tritiated thymidine has previously been used to study the DNA synthesis rate of breast cancers. Tumour samples that showed the highest DNA synthesis rates were a positive indicator of high risk of recurrence [66]. With regards to uveal melanoma, this method has previously been utilized to study radio sensitivity and survival curves of human uveal melanoma cell lines [67].

New colourimetric assays, such as the Sulforhodamine-B assay developed by the National Cancer Institute, replace labelling with radioactive materials [68]. These colourimetric assays, specifically designed for the rapid and sensitive testing of potential anti-cancer agents, have proven valuable in the assessment of proliferation rates of uveal melanoma cell lines [16, 45, 69, 70]. These assays have proven to be reproducible and quite useful for detecting changes in proliferation rates and are used to verify our results.

2.1.4 Invasion Assays

The ability of cells to invade through a basement membrane is important not only for the escape of cells from the primary tumour but also for the

implantation of cells at the site of metastasis. The isolation of this step for *in vitro* study has been made possible by the use of artificial basement membranes such as Matrigel. These artificial basement membranes have been used to study the invasive ability of cells and the possible effects of soluble proteins on invasive rates [71]. We have used these assays to investigate the effect of a newly described soluble protein, melanoma inhibitory activity (MIA), which is secreted by melanoma cells based on the invasive ability of these cells [72]. This has also proven useful in demonstrating the potential effect of novel drug targets on the invasive ability of the cell lines [73]. We have previously characterized the ability of vascular endothelial growth factor (VEGF) to induce high rates of invasion in our cell lines [74]. This therefore allowed us to verify differences in the cells that we isolated from each location of the animal model in their invasive ability towards VEGF.

2.1.5 Soluble Factors

Our laboratory has undertaken several investigations into the expression of soluble factors by uveal melanoma cells in culture. These include the study of MIA expression by the five cell lines and correlating this expression with the presence of tumour associated macrophages [72]. Two other studies have also looked into the expression of interleukin 6 (IL6), prostaglandin E2 (PGE2), hepatocyte growth factor (HGF) and VEGF after exposure of the cells to macrophage conditioned medium [75, 76]. These studies have helped to advance our understanding of the interaction of our cells with tumour associated

macrophages, which play an important role in modulating the tumour microenvironment.

2.2 Animal Models

Throughout the history of modern medicine most major advances in treatment and our basic understanding of disease processes have come from the use of animal models of the human disease. In cancer research, animal models are used to develop a better understanding of the disease progression, spread and therapeutic windows. To be useful, these models must accurately reproduce the human disease as well as being reproducible and predictable. Animal models of uveal melanoma should ideally produce a high rate of intraocular tumours in the animals, with these tumours having similar morphology and molecular biology to what is seen in our patients. A good model should also show a high rate of metastatic disease, which should be present after a reasonable period of time.

There are three different forms of animal models for uveal melanoma [77]. The first is the spontaneous occurrence of uveal melanoma, which has only been documented in dogs and cats [78, 79]. These models have limited utility as they occur rarely and their biological behaviour is different than that of the disease in humans. The second is an induced transformation of normal melanocytes in these animals, often done by oncogenic agents, viruses, or even the use of transgenic mice. The third type of model is the direct inoculation of uveal melanoma cells into these animals and is the method that we utilized for our animal model.

2.2.2 Induced Transformation of Melanocytes

Three different methods have been used to induce the transformation of normal melanocytes in host animals for the establishment of an animal model of uveal melanoma. Oncoviruses have been used, including the feline leukemia-sarcoma virus that induced uveal melanoma in kittens [80]. The tumours were detectable 40 days after the exposure in a relatively high percentage of animals (89 percent). This approach has several disadvantages, however, including the death of the animals due to the viral infection, viral contamination and inability to determine if metastases are due to viral infection or tumour cell dissemination.

Several different carcinogenic substances have been used to induce transformation as well. Ethionine was used to give rise to intraocular tumours in rodents, but no metastases were seen [81]. Nickel sulfate was also used to induce intraocular tumours in rats, but tumour development was no seen until six to nine months following exposure [82]. They did see wide spread metastases in these rats following the development of the intraocular tumours.

Transgenic models have recently been used. The tyrosinase promoter was used to target the expression of oncogenes such as the T24 Ha-ras gene in melanocytes [83]. Unfortunately the intraocular tumours that were derived from these strains were found to be benign. In addition, there was significant hyperplasia seen in the skin, inner ear and meningeal membranes of the brain. A more recent model using the deletion of the Ink4a/Arf tumour suppressor locus (exons 2 and 3) and expressing human H-ras controlled by the human tyrosinase promoter was also assessed [84]. They showed the development of intraocular

tumours in only 15 percent of mice after 6 months and no metastases were detected in the mice.

2.2.3 Intraocular Inoculation of Melanoma Cells

In these models, uveal melanoma cells or xenografts are implanted into the eyes of the host animals. These models do not allow for the study of the processes of malignant transformation of the melanocytes. They do give more reproducible results from the induced models as well as better mimicking the progression of the disease in our patients. Cell lines from three different species have been widely used for inoculation in various animal models, Hamster Greene melanoma, B16 mouse melanoma and human uveal melanoma cell lines.

The most widely used cell line to date is the hamster Greene melanoma. This cell line was isolated in 1958 from a skin melanoma in a hamster [85]. These cells were then injected into the eye of the host and led to the formation of aggressive tumours that fill the eye in three to four weeks [86]. This cell line has also been used in rabbits, due to their larger eye size compared to hamsters [87]. The major limitation of these models is the different biological behaviour of these cutaneous hamster melanomas compared to the human ocular disease.

The B16 mouse melanoma cell line has been used in a wide variety of models ever since its isolation in 1954 [88]. These cutaneous melanoma cell lines have been injected into the anterior and posterior compartment of mice [89, 90]. They were found to metastasize to the lung of these animals in the majority of cases. The procedure of inoculating these cells into the eye of the mice is difficult and poses technical difficulties due to the size of the eye.

In recent years a major advance in the development of experimental models has been the use of human derived cell lines. These models have the benefit of using human cells and therefore lead to a model that better mimics the human disease.

The inoculation of human uveal melanoma cells into an immunosuppresed rabbit was first described in 1989. The model has the advantage of using an animal with a relatively large eye size. The rabbit eye is close to the size of the human eye and traditional clinical methods for observing tumour formation, such as ultrasound and fundus exam, can be carried out. The downside is that these animals must be immunosuppresed for the formation of intraocular tumours and metastases to occur. A dosage scheme for the use of cyclosporin A for this immunosuppression has been described, which we follow in our model [91]. The difference between several human uveal melanoma cell lines has been described as well [92, 70]. In our model we studied the progression of the disease through a 10 week progression of the model [93]. The sacrifice of one animal per week allowed the study of the disease progression and attempts to isolate circulating malignant cells throughout the model.

2.3 Genetic Changes in Uveal Melanoma

Unlike retinoblastoma, which is the most common intraocular tumour in children and is linked to mutations in the Rb gene, there has not been a definitive association between a clearly defined genetic mutation and uveal melanoma. Over the past decade, several different groups have attempted to define the potential

genetic changes that may lead to metastases in uveal melanoma patients. These groups have used a wide variety of methods to investigate the transcriptional and genomic changes that the primary tumours undergo, including fluorescent *in situ* hybridization (FISH) and comparative genomic hybridization (CGH). To date, these studies have focused on the primary tumours and have not sought to investigate the changes present in metastases. This may reflect the difficulties in obtaining metastatic samples from patients or the long time period involved before the formation of metastases in patients is seen.

2.3.1 Transcriptional Analysis

Within the last few years' genomics has provided powerful tools with which we can probe the behaviour of complex biological systems. One of these tools is the high-density DNA microarray, which allows for the identification of changes in transcript abundance for thousands of genes and is useful for the classification of complex traits such as tumour development. These cDNA microarrays are microscopic grids composed of sequences of single stranded DNA that are spotted or printed onto a glass slide. These single strands of cDNA are composed of known sequences that are provided in a file to the researcher along with the glass slides. The sample RNA is subsequently converted into cDNA using a reverse transcriptase, during which step it is fluorescently labelled. This fluorescently labelled cDNA is known as a probe and is allowed to hybridize to the single stranded DNA that is attached to the slide. The resulting probes can be imaged with a micro-array scanner using a high precision laser scanning system. The amount of probe at each spot can be therefore quantified as compared

to a competing standard that was labelled with a different colour fluorescent dye. This technology makes it possible to characterize gene expression in both normal and neoplastic tissues.

In cutaneous melanoma transcriptional studies have shown the up regulation of several genes in the progression of cutaneous melanoma, such as cyclin D1, c-Myc, and pleiotrophin [94-96]. This has also allowed for the direct comparison of cutaneous melanoma and benign nevi [97]. This allowed for the identification of several malignant melanoma genes that were up-regulated in comparison to benign nevi of the skin, such as L1 cell adhesion molecule, NTRK3, and PLAB, a novel gene. Other studies have used this technology to examine potential prognostic indicators as well as to identify differentially expressed genes and pathways [98].

Only one other laboratory group has made use of microarrays to investigate the transcriptional differences in uveal melanoma. Studies using transcriptional analysis of primary tumours from a group of 10 UM patients and classified these patients into two groups: Class 1, having low risk of metastasis, and Class 2 tumours, having a high risk for metastatic death [99]. The down regulation of melanoma specific genes and the helix-loop-helix inhibitor *ID2* was discovered in Class 2 tumours along with a corresponding increase in E-cadherin. This group observed a co-localization of E-cadherin and beta catenin to the plasma membrane in these high-risk patients. Interestingly, when they inhibited *ID2* in cultured cell lines they were able to give rise to a more aggressive phenotype, which resulted in the up-regulation of E-cadherin. This increase in E-

cadherin was then found to promote anchorage-independent growth of the cell lines, revealing a possible mechanism necessary for the progression to metastasis [100].

These results, as a whole, may explain a feature of uveal melanoma that has long been apparent to ocular pathologists but not well understood; tumours with epithelioid cell types are more aggressive than those with spindle cell types. The epithelioid cell type is a reflection of the Class 2 type that Harbour *et al* has described. The cells that we investigated in our animal model of uveal melanoma are epithelioid in morphology and we believe that they would fit into the Class 2 type that is described in these previous transcriptional studies. Although this study was able to make prognostic use of their transcriptional analysis, they were unable to compare these changes to any that had occurred in the metastasis of these patients.

2.3.2 Detecting Chromosomal Abnormalities in Uveal Melanoma

It has long been understood that genetic mutations occur in the progression of normal cells to a malignant phenotype. There have been several different techniques utilized for characterizing these changes. Traditional cytogenetic analysis, using chromosomal preparations and banding, having been used from a series of 42 patients with choroidal melanoma [101]. These results showed a concurrent increase in cytogenetic abnormalities as the size of the tumour increased. In addition this laboratory group found rearrangements of chromosomes 6 and 11, deletions of chromosome 3 and loss of the Y chromosome.

Following the use of cytogenetic analysis, fluorescent *in situ* hybridization (FISH) was used to detect chromosomal changes in fine needle aspiration biopsies (FNABs) from 40 patients with uveal melanoma [102]. This was the first study to introduce the use of FNABs for the detection of genetic changes in the tumour and compared these changes to larger tumour samples from the same patient. They found a strong correlation between the two and concluded that the use of FNABs for detecting chromosomal changes using FISH was a useful technique. The majority of analysis of uveal melanoma tissue for chromosomal abnormalities has been done using FISH [103, 104]. In this method, specific probes for chromosomes 3 and 8 are routinely utilized, covering a variety of regions in the p and q arms from both chromosomes. These regions are typically quite large, spanning the majority of the chromosome arm.

Spectral karyotyping (SKY) has also been used, although the bulk of these studies have focused on UM cell cultures [105, 106]. This allows for the painting of the entire chromosome with specific probes of different colours. This enables the researcher to overcome the specific probes that are necessary when using FISH and allowing for the identification of chromosomal changes for all chromosomes, although at a relatively low resolution.

In the past several years comparative genomic hybridization (CGH) has been used to analyze chromosomal changes with a higher resolution than either of these previous methods have allowed. There are several different types of CGH that can be used. Traditional CGH has used fluorescently labelled tumour DNA, frequently labelled with FITC, and hybridized with normal DNA fluorescently

labelled with a different dye, frequently rhodamine or texas red. Areas of deletion or of amplification has occurred can be seen using an epiflourescent microscope. This has evolved into the use of CGH microarrays where normal DNA is spotted onto glass slides and the genomic DNA isolated from the sample of interest is fluorescently labelled and hybridized to the normal DNA. This is subsequently analyzed like transcriptional microarrays using a scanner with a high-resolution laser.

Initial arrays were printed using bacterial artificial chromosome (BAC) clones. These arrays were printed by the researcher facility and customized by the individual researcher. The average spacing of the probes usually was in the 1 Mb range, yielding an improved resolution as compared to FISH or even SKY [107]. Subsequently, a new generation of CGH arrays has evolved with an increase in resolution down to 70 kb [108]. These CGH arrays use a high density commercialized probe printing method with an average density of 44,000 up to 244,000 probes across the genome. These allow for the detection of small deleted or amplified genomic regions that were previously impossible to detect.

2.3.3 Chromosomal Abnormalities in Uveal Melanoma

The most common chromosomal abnormalities that have been detected in uveal melanoma tumours are in chromosomes 1, 3, 6 and 8. Of these, monosomy 3 has the strongest correlation with poor prognosis and was described as an early event in both ciliary and choroidal melanomas [109, 110]. This abnormality has been described in as many as 50 percent of uveal melanoma cases [101]. However, new evidence using CGH found no correlation between monosomy 3

and patient survival, thus rendering the prognostic significance of monosomy 3 in uveal melanoma patients controversial [111]. White *et. al* have also suggested that small rearrangements of chromosome 3 may be more frequent than loss of the entire chromosome [105]. These rearrangements may take the form of small deletions or translocations that are unable to be detected by traditional fluorescence *in situ* hybridization or even comparative genomic hybridization.

In 50–60 percent of uveal melanoma cases, trisomy 8 was identified and coincided with monosomy 3 in approximately half of the cases [101]. Monosomy 3 and gain of chromosome 8 correlated with a ciliary body location [102], epithelioid phenotype [112] and decreased survival [113, 114]. Using comparative genomic hybridization, it has been shown that gains of 8q strongly correlated with the expression of DDEF1 and that the over expression of this gene made low grade uveal melanomas more aggressive by increasing their motility [115].

Losses of 6q and gains of 6p were also identified in approximately 40 percent of uveal melanomas and appeared to be associated with a better prognosis [101, 114]. Deletions or rearrangement of 1p were observed in 25–30 percent of posterior uveal melanomas and these changes were only found in primary uveal melanomas that had metastasized [116]. Recently, using a 24 colour multiplex fluorescence *in situ* hybridization (M-FISH) method, spindle melanomas were found to have rearrangements affecting chromosomes 6, 15 and 18, which may relate to early changes in uveal melanoma development or associate with those melanomas of a more differentiated status [117]. The same study that questioned the correlation between monosomy 3 and prognosis identified an amplification of

chromosome 18 in band q11.2 as an alternative and powerful predictor of poor prognosis. Microarray techniques, CGH arrays, and spectral karyotyping have shown abnormalities in 7q, 9p and 13q [118], although the significance of these changes has yet to be fully characterized.

To date, no study has made use of the latest generation of CGH arrays to investigate possible small deletions or amplifications that may be present in these tumours. These CGH arrays have only recently become available for use and have an average resolution approaching 75 kb [108]. The ability to extract genomic DNA from paraffin embedded tissue has only been demonstrated in a handful of studies [119-121]. To the best of our knowledge, none of these techniques for extracting genomic DNA from archival material has been used before for these CGH arrays.

Chapter 3

MATERIALS AND METHODS

3.1 Ethical and Biohazard Approval

Animal experimentation was carried out in compliance with the Association of Research in Vision and Ophthalmology Resolution on the use of Animals in Ophthalmic and Visual Research according to the declaration of Helsinki. The approval of both the Animal Care Committee and the Ethics Subcommittee at McGill University, was obtained before any experiments were carried out (Appendix).

Approval for using Biohazardous materials was granted for culturing the human uveal melanoma cell lines by the University Biohazard Committee (Appendix). University health and safety compliance was ensured throughout the culturing of these cell lines and in the proper disposal of all waste products throughout the experiments.

3.2 Human Uveal Melanoma Cell Culture

Five human uveal melanoma cell lines were utilized; 92.1, SP6.5, MKT-BR, OCM-1 and UW-1 had been established by Dr. Jager (University Hospital Leiden, The Netherlands), Dr. Pelletier (Laval University, Quebec, Canada), Dr. Belkhou (CJF INSERM, France) and Dr. Albert (University of Wisconsin-Madison, USA) [122, 123]. We received the five human uveal melanoma cell lines from Dr. Antonia Saornil of the Institute of Ophthalmology and Visual Sciences (IOBA) of the University of Valladolid Spain, in 2001 (Appendix).

The five previously characterized human uveal melanoma cell lines (92.1, SP6.5, MKT-BR, OCM-1, UW-1) were incubated at 37°C in a humidified 5 percent CO_2-enriched atmosphere [16, 70]. The cells were cultured in RPMI-1640 medium (500 ml) (Invitrogen Life Technologies, Burlington, Ontario, Canada), supplemented with 5 percent by volume heat inactivated fetal bovine serum (FBS; Invitrogen), 1250 μg of fungizone (Invitrogen), and 50,000 units of penicillin-streptomycin (Invitrogen). Cells were cultured as a monolayer in 25 cm^2 flasks (Fisher, Whitby, Ontario, Canada) and observed twice weekly, at every media change, for normal growth by phase contrast microscopy. The cultures were grown to confluence and passaged by treatment with 0.05 percent trypsin in EDTA (Fisher) at 37°C and washed in 7 ml RPMI-1640 media before being centrifuged at 120 g for 10 minutes to form a pellet. Total RNA was then extracted from each cell line and re-cultured cells, following the manufacturer's protocol (Qiagen, RNeasy). Four separate total RNA samples were extracted from each cell line.

3.3 Uveal Melanoma Animal Model

3.3.1 Animals

Twenty-eight male New Zealand albino rabbits (Charles River Canada, St-Constant, Quebec, Canada) with a mean initial weight of 3.3 ± 0.2 kg (range: 2.9-3.6 kg) were used in this study. The animals were allowed to acclimatize for one week after arrival at the facility before the beginning of the experiments. They were kept in individual steel cages in the animal facility at the Lyman Duff building and routinely checked by animal care technicians for overall health.

Male rabbits were used to eliminate any chance of changes due to hormonal fluctuations in the female rabbits. Albino rabbits have been chosen because the ocular examination in these animals is more accurate than that in pigmented rabbits due to the lack of pigment in the eye. Animals with an initial weight of 3 kg or greater were chosen to better resist the toxic side effects of cyclosporin-A (CsA).

3.3.2 Immunosuppression with Cyclosporin-A

The animals were immunosupressed using daily intramuscular injections of cyclosporin A (CsA; Sandimmune 50 mg/ml, Novartis Pharmaceuticals Canada Inc., Dorval, Quebec, Canada) in order to avoid rejection of the human cells. CsA administration was maintained throughout the 10-week experiment to prevent spontaneous tumour regression. The dosage schedule recommended in previous studies was employed: 15mg/kg/day, three days before cell inoculation and during the following four weeks, followed by a decrease to 10mg/kg/day during the last six weeks of the experiment [91]. CsA doses were adjusted weekly according to the animal weight to compensate for decreased animal weight and possible toxicity.

3.3.3 Surgical Procedure

The surgical procedure was carried out under aseptic conditions. The right eye of each rabbit was dilated 10 minutes for ophthalmoscopic examination before the operation using drops of phenylephrine hydrochloride (Mydfrin, Alcon Canada Inc., Mississauga, Canada) and tropicamide (Mydriacyl, Alcon Canada Inc.). A fundoscopic examination, using an indirect binocular ophthalmoscope,

was performed on each rabbit to rule out any pre-existing ocular pathology. Ocular anesthetic (Proparacaine Hydrochloride; Alcaine, Alcon Canada Inc.) was applied topically in the right eye of the animal one-minute before the surgery. Ketamine (35mg/kg; Vetalar, Vetrepharm Canada Inc., Belleville, Ontario, Canada) and xylazine (5mg/kg; Anased, Novopharm Limited, Toronto, Ontario, Canada) were used as general anaesthetics during the surgical procedure.

The injection of the cells was performed according to a previously described technique [91]. Briefly, an incision of 2-3 mm was made in the temporal superior sclera (sclerotomy) up to the suprachoroidal space, which is recognized by a brown colour, using an ophthalmic surgical blade. If a vitrectomy (perforation of the vitreous cavity) had occurred, the animal would not have been used for the experiment. A paracentesis of the anterior chamber of the eye (removal of aqueous humor) was performed using an insulin-like syringe (Becton Dickinson) to release intraocular pressure. The extracted volume was approximately 0.2 ml. A tunelizer was used to make a tunnel in the suprachoroidal space by the incision already made. One end of the incision was sewed forming a U. An insulin-like syringe with the cannula loaded with one million cells (cellular viability greater than 98 percent) suspended in 0.1 ml of RPMI-1640 media was introduced into the tunnel and the cells were injected. The suture was knotted when the cannula was extracted.

Post-operative fundoscopy was performed to rule out any immediate complications. Antibiotic ointment (BNP, Vetcom Inc., Upton, Quebec, Canada) was then applied to the eye. In the first two days after surgery, the analgesic

buprenorphine (0.02 mg/Kg; Temgesic, Schering-Plough, Pointe Claire, Quebec, Canada) was administered when determined necessary by the animal care technician and veterinarian.

3.3.4 Weekly Follow-Up

The animal care technician and veterinarian from the animal facility assessed overall animal health weekly. During the 10-week experiment the doses of CsA were adjusted weekly based on animal weights. Signs of CsA toxicity that have previously been described were noted if seen, including weight loss, hyper salivation and diarrhoea.

Indirect ophthalmoscopy of the rabbit fundus was carried out each week using Mydfrin to dilate the pupils. This fundoscopy was carried out to document the growth of the intraocular tumours throughout the 10 weeks. Photographs of the fundus were also taken during the length of the experiment using a digital camera (Kodak DCS 620; Kodak Canada Inc., Toronto, Ontario, Canada) mounted on a fundus camera (Zeiss FF450 Plus; Carl Zeiss Canada Ltd., Ontario, Canada).

3.3.5 Ultrasound Examination

Ultrasound examination using a 10-MHz B-Scan and standardized A-scan (I^3 System-ABD; Innovative Imaging Inc., Sacramento, CA) was performed for the 15 animals remaining at the last week of the experiment. This allowed us to determine the echographic characteristics, location and final dimensions of the tumours in each animal.

3.3.6 Euthanasia

Beginning one week after the inoculation of cells into the eyes of the animals, one animal per week was sacrificed. This allowed for the documentation of the disease progression during the 10-week experiment. The selection of the rabbit for sacrifice was based on signs of CsA toxicity and was made with consultation of the veterinarian. The remaining rabbits were sacrificed at the end of the experiment. The method of euthanasia was exsanguinations and anaesthetic overdose following general anesthesia using an intramuscular combination of ketamine and xylazine (35 mg/kg-5 mg/kg). Cardiac punctures were performed while the animals were ansethetized using a Vacutainer (BD Biosciences, etc) containing EDTA to prevent coagulation.

3.3.7 Blood Sample Processing

We attempted to culture circulating malignant cells (CMCs) from the blood obtained at the time of sacrifice. Mononuclear layers extracted from the blood of the rabbits at the time of sacrifice were isolated using the Ficoll-Paque Plus method (Amersham Biosciences, Quebec, Canada) as previously described [124]. Ficoll-Paque Plus is a density-gradient procedure used to separate the different blood cell types into layers. Two millilitres of fresh rabbit blood was diluted in 2 ml of PBS and mixed. The diluted blood sample (4 ml) was carefully layered on top of 3 ml of Ficoll-Paque solution in a 15 ml centrifuge tube and centrifuged at 400 g for 30-35 minutes at 18-22°C. The upper layer of plasma was removed using a Pasteur pipette and stored at -20°C for future studies. The mononuclear layer containing the malignant cells was transferred, using a Pasteur pipette, to a sterile tube and centrifuged at 120 g for 10 minutes. The supernatant

was removed and the resulting pellet was re-suspended in 2 ml of 10 percent FBS supplemented RPMI-1640 media.

Cells were then seeded into a six well plate (Becton Dickinson) and placed in a 5 percent-supplemented CO_2, 37°C incubator under normal culture conditions. After three days of incubation the media was changed and all non-adherent cells were washed off. Cells were grown to confluence and subcultured. Each culture was immediately frozen in liquid nitrogen as soon as a sizeable colony had formed in the well.

3.3.8 Isolation of Tissue and Cells

Following autopsy of the sacrificed animals, samples were immediately taken from the intraocular tumour and any macroscopically observed metastases. A pathologist was present to examine the organs and identify tumours and metastases. Intraocular tumour samples were taken after a pupil to optic nerve section was performed. Lung metastases were dissected using scalpels to remove as much tissue as possible from the metastatic nodules.

Pieces of both intraocular tumours and metastases were snap frozen in liquid nitrogen at the time of autopsy. At the same time, cells were isolated for re-culturing. Collected samples for re-culturing were homogenized using 0.05 percent trypsin in EDTA (Fisher Scientific Limited) at 37° C for 10 minutes, washed and re-suspended in fresh culture media. Cells were then seeded into 6 well plates (Becton Dickinson) and placed in a 5 percent-supplemented CO_2, 37°C incubator. After three days of incubation the media was changed. Cells were

grown to confluence and subcultured. A portion of each culture was frozen in liquid nitrogen as soon as sizeable colonies had formed.

3.3.9 Histopathological Studies

Formalin-fixed, paraffin-embedded sections of the collected specimens including eyes, lungs, livers and kidneys, were Hematoxylin and Eosin (H&E) stained for histopathologic assessment. The enucleated eyes were microscopically examined to determine tumour presence and morphology. A study of intraocular tumour progression was performed throughout the 10-week experiment. The lungs, livers and kidneys were inspected for the presence and form of presentation of metastatic disease. Other general histopathological findings were also recorded.

Uveal melanoma histopathological prognostic factors were evaluated in the intraocular tumours, weekly during the course of the experiment and in 10 animals at the end of the experiment. The prognostic factors evaluated included cell type, tumour size, tumour infiltrating lymphocytes (TIL), vascular loops, mitotic rate, cytomorphometry (mean of the 10 largest nucleoli) and extraocular extension.

3.3.10 Immunohistochemistry

Immunohistochemistry using the HMB-45 monoclonal antibody (mAb) (DakoCytomation, Mississauga, Ontario, Canada) was performed to verify the presence of melanoma cells in all tumours and suspected metastases. Immunohistochemistry was performed according to the streptavidin-biotin complex method as previously described [49].

Tissue sections of 5 μm thick were deparaffinized with xylene and rehydrated in graded ethanol series. The sections were washed for 10 minutes with 3 percent hydrogen peroxide and methanol to block the activity of the endogenous peroxidase. Microwave citrate treatment (citrate buffer pH 6.0) was used as the heat antigen retrieval technique. In order to block non-specific binding of the antibodies, the slides were washed for 30 minutes in one percent bovine serum albumin (BSA) and tris buffered saline (TBS; pH 7.6). The sections were incubated for 1 hour at 37°C with the mouse mAb against HMB-45 (dilution 1:50) in a humidity chamber. On negative control sections, non-immune serum (0.1 percent BSA/TBS) was applied instead of the primary antibody. The sections were then incubated with the biotinylated rabbit anti-mouse secondary antibody (dilution 1:500; DakoCytomation) for 30 minutes at 37°C. Subsequently, horseradish peroxidase conjugated streptavidin-biotin complex (DakoCytomation) was applied to the sections and they were incubated for 30 minutes at 37°C. The visualization of the antibody-antigen reaction was achieved by using 3-amino-9-ethylcarbazole (AEC) chromogen (DakoCytomation). The sections were then counterstained with hematoxylin, mounted with an aqueous mounting medium (Faramount, DakoCytomation) and cover slipped.

3.4 Transcriptional Profiling Studies

3.4.1 Total RNA Extraction

Following the confirmation of intraocular and metastatic nodules by immunohistochemical staining, when possible paired tissue samples were used from five different animals. Samples of the 92.1 human uveal melanoma cell line

that were used to inject into the eyes of the rabbits were thawed at the same time. Re-cultured cells isolated from the intraocular tumour, circulation and metastasis were grown as well.

Total RNA was then extracted from the tissue and cell samples using the Qiagen RNeasy kit as per the manufacturer's recommendations. Briefly, tissue was disrupted and homogenized using the included lysate buffer and ground with a mortar and pestle. The lysate was then centrifuged to remove any insoluble material. One volume of 70 percent ethanol was added to the lysate and mixed, before the solution was added to the included Rneasy mini column. Following centrifugation, the columns were then washed twice using the included buffer solutions. Total RNA was then eluted using RNase free water.

3.4.2 Total RNA Quantity and Quality

The quality of the extracted total RNA was verified using a 2100 Bioanalyzer (Agilent, Foster City, CA) with the 6000 RNA LabChip kit (Agilent) as per the company recommendations. The LabChip is designed for the analysis of total RNA and messenger RNA from either eukaryotic or prokaryotic samples. A gel-dye mix is prepared using 130 µl of RNA gel matrix with 2 µl of RNA dye. The combined RNA gel matrix and RNA dye are loaded into the LabChip using a proprietary Chip Priming Station (Agilent) using a syringe. Five microliters RNA 6000 nano marker was added to a control well and 1 µl of RNA 6000 ladder was added to the ladder well. The RNA samples were then diluted to approximately 200 – 500 ng/µl with DEPC H_2O and 1 µl of sample was pippetted into the

sample wells. The chips are vortexed for one minute at 2400 RPM. Samples were read using the 2100 Bioanalyzer.

The quantity of the extracted total RNA was measured using a fluorescent plate reader and ribogreen dye (Molecular Probes, Eugene, OR, USA) as well as traditional ultraviolet spectrophotometry ratios of 260/280 nm (Biochrom, Ultraspec 2000).

RiboGreen labelled the total RNA and fluoresced under excitation by a 500nm wavelength source, with an emission of 520nm. Ribosomal RNA standard (Molecular Probes) was used as a known control, containing 100 μg of 16S and 23S RNA isolated from *E. Coli.*

3.4.3 Universal Human Reference RNA

Universal human reference RNA (Strategene) was used for comparison on the microarrays for all cell lines, tumour samples and re-cultured cells. This human reference RNA contained total RNA extracted from 10 different established human cancer cell lines at a known concentration of 200 micro grams per tube with guaranteed quality and lack of degradation. Quality was assessed by observing distinct 28S and 18S ribosomal bands on an agarose gel under denaturing conditions. These 10 cell lines are:

1) Adenocarcinoma, mammary gland
2) Hepatoblastoma, liver
3) Adenocarcinoma, cervix
4) Embryonal carcinoma, testis
5) Gliobastoma, brain

6) Melanoma, skin

7) Liposarcoma

8) Histiocytic lymphoma, macrophage, histocyte

9) Lymphoblastic leukemia, T lymphoblast

10) Plasmacytoma, Myeloma, B lymphocyte

The same lot number of universal reference RNA was purchased to be used for all microarray experiments.

3.4.4 cDNA Preparation and Labelling

A master mix was prepared on ice containing 8 ul of 5X first strand buffer (InVitrogen), 1.5 µl of AncT mRNA primers, 3 µl of 20 mM nucleotide mix (d-ATP, d-TTP, d-GTP), 1 µl of 2 mM d-CTP (InVitrogen), and 4 µl of 0.1 M DTT (InVitrogen). We then added 10 µg of our sample or reference total RNA to the master mix which was then incubated at 70°C for 10 minutes, followed by an incubation on ice for two minutes. Following these incubations 2 µl of 1mM Cy3 labelled dCTP or 1 µl of 1 mM Cy5 labelled dCTP (Perkin-Elmer) were added to the samples. The mixture was then heated to 42°C and 2 µl of Superscript II reverse transcriptase was added to each sample and incubated for three hours, with an additional 1 µl of enzyme added halfway through the incubation period.

The resulting cDNA probes were purified using a QIAquick spin column (Qiagen) as per manufacturers recommendations. Two hundred microliters of buffer with 2.7 µl of 3M NaAc at pH 5.3 was added to the columns. The flow through was then discarded and 750 µl of PE buffer was used to wash the column

five times. The cDNA probes were then eluted from the column using 30 µl of DNase free H_2O pre-heated to 37°C.

The volume of the probes was then reduced using a SpeedVac centrifuge until approximately 5 µl remained. The sample and reference probe sets were then combined with 90 µl of hybridization buffer containing 20 µl yeast total RNA (10mg/ml), 20 µl salmon sperm DNA (10mg/ml), and 400 µl Dig Easy Hyb (Roche Diagnostics) and heated to 95°C for three minutes.

The mixture was then placed onto the microarray chips, which contained 19,008 characterized and uncharacterized expressed sequence tags (ESTs) produced by the University Health Network (http://www.microarrays.ca/). Probes were allowed to hybridize overnight at 37°C in a humidified incubator.

The following morning the chips were washed three times in a solution of 0.1 percent SSC and 0.1 percent SDS at 50°C in a slide dish with a magnetized stirring bar for 10 minutes, followed by four washes in a solution of 0.1 percent SSC at room temperature for three minutes. The chips were then dried in a centrifuge at 700RPM for five minutes. Fluorescence was measured on a ScanArray lite microarray scanner and quantitated with ScanArray software (Perkin-Elmer).

Four microarrays were used for each cell line and re-cultured tumour sample, with two of these used for dye swap. Two microarray hybridizations, including dye swaps, were conducted for each tumour or metastatic tissue sample. Studies involving re-cultured cell lines were performed with four-microarray hybridization that were conducted on four independently-produced cell lines. Two

were labelled with Cyanine 3 (Cy3) and the other two with Cyanine 5 (Cy5) and compared to reciprocally labelled Universal RNA.

3.4.5 Data Normalization and Statistical Analysis

All of the data normalization and analysis were performed in GeneSpring version 7.4 (Agilent Technologies). For the normalization, a Lowess curve was fitted to the log-intensity versus log-ratio plot and 20 percent of the data was used to calculate the Lowess fit at each point. To identify genes with statistically significant changes in transcript abundance between two conditions, we used Welch t-test with a Benjamin and Hochberg False Discovery Rate. Significant genes had an FDR of less than 0.05. We also compared these results with gene lists obtained with the non-parametric Wilcoxon-Mann-Whitney test. Because the number of replicates was too low for the application of multiple testing correction, we reduced the significant p-value threshold to less than 0.002. The application of parametric or non-parametric methods did not change our conclusions and all of the validated genes were selected by both methods.

3.5 Gene Validation

3.5.1 Quantitative Real Time Polymerase Chain Reaction

Quantitative real-time PCR was performed using a Quantitect one step SYBR Green PCR kit (Qiagen) as per the manufacturer's instructions. A Chromo4 thermocycler (MJ Research) was used for all experiments and all results were analyzed using the included GeneEx software. SYBR Green fluoresces when bound to double stranded DNA, thus, allowing for quantification of different

targets, based on the primers used, without the need for sequence-specific fluorescent probes. SYBR Green has an excitation wavelength of 494 nm and an emission maximum of 521 nm. The Chromo4 thermocycler includes an optional light shuttle that passes over each well, exciting the bound SYBR Green and measuring the emission.

Six genes identified during microarray analysis (APK-3, ATF4, Fibronectin 1, Insulin Receptor Substrate-2, Melan-A, and Septin 7) were chosen for verification of their mRNA expression levels. Beta actin was used as a housekeeper gene for purposes of normalization. QuantiTect primer assay pairs (Qiagen) were designed and used for each gene product of interest. The assay was performed in triplicate for each gene of interest.

Total RNA from the cell lines was isolated as described above. The same RNA from the intraocular and metastases samples were used as those used in the microarray analysis due to lack of material.

From this previously quantified total RNA, 10 μg of RNA was taken for each well of the real time PCR plate (iCycler iQ, Bio-Rad, Hercules, CA). A Quantitect RT Mix containing Oniscript Reverse Transcriptase and Sensiscript Reverse Transcriptase (RT) was used. Omniscript RT is optimized for use with RNA amounts of greater than 50 ng, while Sensiscript RT is optimized for small amounts of RNA, less than 50 ng. A master mix containing HotStarTaq DNA Polymerase, buffer, SYBR Green and dNTP mix was then added to each well. The included RT-PCR buffer was composed of 5 mM $MgCl_2$, Tris, KCl,

$(NH_4)_2SO_4$, and balanced to pH 8.7. The dNTP mix contained dATP, dCTP, dGTP, and dTTP at ultrapure quality.

A total of 12.5 µl of the master mix was added to each well, along with 2.5 µl of the primer pairs and 0.25 µl of the RT mix. The total volume available in each well was 25 µl, leaving 9.75 µl available for our samples. RNase free water was used to fill any remaining amount that was left after the addition of the sample RNA. The wells were then capped using PCR tube strips (Flat Cap Strips, Bio-Rad). The plates were then briefly centrifuged at 900 g to settle all liquid to the bottom of the wells in preparation for the thermal cycler.

Reverse transcription was carried out for 30 minutes at 50°C. The polymerase is inactive at room temperature, but is activated by a 15 minute 95°C incubation step following the reverse transcription. This step also inactivates the reverse transcriptase. A three step cycle was then used with denaturation for 15 seconds at 94°C, annealing for 30 seconds at 55°C, and extension for 30 seconds at 72°C. Following this step the Chromo4 thermocycler scanned the wells for fluorescence data collection. This three-step cycle was repeated for a total of 35 cycles.

At the end of these 35 cycles a melting curve was performed for the real time PCR products. To carry out this analysis the temperature in the wells was slowly increased from 65°C to 95°C with a fluorescence read following every 1°C increase.

3.5.2 Proliferation Assay

To validate the change in expression of ribosomal proteins that was seen from cells isolated from different locations, a proliferation assay was carried out as previously described [69, 65]. The Sulforhodamine-B based assay kit (TOX-6, Sigma-Aldrich, St. Louis, Missouri, USA) was performed as per the National Cancer Institute protocol. The re-cultured cells isolated from the intraocular tumour, CMCs and metastases were seeded into wells at a concentration of $2.5x10^3$ cells per well, in a minimum of six wells per cell line. A row of eight wells containing only RPMI-1640 medium was used as a control. Cells were allowed to incubate for 48 and 72 hours following cell seeding. Following these time periods, the cells were fixed to the bottom of the wells using a solution of 50 percent Trichloroacetic acid (TCA) for one hour at 4°C. Plates from each time point were then rinsed with distilled water, to remove TCA and medium, and air dried. The Sulforhodamine-B dye solution was then added to each well and allowed to stain for 25 minutes. The Sulforhodamine-B solution was subsequently removed by washing with a 10 percent acetic acid solution and once more allowed to air dry. The dye that had become incorporated into the fixed cells at the bottom of the wells was solubilized in a 10 mM solution of Tris. The absorbance of the solute was then measured using a microplate reader at a wavelength of 510 nm.

3.5.3 Invasion Assay

To examine potential changes in response to chemoattractants, a matrigel invasion assay was carried out using the same re-cultured cells as those for the proliferation assay. We selected a previously described chemoattractant (VEGF

with 10 percent FBS), which was found to induce invasive ability in the original 92.1 cell line.

A modified Boyden chamber consisting of polyethelene teraphthalate membrane (PET) with 8-um diameter pores precoated with Matrigel, an artificial basement membrane, (Beckton Dickenson Labware, Bedford, MA, USA) was used as previously described to assay for invasive ability [71]. A PET membrane without Matrigel was used as a control. Recombinant human VEGF (R&D Systems Inc, Minneapolis, Minnesota, USA) was used as a chemoattractant.

Briefly, $1.25x10^5$ re-cultured cells were added to the upper chamber in RPMI-1640 medium with 0.1 percent FBS. RPMI-1640 medium with 10 percent FBS was added to the lower chamber as a chemoattractant to obtain the baseline invasive ability of the cell lines. The effect of VEGF was assayed by adding 20 ng/ml to the RPMI-1640 10 percent FBS medium in the lower chamber. The chambers were then incubated at 37°C in 5 percent CO_2-enriched atmosphere for 48 and 72 hours to allow for cellular invasion through the Matrigel.

Non-invading cells were removed from the upper chamber by gently wiping the surface of the membrane with a moist cotton swab. Membranes were removed and then stained using a Diff-Quick staining set, which stains cell nuclei purple and cytoplasm pink. Stained cells were counted microscopically in 20 high-powered (x400) fields. Only cells whose nuclei had completely invaded through the membrane were counted. Each experimental condition, including control, was performed in triplicate and the average number of invading cells was then calculated for all experimental conditions. The mean number of invading

cells was then determined and the re-cultured cells were compared to the original 92.1 cell line using the Student's T test.

3.5.4 Fibronectin Adhesion Studies

The ability of the five human uveal melanoma cell lines as well as the re-cultured cells isolated from the intraocular tumour, CMCs and metastases to bind to fibronectin was tested. The human fibronectin matrix strips were purchased from Chemicon International (Temecula, California, USA). The fibronectin strips were hydrated with PBS, immediately preceding the experiment.

The cells were harvested with 0.05 percent trypsin in EDTA (Fisher, Whitby, Canada), which was subsequently inactivated in 7 ml RPMI-1640 medium with 5 percent FBS. The cells were centrifuged at 120 *g* for 10 minutes to form a pellet and re-suspended in 1 ml RPMI-1640 medium. Each of the re-cultured cells was seeded at a concentration of 5 x 10^5 cells/ ml in nine fibronectin-coated wells and in three negative control wells coated with BSA. The wells were incubated for one hour. Then they were washed with PBS and the remaining cells adhering to the fibronectin were stained with 100 ul 0.2 percent crystal violet in 10 percent ethanol. The stain was removed and the wells were again washed with PBS. Finally, 100 ul of solubilization buffer (50 percent NaH_2PO4, pH 4.5 and 50 percent ethanol) was added into each well. The absorbance was determined at 540nm with a microplate reader (Bio-Tek, Vermont, USA). The results were averaged for the different cell lines and re-cultured cells, and differences between the ability of the cell lines to adhere to fibronectin were determined using the Student's T test.

3.6 Genomic DNA Extraction from Paraffin Embedded Tissue

3.6.1 Paraffin Embedded Sections

Formalin fixed paraffin embedded, specimens from the immunosuppressed rabbit model of uveal melanoma were used for this study. The tumours were selected based on the size of the embedded material available for extraction. Three intraocular tumours were used for all studies, each one from an animal that was sacrificed for the last week of the animal model (Rabbits: 21, 26, 28).

Ten micron serial sections were made using a microtome (Finesse 325, ThermoShandon) and placed on Superfrost Plus (Fisher Scientific) glass microscope slides. Sections were made prior to each of the DNA extraction techniques from the same intraocular tumours that were used during the transcriptional analysis.

3.6.2 Laser Capture Microdisection

Ten micron sections of the intraocular tumours were stained with a modified hematoxylin and eosin stain for visualization of the sections during laser capture microdisection (LCM). Sections were stained immediately prior to tissue isolation using LCM. Slides were deparaffinized using two xylene baths for five minutes each followed by a wash in 100 percent, 95 percent and then 70 percent ethanol and distilled H_2O. A final wash in pure distilled H_2O was then done to remove any remaining ethanol or xylene. The sections were then stained for one minute in Mayer's hematoxylin followed by a wash in distilled H_2O. A bluing reagent was then used for 30 seconds followed by a 70 percent and 95 percent

ethanol wash. The sections were then stained with Eosin for one minute followed by 95 percent and 100 percent ethanol washes with a final xylene wash for one minute. Slides were then air dried to remove any traces of xylene prior to LCM.

An Acturus Pixcell II LCM was used (Arcturus, Mountain View, CA) for this extraction. Stained slides were used immediately after staining to diminish DNA degradation. Slides were placed onto the stage of the Pixcell II and imaged prior to LCM. In the LCM holder a CapSure Macro LCM cap was placed. The cap contained a heat sensitive polymer, which became activated when the laser was used, melting the polymer to adhere to the cells of interest. These cells are then removed with the cap. Our tumour cells were imaged and then roughly 800 cells per slide were melted onto the polymer cap. These caps were then imaged after removal from the slide to ensure the adherence of the cells of interest.

The DNA was then extracted from the captured cells using the Pico Pure DNA Extraction Kit (Arcturus) as per the manufacturers recommendations. The caps were inserted into the top of a Eppendorf tube containing 50 µl of digestion buffer (0.04 percent Proteinase K, 10 mM Tris-HCl, pH 8.0, 1mM EDTA, 1 percent Tween-20). The tubes were placed upside down in an oven and incubated overnight at 65°C. Proteinase K was then inactivated by heating the tubes to 95°C for 10 minutes and then cooled on ice prior to storage for use.

3.6.3 Pin Point Slide DNA Isolation System

The Pin Point slide DNA isolation system was also tested for its ability to extract genomic DNA from paraffin embedded sections (Zymo Research, Orange, CA). Unstained paraffin embedded slides were sectioned as described above. A

proprietary Pin Point isolation gel (Zymo Research) was spread across the area of the slide containing the intraocular tumours after microscope verification of the tumour area. The solution was allowed to dry over the tumour area at room temperature for 30 minutes. The embedded tumour section was then removed from the slide using a scalpel to circumscribe the tumour and gently lift the film containing the piece of tumour. The gel and tumour mixture was then placed into an Eppendorf tube and centrifuged to bring the fragment to the bottom. Fifty microliters of extraction buffer containing 5 µl of Proteinase K was added to the tube and mixed. The tubes were then incubated at 55°C for four hours. Proteinase K was then inactivated by heating the tubes to 95°C for 10 minutes and then cooled on ice.

The extracted DNA was then purified using the included Zymo-Spin Column (Zymo Research). The DNA solution was loaded onto the column along with 100 µl of DNA binding buffer. The column was then centrifuged for ten seconds at 16,000 g and the flow through discarded. The column was washed twice with the included wash buffer before being transferred to a new centrifuge tube. The DNA was then eluted using 10 µl of ultrapure H_2O and stored for future analysis.

3.6.4 Macroscopic Tumour Isolation and DNA Extraction

The third method tested for extracting genomic DNA was placing the unstained slide under a stereo-microscope to see the intraocular tumours. A disposable scalpel blade was then used to scrape the paraffin embedded tissue off the microscope slide and directly into an Eppendorf tube. To obtain sufficient

material, tumour cells were removed from two serial sections using this method. Genomic DNA was then extracted from this isolated material using a Genomic DNA Purification Kit (Gentra, Minnesota) with a modified manufacturer's protocol. To each Eppendorf tube 100 µl of xylene was added and incubated for five minutes with constant shaking before being centrifuged at 13,000 g for two minutes. The supernatant was then discarded and the pellet washed with 100 percent ethanol for five minutes with constant mixing before being centrifuged at 13,000 g for two minutes. This washing procedure was repeated for a total of two washes in 100 percent ethanol.

The remaining deparaffinized cells were then lysed with the addition of 200 µl of lysis solution and homogenized using a microfuge tube and pestle. The lysate was then incubated at 65°C overnight after the addition of 1 µl of proteinase K solution (20 mg/ml). RNase A, 1 µl of 4 mg/ml solution, was added to the cell lysate following the overnight incubation and the mixture was then incubated again for one hour at 37°C.

The sample was then cooled to room temperature and 33 µl of protein precipitation solution was added. The solution was vortexed vigorously for 20 seconds and then incubated on ice for five minutes. The mixture was then centrifuged at 13,000 g for three minutes to form a pellet of protein precipitate. The supernatant was removed and placed into a clean 1.5 ml eppendorf tube.

This supernatant was then mixed with 200 µl of 100 percent isopropanol and 4 µl of Glycogen solution (5 mg/ml). This was mixed vigorously and centrifuged at 13,000 g for five minutes. The DNA in solution then formed a

pellet and the supernatant was poured off. The DNA pellet was allowed to dry before being washed with 200 µl of 70 percent ethanol and centrifuged again at 13,000 g for one minute. The ethanol was carefully poured out of the tube and the DNA pellet allowed to dry for 10 minutes at room temperature.

This genomic DNA was then hydrated with 25 µl of DNA Hydration Solution (Gentra) and incubated at 65°C for one hour. The DNA was then stored for later use.

3.6.5 Genomic DNA Quantification and Validation

The DNA extracted from each of the three methods was verified using a variety of different techniques to check for purity, concentration and degradation. The ultraviolet spectrophotometry ratios (Biochrom, Ultraspec 2000) were checked for each sample. Following this, each sample was then run on an agarose DNA gel to check for the presence of degraded genomic DNA. Finally, a microscale spectrophotometer was used to verify the previous results (ND-1000, Nano Drop, Delaware, USA). The company that produced the array genomic hybridization chips believed that the microscale spectrophotometer was the best way to measure the DNA extracted from paraffin.

3.6.6 Array Comparative Genomic Hybridization

Nine different array Comparative Genomic Hybridization (aCGH) chips containing 44,370 different *in situ* synthesized 60 mer oligonucleotides were used for this study [108]. These chips consisted of oligonucleotide probes that span the human genome with an average spacing of approximately 75 kb. These probes are spaced across the genome and include areas of coding and noncoding sequences,

with an average of one probe for each characterized gene and three probes for known cancer genes of interest.

The DNA that was isolated from the three previous methods was used if there was at least 500 ng of extracted DNA. The DNA isolated using the LCM method was of insufficient quantity. We therefore attempted to amplify the DNA using two rounds of ligation-mediated PCR (LM-PCR) followed by another purification with the Gentra DNA purification columns. The DNA isolated using the Pin Point Slide DNA Isolation system was of poor quality but sufficient quantity; therefore, it was purified again using the Gentra DNA purification column. The DNA isolated using the macroscopic technique was of sufficient quality and quantity to attempt direct labelling without any amplification or purification.

The genomic DNA was labelled according to the aCGH manufacturers recommendations (Agilent). In brief, 500 ng of genomic DNA was incubated with a Digestion Master Mix containing 2.6 µl of 10 times Buffer C, 0.2 µl of Acytelated BSA, 0.5 µl of Alu I, and 0.5 µl of Rsa I and incubated for two hours at 37°C. The restriction enzymes (Alu I and Rsa I) were then inactivated by heating to 65°C for 20 minutes. The resulting fragments of genomic DNA were then labelled.

The genomic DNA mix was mixed with 5 µl of random primers (Agilent) and incubated at 95°C for three minutes before being cooled on ice. This was then used with a master mix containing 10 µl of 5 strand buffer, 5 µl of dNTP, 1 µl of Exo-Klenow fragment and 3 µl of either Cyanine 3 labelled dUTP or Cyanine 5

labelled dUTP. This mixture was incubated at 37°C for two hours. A known sample of female genomic DNA was used as a control for each of the aCGH experiments.

The enzymes were then inactivated by heating to 65°C for 20 minutes and cooling on ice. At this point the labelled genomic DNA was assessed for its quality by measuring the fluorescent intensity of the label with a NanoDrop micro spectrophotometer (Agilent). These DNA samples which were deemed to have sufficiently been labelled and contained sufficient specific activity were then hybridized to the arrays.

The appropriate Cy3 and Cy5 labelled samples and known controls were then combined and hybridized together on the 44k aCGH chips. This mixture was loaded onto the arrays, which were then sealed with a SureHyb gasket (Agilent). The arrays were then placed in a hybridization oven at 65°C and incubated for 40 hours at a revolution of 20 rpm. Following this hybridization, the slides were removed from the gaskets and washed in an ozone-controlled environment. The slides were washed with three different wash buffers to remove any unbound labelled DNA or Cy3 and Cy5. The slides were then scanned using an Agilent scanner with the Agilent version 7.0 control software. The resolution of the scanner was set to 10 μm and the barcode of each slide was then recorded. All information from the aCGH chips was then transferred to the CGH analytics software version 3.3.31 for quality control calculations and viewing of genomic abnormalities.

Chapter 4

RESULTS

4.1 Human Uveal Melanoma Animal Model

4.1.1 Survival Rate and General Condition

The 10-week animal model of uveal melanoma was carried out without major complications. The survival rate in this model was 90 percent. Since one animal was sacrificed per week, 19 of the initial 28 animals were supposed to survive until the last week of the model. Seventeen rabbits survived until the end of the experiment, with two rabbits having to be euthanized before planned due to veterinary recommendations. The first animal was euthanized during the first week and the other in week 8, due to poor general conditions including more than 20 percent weight loss, which was one of our experimental endpoints.

We observed an initial acute weight loss one week after cell injection that can be partly attributed to the surgery and the initiation of CsA dosage. After week 1, the average weight of the animals was maintained until the end of the experiment (Figure 4.1).

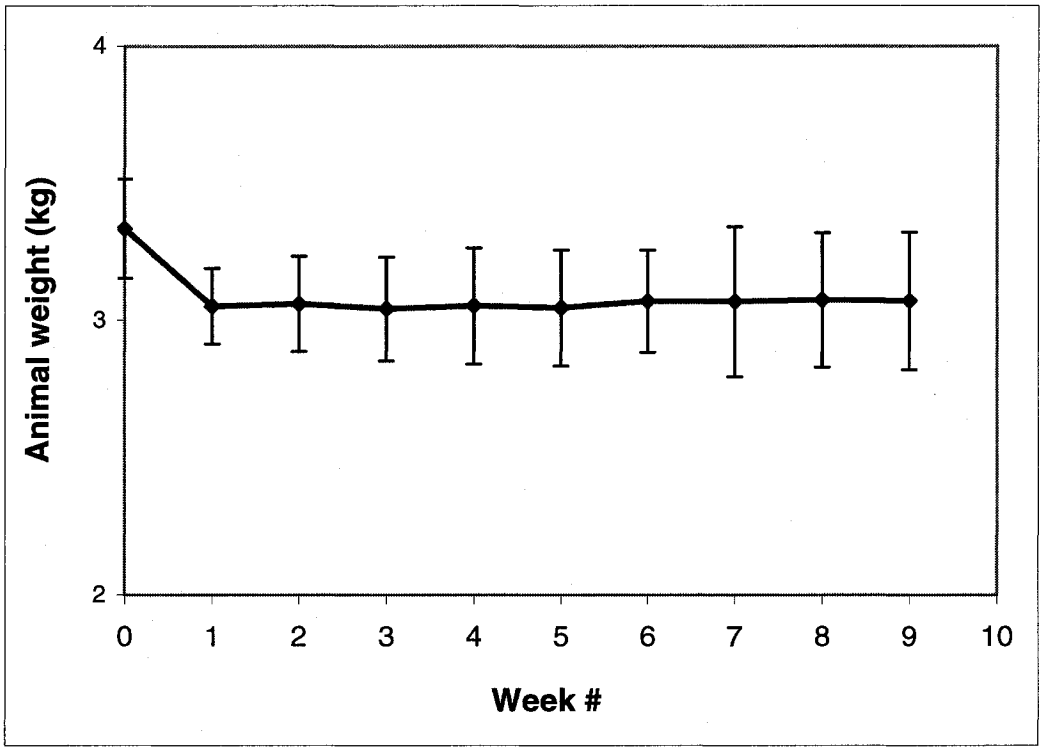

Figure 4.1) Animal weight during the experiment

The mean animal weight was calculated for the number of remaining animals each week. Values presented are the mean ± standard deviation.

4.1.2 Intraocular Tumour Detection by Fundoscopy

The fundoscopic examination performed prior to the surgery demonstrated that all animals were free of ocular disease at the beginning of the experiment. During the 10-week experiment, fundoscopic examination detected the formation of intraocular tumours in 67 percent of the animals as seen in Figure 4.3. Of these animals with detectable tumours, seven were detected two weeks after the intraocular cell injections, with the remaining nine intraocular tumours being detected later on in the study. The number of tumours remained stable following the fifth week of the experiment as shown in Figure 4.2.

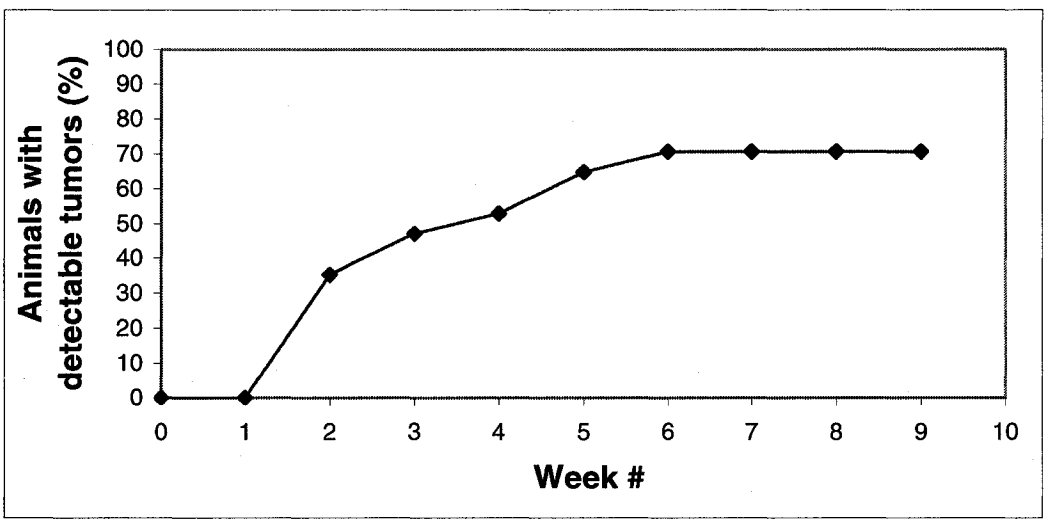

Figure 4.2) Intraocular tumour detection by fundoscopy

Percentage of animals with detectable tumours by fundoscopy vs week of the experiment.

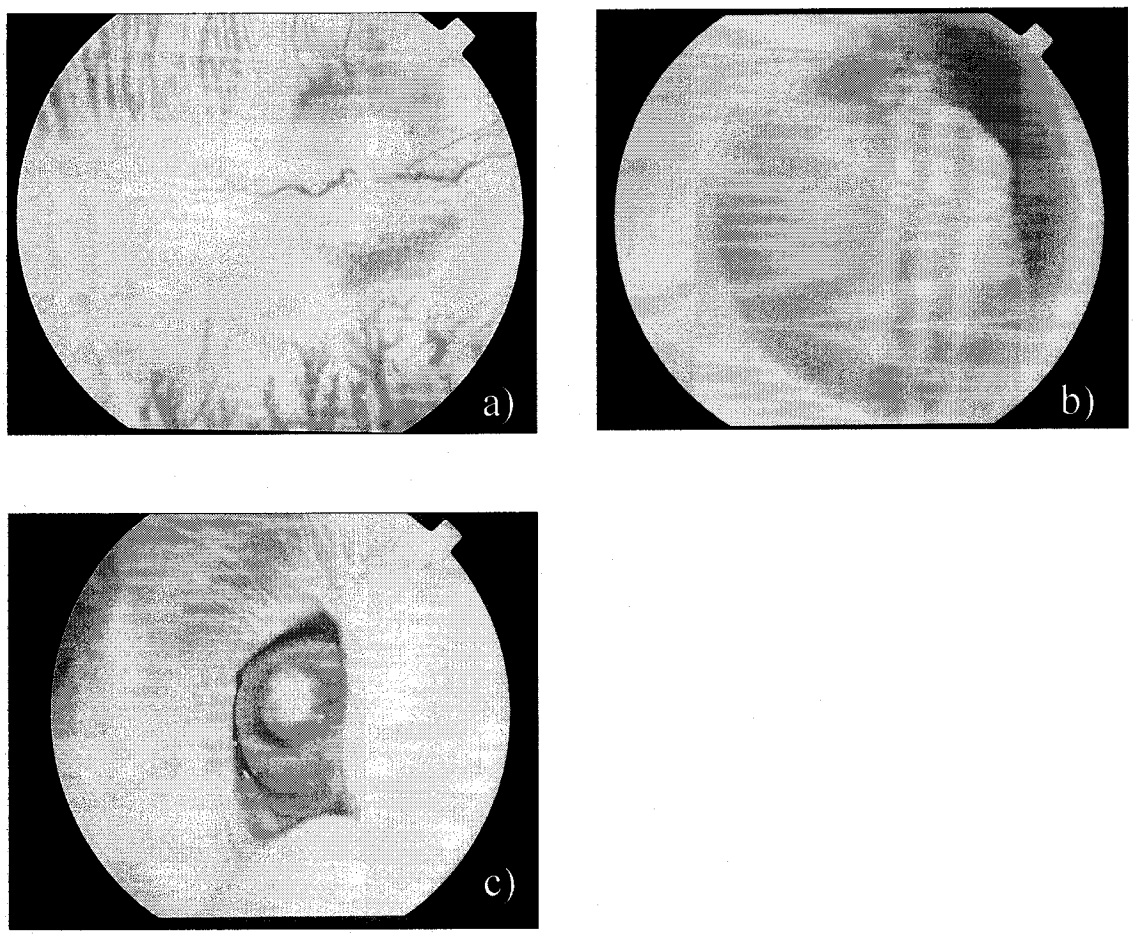

Figure 4.3) Fundus photographs of rabbits' eyes

Photographs of the fundus from the rabbits: a) Normal eye fundus photo; b) Intraocular melanoma in a rabbit, nine weeks after cell injection; c) Large tumour mass observed with the naked eye, nine weeks after cell injection.

4.1.3 Ultrasound Evaluation of Intraocular Tumours

Ultrasound examination was performed to determine the echographic characteristics, location and final dimensions of the intraocular tumours *in vivo*. Using A-scan, intraocular tumours presented as solid lesions with low to medium, regular, internal reflectivity; all characteristic features of uveal melanoma (Figure 4.4). Using B-scan, intraocular tumours were shown to consist mainly of large choroidal masses with a tendency for extraocular extension (Figure 4.4). Ultrasound revealed the presence of intraocular tumours in all 15 animals that were examined. Ten weeks after cell inoculation, tumours presented with an average length of 10.1 ± 1.5 mm (n=9), an average width of 10.0 ± 1.8 mm (n=9) and an average height of 7.5 ± 2.3 mm (n=15). In six cases, the tumour was so large that it exceeded the boundaries of the ultrasound field.

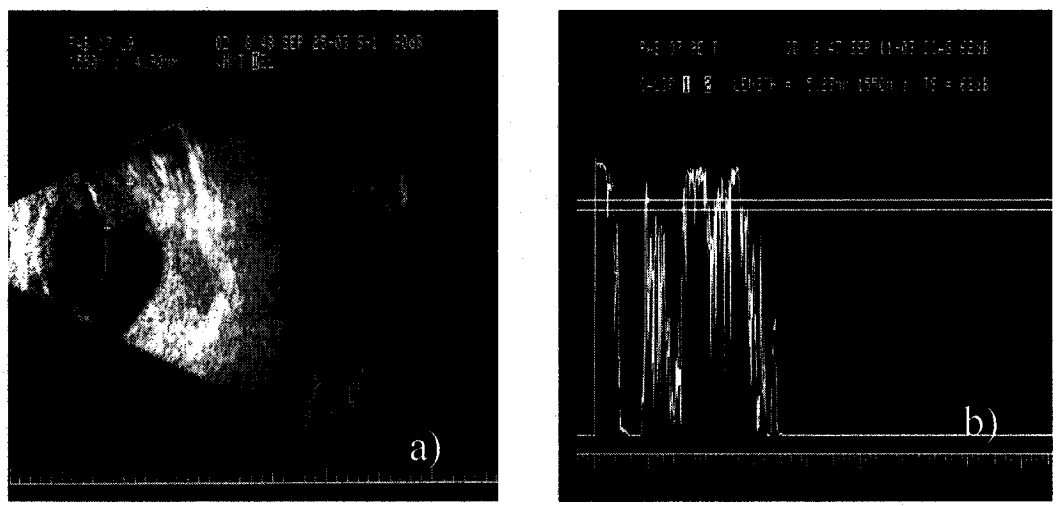

Figure 4.4) Ultrasound examination

The ultrasound results from the rabbit eye. a) A and b) B-scan echograms showing mushroom-shaped lesions in the rabbits' eyes, nine weeks after cell injection.

4.1.4. Macroscopic and Microscopic Intraocular Tumour Findings

The eyes were examined following enucleation with the aid of an ocular pathologist to determine the presence of intraocular tumours. When tumour size was sufficient, samples were taken for snap freezing in liquid nitrogen and to be re-cultured.

Macroscopically, intraocular tumours were found in 82 percent of the animals (22 out of 27) (Figure 4.5). Ocular tumour development was observed in the first sacrificed animal, one week after cell injection. Histopathological evaluation of the enucleated eyes further revealed that tumours were present in 89 percent of the animals (24 out of 27). Melanomas were positively identified by immunostaining with a mAb to the melanoma-specific marker HMB-45 (Figure 4.6).

Intraocular tumour development was monitored throughout the experiment (Figure 4.6). Tumours grew diffusely within the choroid during the first two weeks. The site of cell injection could sometimes be identified as a thickened choroidal area. By week 3 and 4 after cell injection, tumours began to grow in height, adopting a nodular or dome-shaped configuration. From week 5 onwards, most of the eyes examined showed large tumours that varied in shape. The majority of these large tumours exhibited a mushroom-like appearance, with a considerable part of the tumour filling the vitreous cavity. At the end of the experiment, tumours completely filled the globe in 30 percent of the remaining animals.

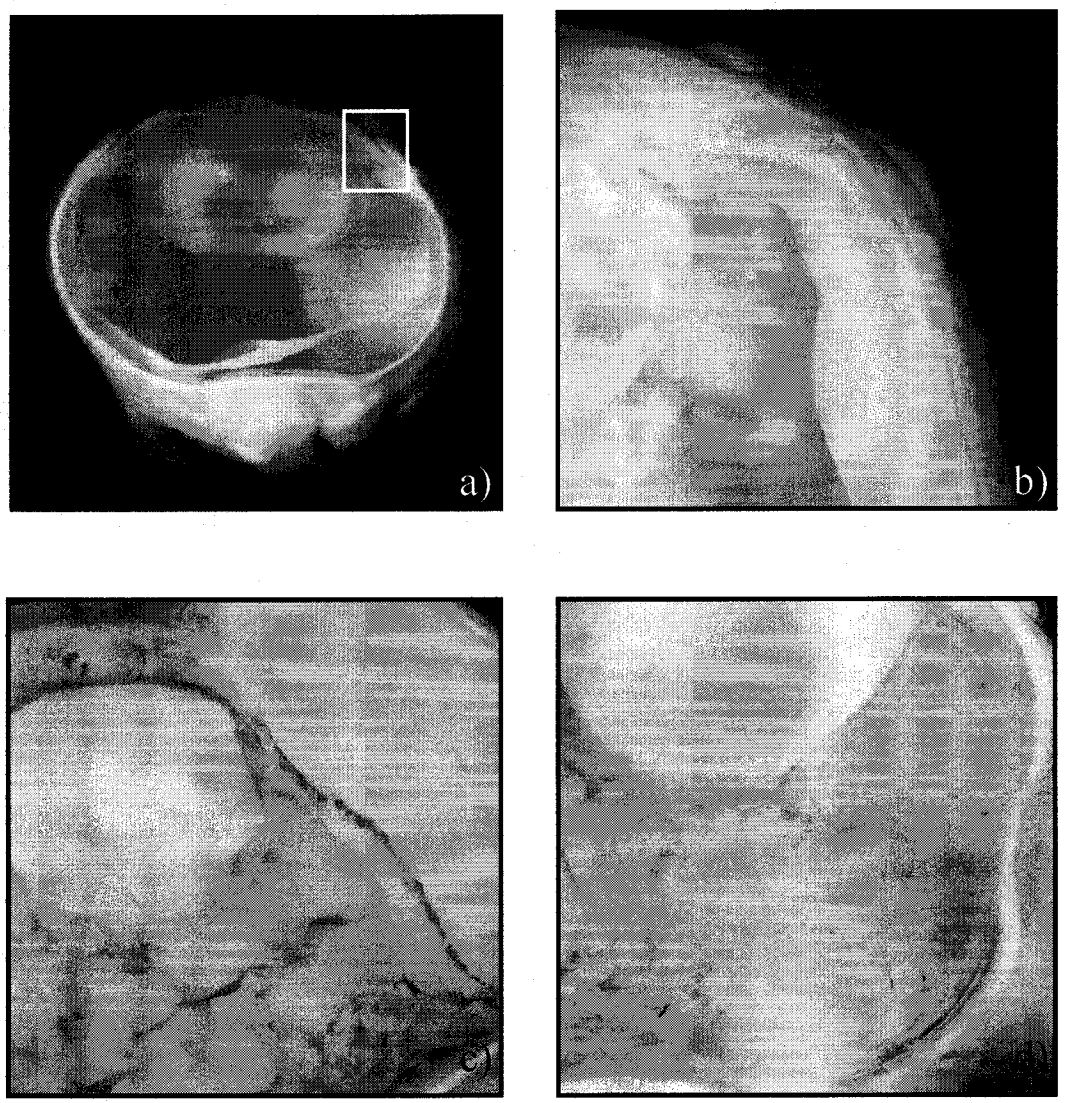

Figure 4.5) Progression of the intraocular tumours: macroscopic findings

a) Normal rabbit eye, x5; b) Intraocular melanoma in a rabbit, one week after cell injection (x 10 magnification of the area indicated in Figure a); c) Intraocular melanoma in a rabbit, six weeks after cell injection, x10; d) Intraocular melanoma filling the ocular cavity of the rabbit, nine weeks after cell injection, x10.

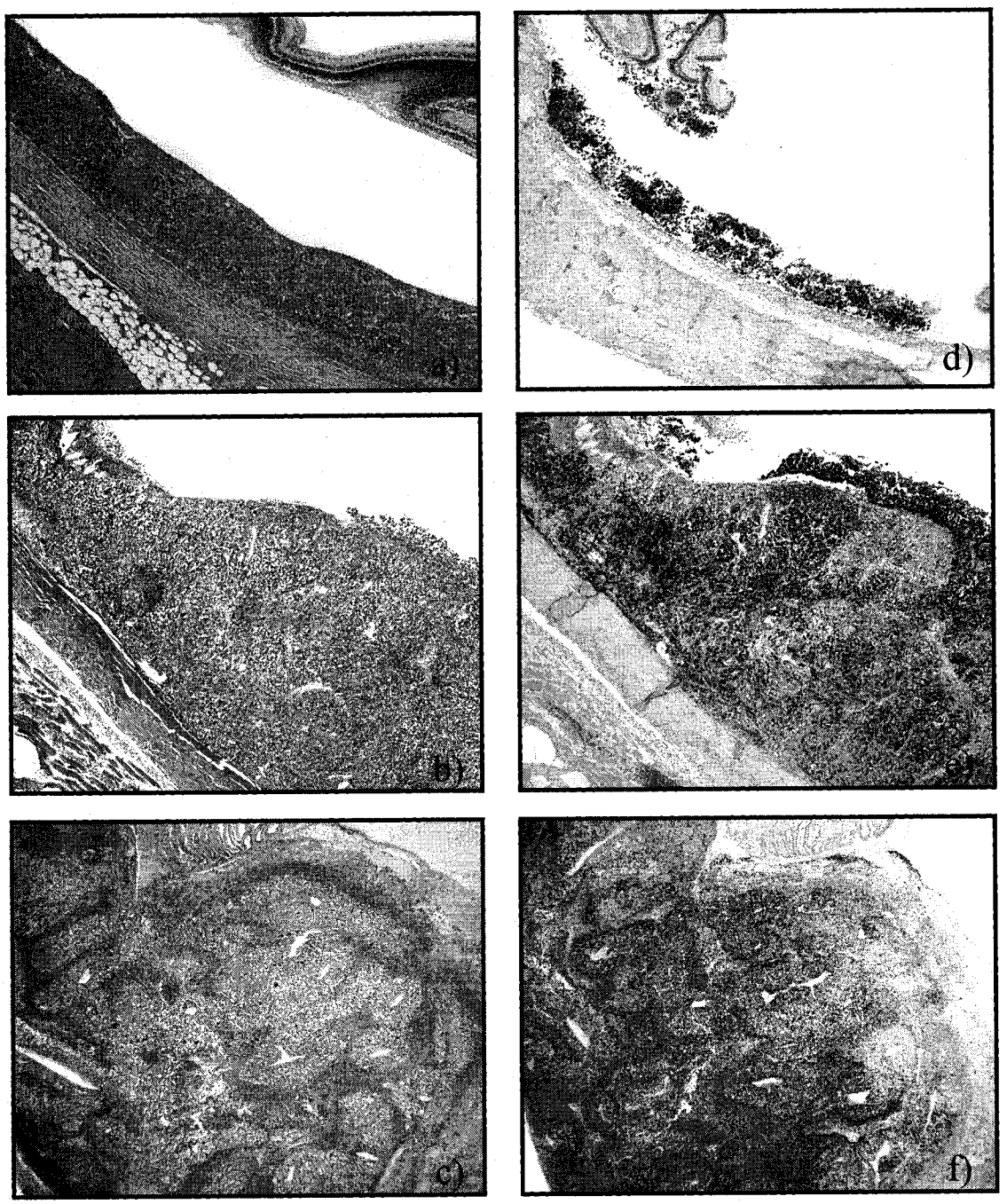

Figure 4.6) Microscopic progression of the intraocular tumours

Histopathological sections showing tumours a) 10 days (H&E, 5x), b) three weeks (H&E, 5x) and c) eight weeks (H&E, 2.5x) after cell injection. Photomicrographs d), e) and f) are HMB-45 immunostained specimens a), b) and c), respectively at x100 magnification.

4.1.5 Re-Culture of Intraocular Tumour Cells

We were able to isolate and re-culture cells from 16 intraocular tumours. Cell cultures were positively immunostained using the melanoma specific markers, Melan A and Tyrosinase mAb (Figure 4.7). Large pieces of intraocular tumours were snap frozen from six of the animals after the ninth week of the experiment.

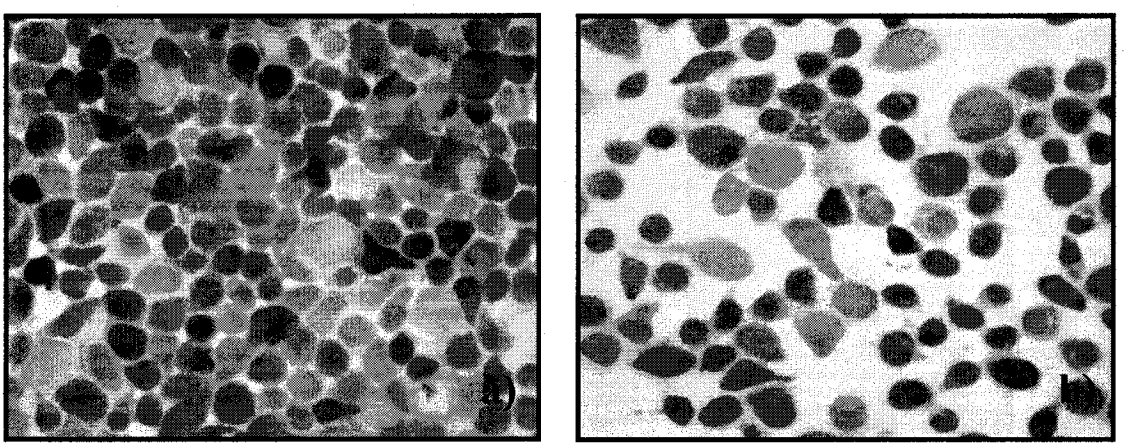

Figure 4.7) Cultured intraocular tumour cells isolated from rabbit eyes

a) Cytospin immunostained with Melan A monoclonal antibody (400x); b) Cytospin immunostained with Tyrosinase monoclonal antibody (400x).

4.1.6 Circulating Malignant Cells

We successfully isolated CMC from blood samples obtained at the moment of euthanasia from five rabbits. Colonies, usually two or three per sample, were observed two weeks following the seeding of the mononuclear layers. The cells were positively identified as uveal melanoma cells through immunostaining using HMB-45, Melan A and Tyrosinase mAbs (Figure 4.8). *In vitro* proliferating CMC were first isolated six weeks after cell inoculation when we first attempted to culture mononuclear cells from the blood. CMC were detected in five of 19 (26 percent) cultured blood samples. Examination of cultured CMC grown on coverslips revealed that the cellular morphology resembled of the original 92.1 human uveal melanoma cell line. As soon as sufficient amounts of cells were present in the plate, the CMC were harvested and kept frozen for future studies.

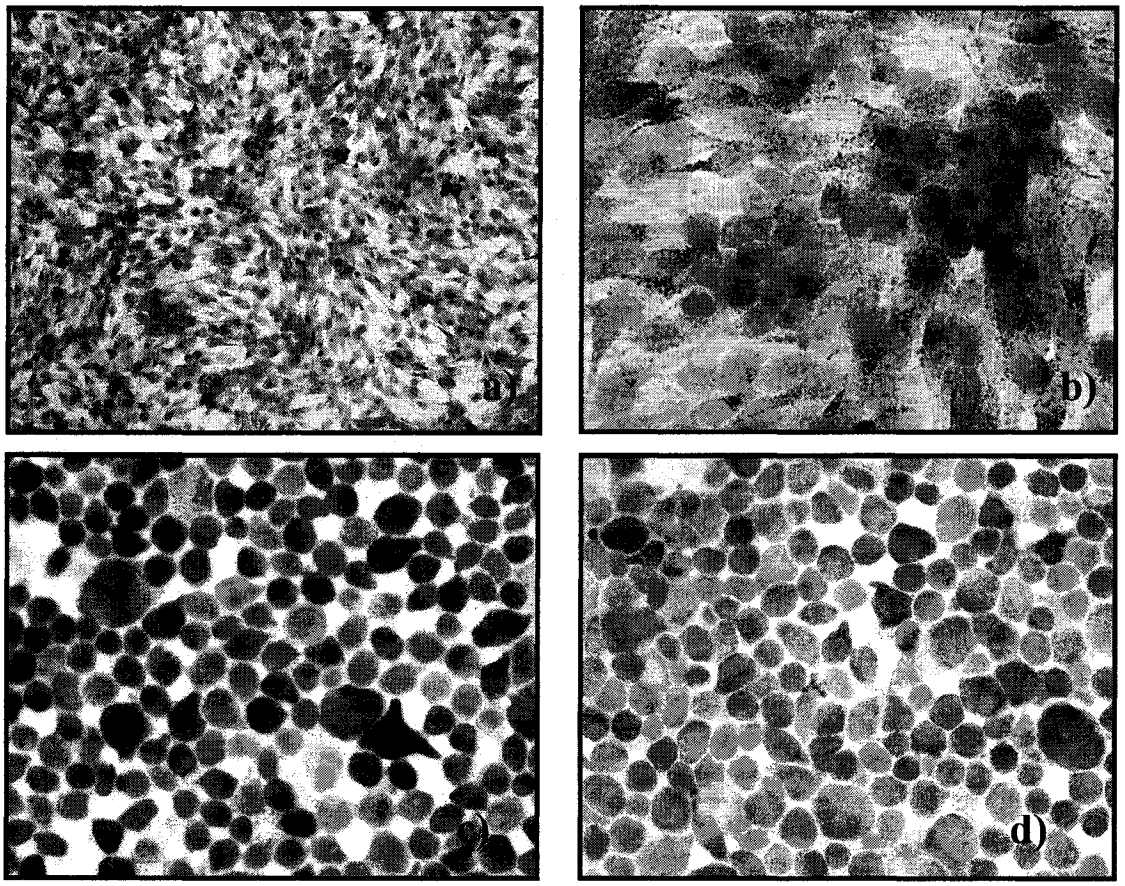

Figure 4.8) Cultured circulating malignant cells isolated from rabbits' blood

a) and b) CMC grown on coverslip were immunostained using the HMB-45 monoclonal antibody (100x and 400x, respectively); c) Cytospins immunostained with Melan A monoclonal antibody (400x); d) Cytospins immunostained with Tyrosinase monoclonal antibody (400x).

4.1.7 Macroscopic and Microscopic Metastasis Findings

Gross examination of the lungs with a pathologist seven weeks after surgery revealed multiple nodular lesions that appeared to be metastases (Figure 4.9). Lung metastases were macroscopically observed in 41 percent of the animals remaining at the end of the experiment. They presented as firm elevated lesions of less than one centimetre in diameter. No macroscopic metastatic lesions were observed in any of the rabbit livers.

Microscopic pulmonary metastatic foci were first observed four weeks after cell injection. By the end of the experiment, all remaining animals (100 percent) showed histopathologically confirmed lung metastases (Figure 4.10). Metastatic lesions were HMB-45 positive (Figure 4.11). The lesions usually presented as multiple subpleural micronodules surrounded by a peripheral rim of lymphocytes. In some cases, areas of diffuse infiltrate were also observed probably causing the breathing difficulties observed in some of the animals. Interestingly, micrometastatic lesions were found in the liver of three out of 17 (17.6 percent) animals remaining at the end of the 10^{th} week (Figure 4.12). Five rabbits at the time of the autopsy had large enough metastatic nodules in the lung to be isolated and snap frozen. These metastatic tissue samples were all from lungs with metastatic lesions that were verified using immunohistochemical staining with HMB-45, Melan A and Tyrosinase. No metastatic lesions from the livers were large enough to be isolated prior to microscopic examination after the livers were fixed in formalin and embedded in paraffin blocks. Therefore, none of the three liver micrometastases were available for transcriptional analysis.

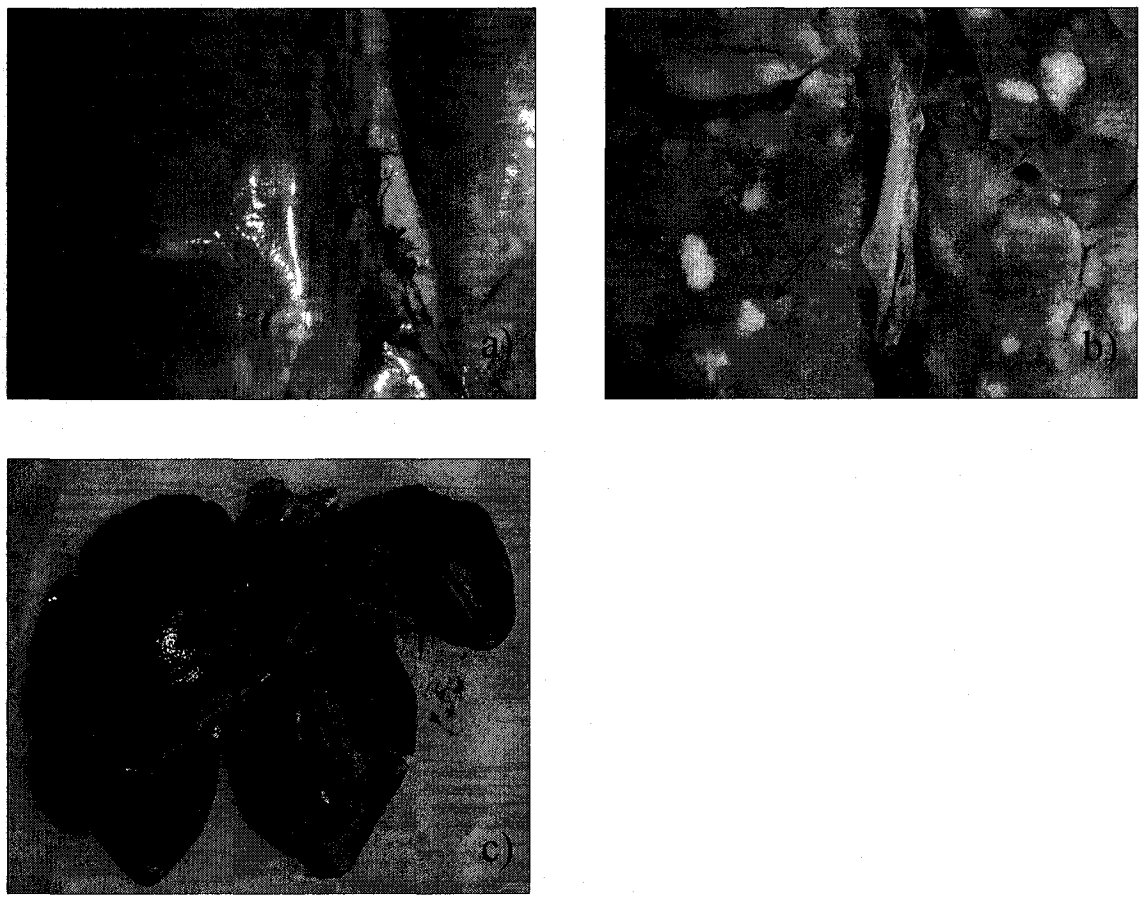

Figure 4.9) Metastases: macroscopic findings

a) Normal rabbit lungs; b) Gross examination of a rabbit lung, 7 weeks after cell injection. Arrows indicate multiple nodules compatible with metastasis. c) A normal rabbit liver.

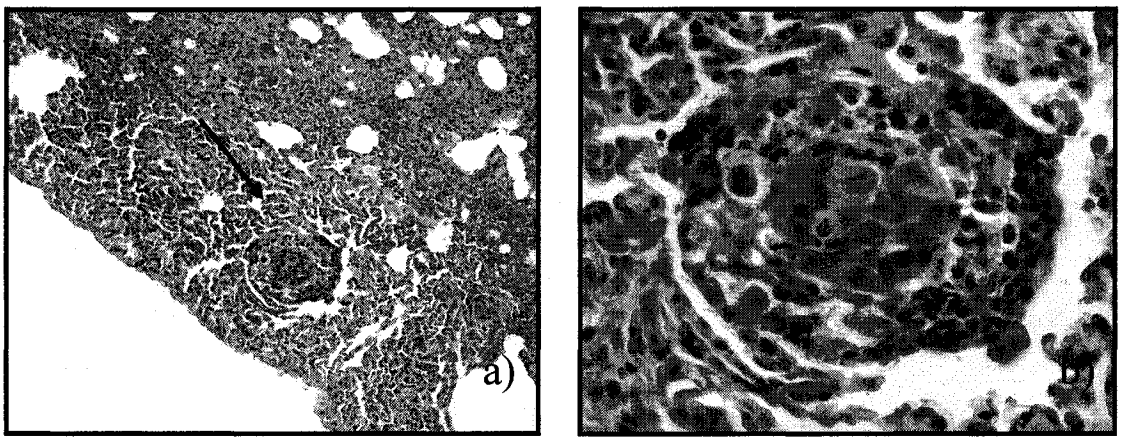

Figure 4.10) Lung metastases: microscopic findings

a) and b) Photomicrographs of a H&E stained specimen showing a subpleural micronodule (100x and 400x respectively);

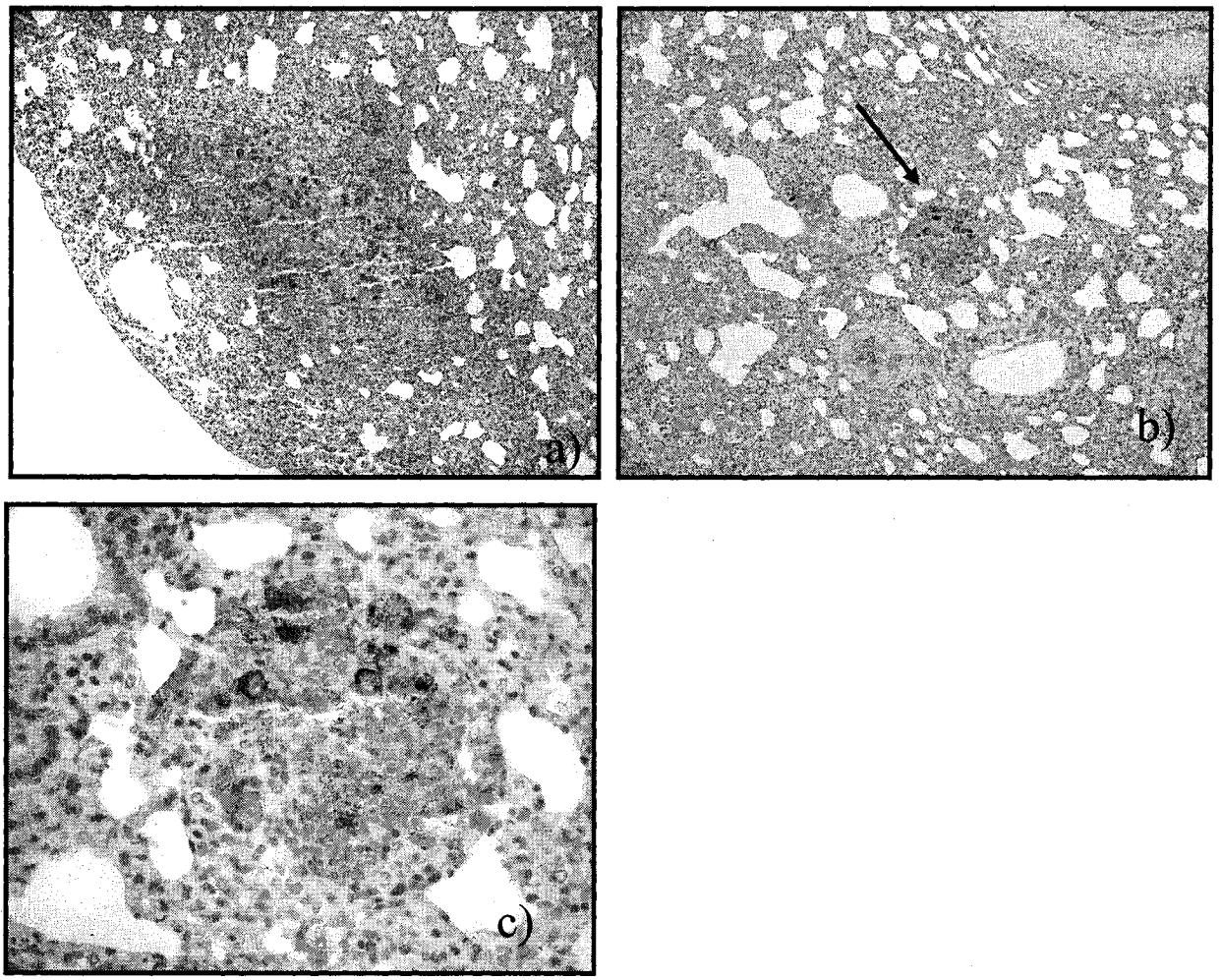

Figure 4.11) Photomicrographs of HMB-45 immunostained lung metastases

a) Subpleural metastasis (100x); b) and c) Lung micrometastatic nodule (100x and 400x, respectively).

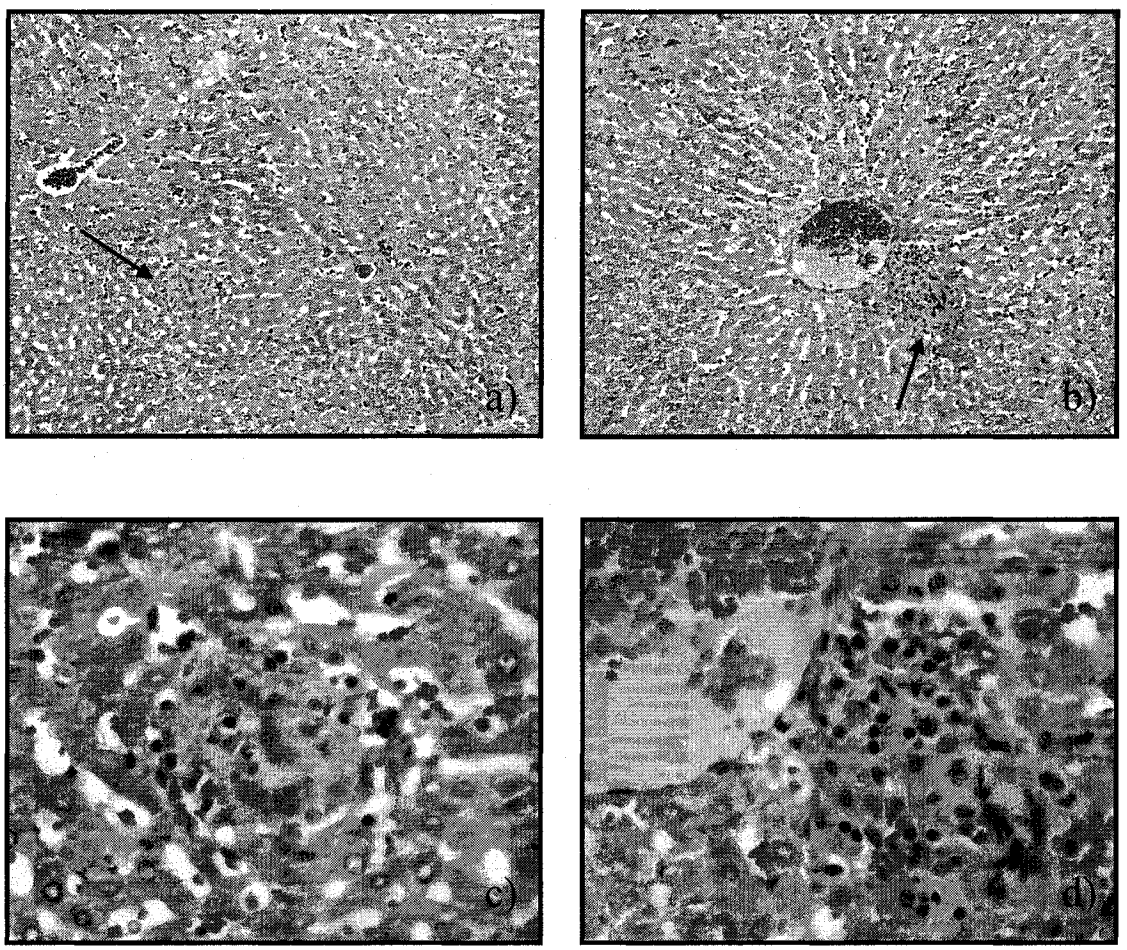

Figure 4.12) Liver metastases: microscopic findings

a), b) and c) Metastatic foci in the rabbit liver (H&E; 100x, 200x and 400x, respectively); d), Malignant cells shown invading the rabbit liver (H&E; 400x)

4.1.8 Culture of Metastatic Cells

Cells from five of the metastatic lung lesions were successfully isolated and grown *in vitro.* These rapidly proliferating metastatic cells were positively immunostained with specific antibodies against melanoma markers (Figure 4.13). Metastatic cells were preserved frozen for future experiments.

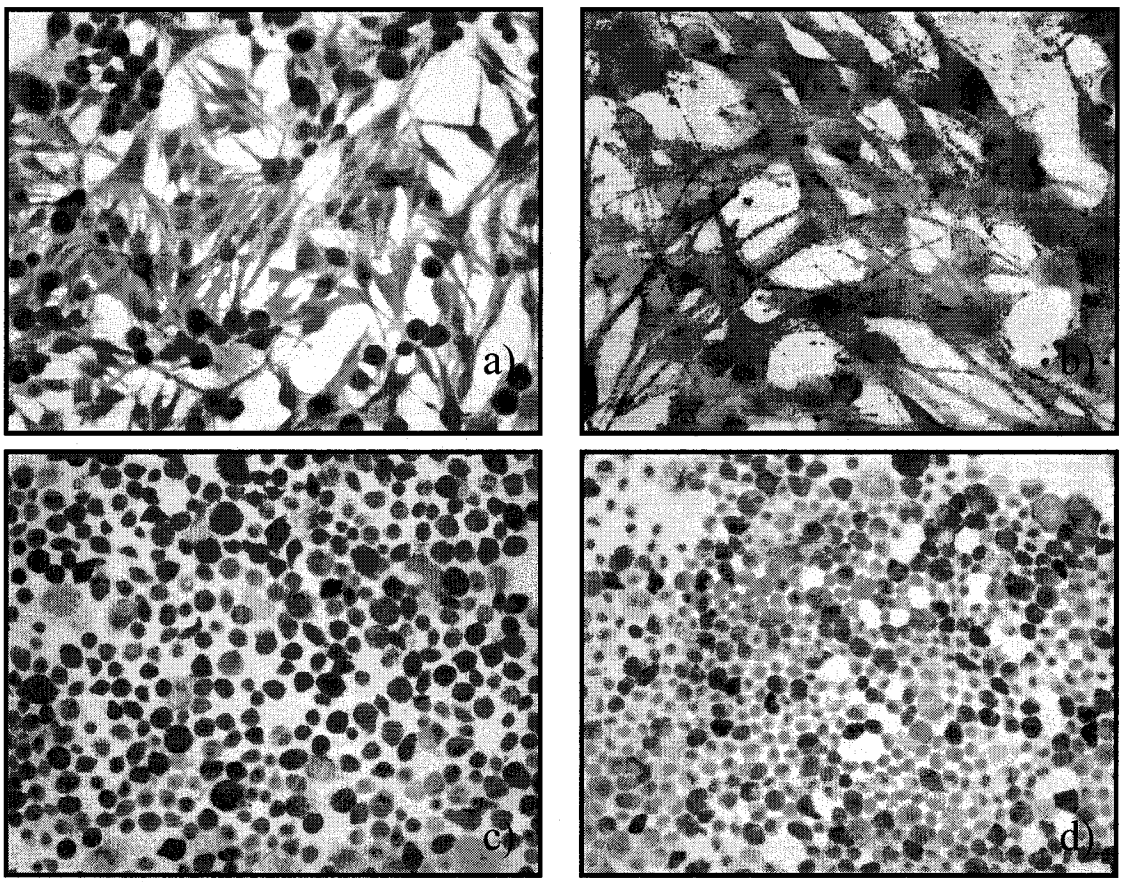

Figure 4.13) Cultured metastatic cells isolated from rabbit lung lesions

a) and b) Cultured metastatic uveal melanoma cells grown on a cover slip were immunostained using the HMB-45 monoclonal antibody (200x and 400x, respectively); c) Cytospin immunostained with Melan A monoclonal antibody (200x); d) Cytospin immunostained with Tyrosinase monoclonal antibody (200x).

4.2 Transcriptional Microarray Results

4.2.1 Total RNA Quality and Quantity

The total RNA that was extracted from the five human uveal melanoma cell lines was of good quality and a large amount of total RNA was present. These RNA samples were deemed to be acceptable for use with the transcriptional microarray analysis.

From the six different intraocular tumour samples that were snap frozen (Rabbits 4, 5, 8, 14, 15, 18), sufficient total RNA that was of good quality was extracted from five of them (Rabbits 4, 5, 14, 15, 18). The extracted RNA was found to be of good quality with no sign of degradation products or contamination. The remaining intraocular tumour sample, from rabbit 8, contained only 5.58 ng/μl of total RNA as measured by the Bio Analyzer. This provided insufficient total RNA to be used for microarray analysis that required a minimum of 10 μg of RNA per sample; therefore this sample was not used for microarray analysis.

The five large metastatic nodules that were isolated and snap frozen (Rabbits 5, 9, 14, 15, 18), yielded sufficient total RNA to be used during the transcriptional microarray analysis. One of the five samples (Rabbit 15) had some contamination present in it, potentially ethanol from the RNA extraction process. The contamination was judged to be within tolerance for use and the RNA was utilized for microarray analysis.

The Bio Analyzer results for each of the intraocular and metastasis tissue samples are shown below (Figure 4.14) along with the included reference sample

from Agilent that was used as a comparison. An example of an RNA sample with degradation products is also shown (4.17). None of our samples showed any presence of degradation, an important consideration when using the transcriptional microarrays. The small peak present at approximately 24 seconds is indicative of 5S and 5.8S RNA as well as tRNA. The peak for 18S ribosomal subunit RNA is usually located at approximately 44 seconds with the larger 28S subunit at approximately 50 seconds. Typically the 28S peak is roughly twice the size of the 18S peak.

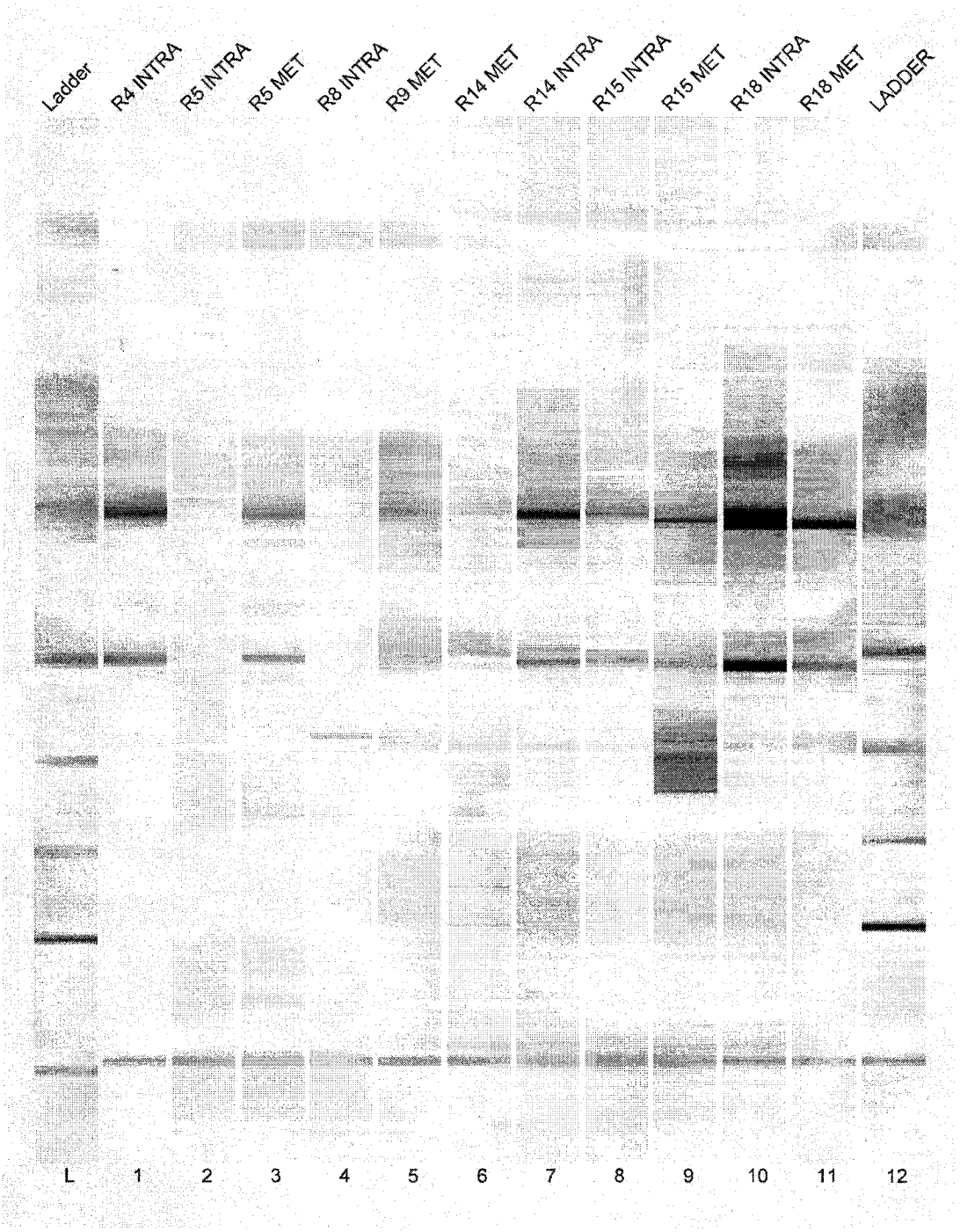

Figure 4.14) Bio Analyzer Results

This graphical representation of the bio analyzer results shows the bands associated with total RNA extracted from each of our intraocular and metastatic tissue samples.

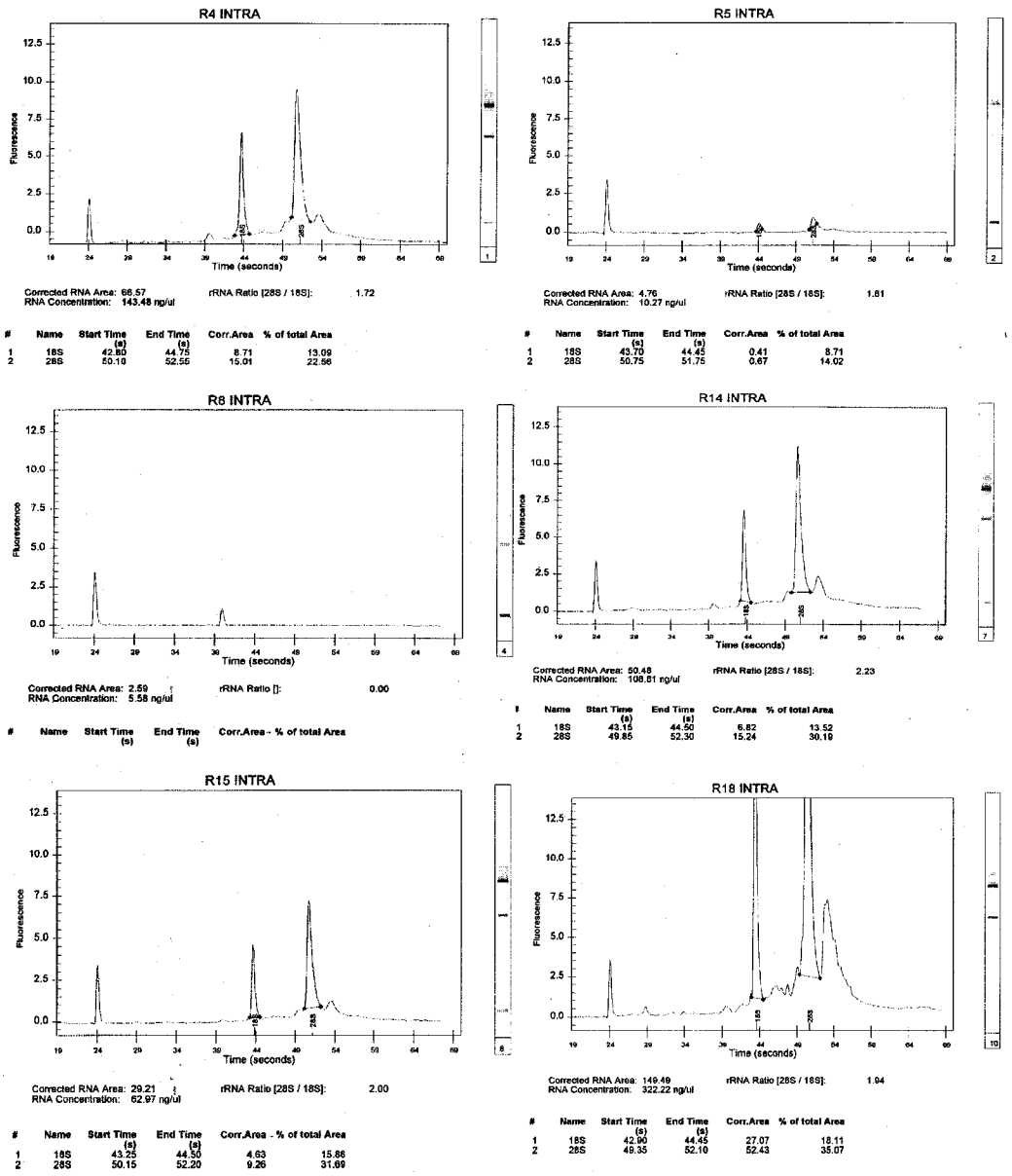

Figure 4.15) Bio Analyzer Results from the Intraocular Tissue

The bio analyzer peaks for the total RNA from each of the intraocular tissue samples. The two large peaks for each of the rabbits with sufficient total RNA (R4, R5, R14, R15 and R18) show the 18S and 28S RNA peaks. The RNA isolated from the intraocular tumour of rabbit 8 did not show either peak when analyzed and had low levels of detectable RNA.

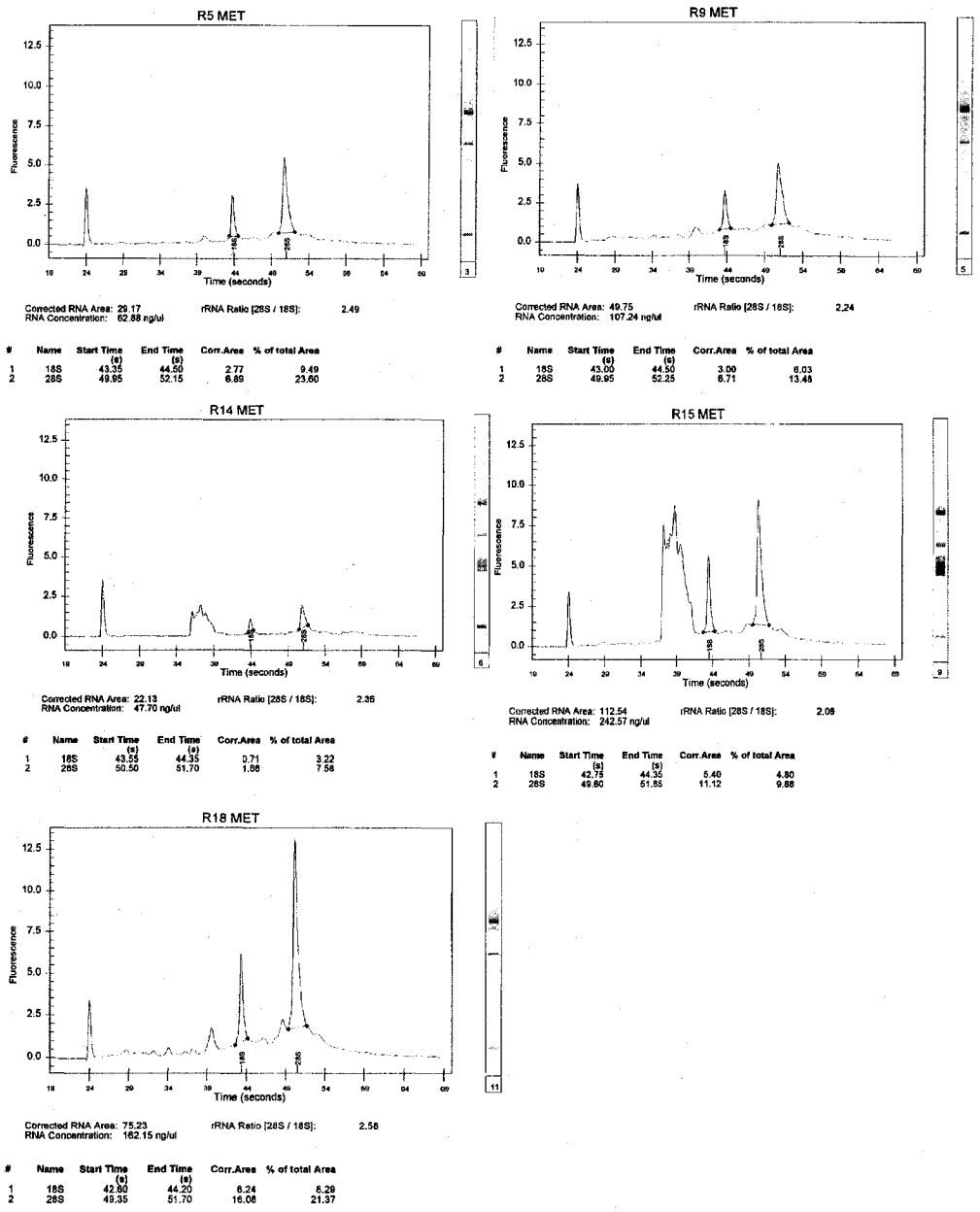

Figure 4.16) Bio Analyzer Results from the Metastatic Tissue

The bio analyzer peaks for the total RNA from each of the metastatic tissue samples. Large peaks for each of the samples were seen for 18S and 28S products. The RNA from the metastatic lesion of rabbit 15 displayed some contamination, as seen by the broad peak located before the 18S peak.

Severely Degraded total RNA

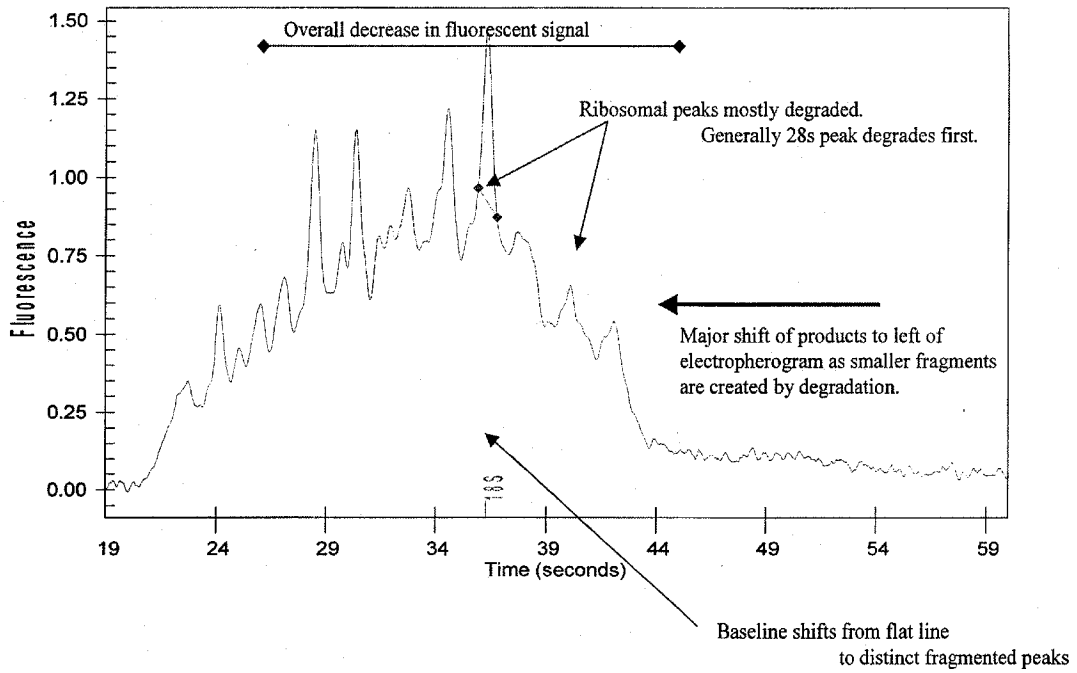

Figure 4.17) Bio Analyzer Results from Degraded Sample

These results show what an RNA sample with degradation products would look like. None of our samples presented with typical signature featuring a large multi-peaked hump through the middle of the analyzer results.

4.2.2 Transcriptional Profiling of the Human Uveal Melanoma Cell Lines

The RNA that was isolated from the five human uveal melanoma cell lines (92.1, SP6.5, MKT-BR, OCM-1, UW-1) was used to run the first set of microarrays. This allowed us to profile the five cell lines, one of which, 92.1, was used to inoculate the eyes of the immunosuppressed rabbits leading to the formation of the intraocular tumours and subsequent metastases. The RNA isolated from these five cell lines was labelled and hybridized to DNA microarrays. As a control, we used a commercially available universal RNA that is produced from a variety of cell lines, which allowed us to compare the results from all the microarrays to each other since the on-chip control was the same. Figure 4.18 shows the comparison of a dye swap from the 92.1 cell line.

The results from this first set of chips indicated that all five cell lines are relatively homogenous when compared to the control sample since the Welch T-test did not identify any transcripts with a statistically-significant change in abundance that could distinguish any one of the cell lines from the others. Four different microarrays were used for each cell line, two with a dye swap to correct for any differences due to the Cyanine dye.

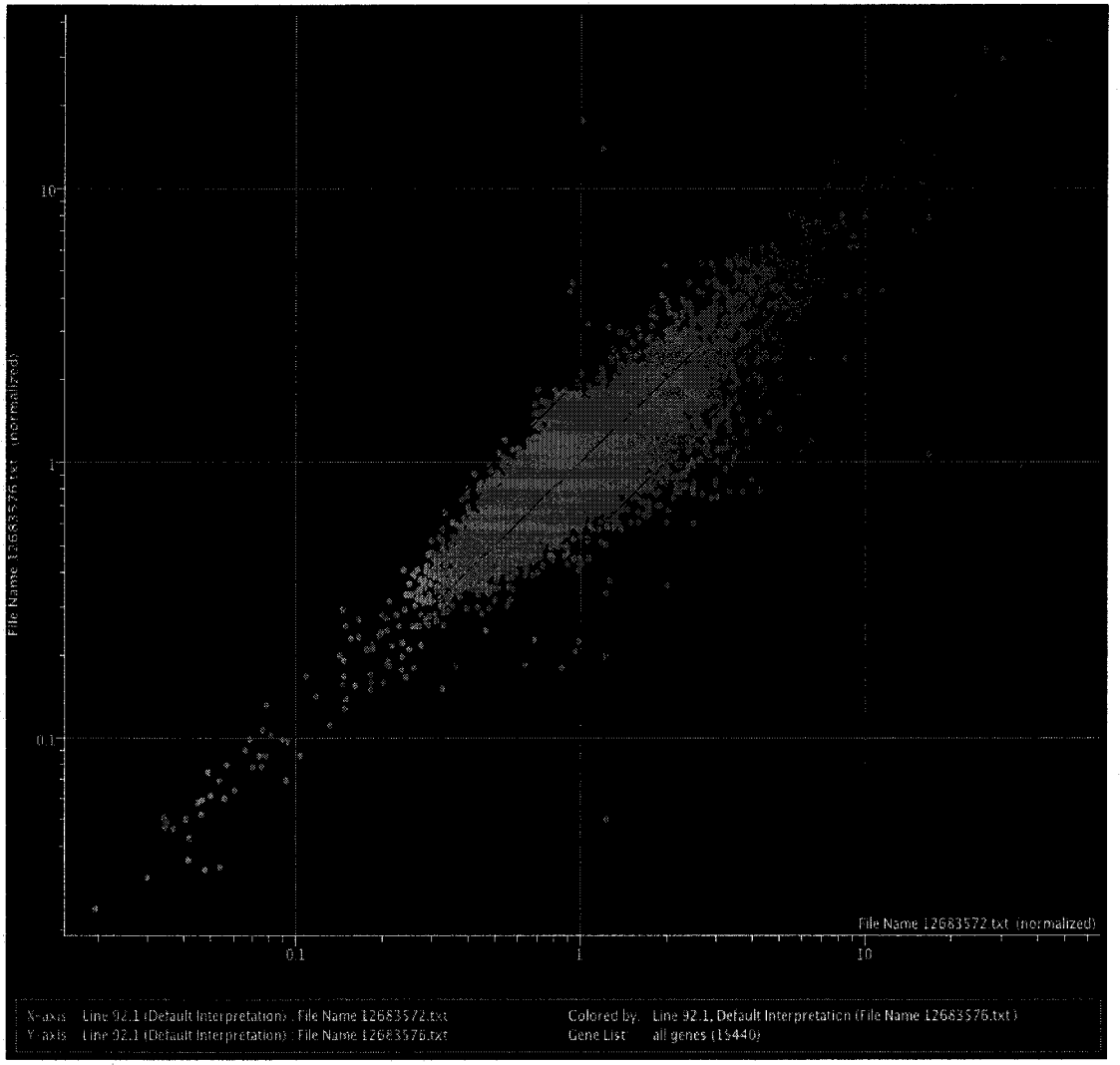

Figure 4.18) Fold Change of Trancripts from the 92.1 Cell Line

The fold change of transcripts from one microarray using the 92.1 cell line compared to another microarray using the same cell line with a dye swap. This comparison checks for reproducibility and any potential bias due to the Cyanine dye. The linearity of the comparison shows no bias due to dye swap.

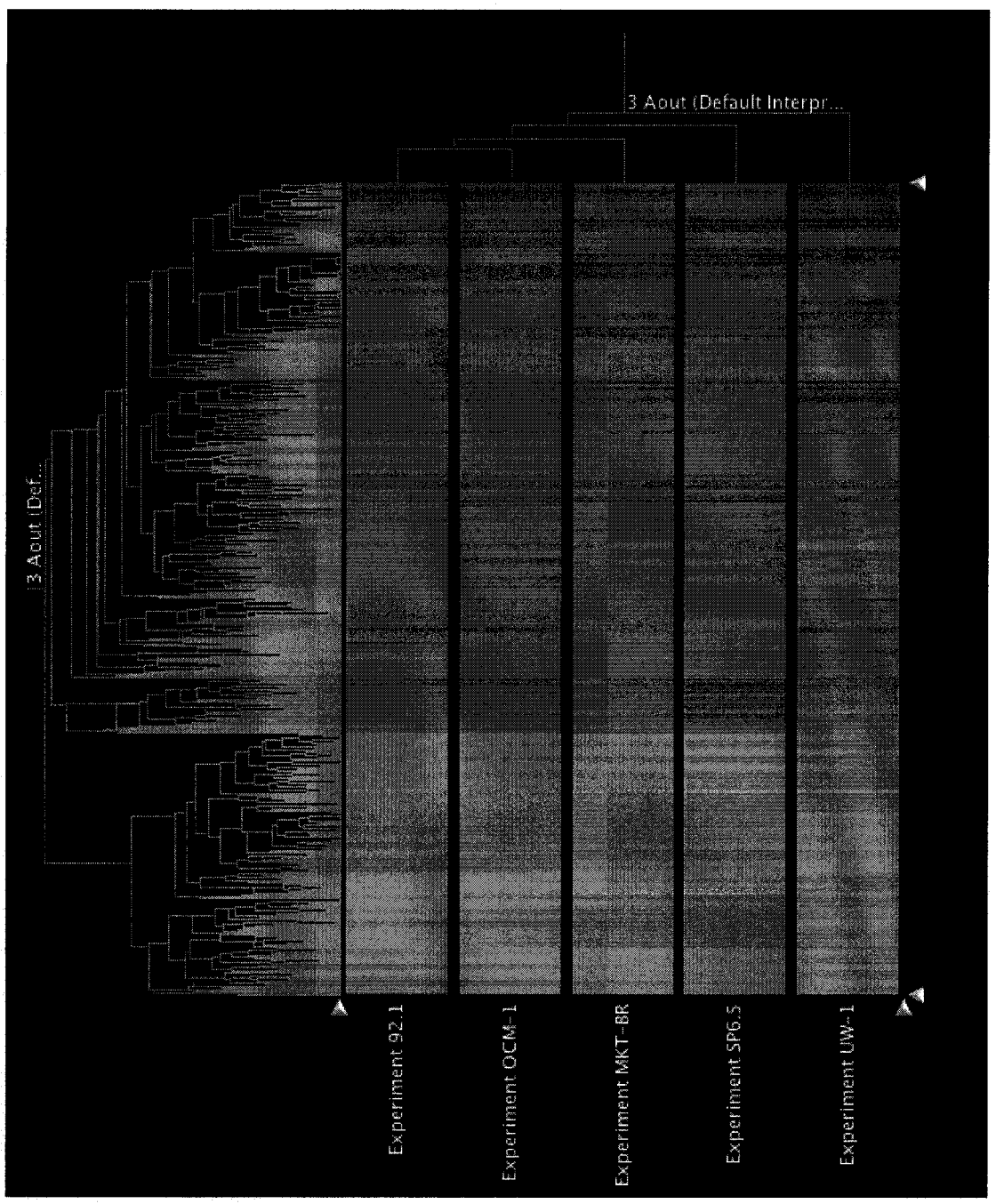

Figure 4.19) Transcriptional Profile of the Uveal Melanoma Cell Lines

The transcriptional profile of the five human uveal melanoma cell lines is shown. The five cell lines showed no significant differences between their respective transcriptional profiles.

4.2.3 Transcriptional Profiling of the Intraocular and Metastatic Tissue

Tissue samples from the intraocular tumours and metastastic lesions were isolated from our immunosuppressed animal model of uveal melanoma. We were able to profile five large intraocular tumours and five large metastatic lesion samples from which good quality RNA was obtained. Four of these sample sets were taken from the same animal (Rabbit 5, 14, 15, 18), while one came from a different animal pair due to small metastatic lesion of insufficient size (Intraocular tumours: Rabbit 4. Metastatic tumours: Rabbit 9).

Microarray data and complete lists of significantly-modulated transcripts are listed in the Appendix. We used the same microarrays and the same Universal RNA as in the cell line analysis. Principal Components Analysis separated each individual hybridization into three distinct clusters according to the tissue of origin (cell line, primary intraocular, metastasis) as shown in Figure 4.20. In addition, we could not identify any significant correlation between the primary tumours or metastatic lesions that came from different animals. This observation is also illustrated in Figure 4.21, suggesting that samples from the same origin show remarkably consistent profiles.

As illustrated in Figure 4.22, ANOVA testing (Welch test coupled with a Benjamini and Hochberg multiple testing correction algorithm) was used to identify the numerous changes in transcript abundance that varied between the original *in vitro* cell lines and the tissue samples. Because of the relative homogeneity between the five cell lines, we decided to increase our sample size

by combining the profiling data from all five cell lines instead of the two individual profiles from the 92.1 line that was actually injected in the rabbits. As can be expected, the transition between cultured cells and solid tumours produced numerous changes which are exemplified by the 1149 transcripts with detectable differences between the *in vitro* cell lines and the intraocular tumours and the 1672 transcripts that distinguish the cell lines and the metastatic lesions. These gene lists are of only marginal interest because of the extensive difference in growth environment between in vitro cultures and solid tumours. We thus chose to focus on the transition, which occurred between intraocular tumours and metastasis, which is characterized by significant changes in abundance in 314 transcripts, shown in the Appendix. Comparison of the intraocular and metastatic profiles with the non-parametric Wilcoxon-Mann-Whitney test ($p<0.002$) identified 268 significantly modulated genes (also listed in Supplementary File 1), 239 (89 percent) of which were also part of the list of 314 genes identified by the parametric Welch test.

Principal Components Analysis (PCA) was then used to cluster the larger list of 314 transcripts that best distinguished intraocular tumour samples from metastatic tumour samples. As shown in Figure 4.23, these transcripts could be separated between four distinct groups that were labelled as Groups A, B, C and D. A complete list of all of these genes can be found in Supplementary File 1.

Group A genes showed an increase in expression between intraocular and metastasic tumours but not between the transition from cell lines to intraocular tumours. It includes Insulin Receptor Substrate 2, Fibronectin 1 (Figure 4.24),

Septin 7, Alpha Kinase 3, Transcription Factor AP-2 Beta, Interleukin 1 receptor accessory protein, Neurofibromin 2, RAB26, Heparin sulfate proteoglycan-2 and Cytokeratin 18.

Group B showed a gradual decrease in expression from the cell lines to intraocular tumours to metastasis and includes the melanoma markers Melan A, CD63 and SILVer along with Activating Transcription Factor 4 and Vimentin. Several genes encoding for ribosomal proteins were also clustered together in Group B (Figure 4.25).

Group C showed a decrease in expression from intraocular to metastasis but, like Group A, no significant changes between the cell lines and the solid tumours. Gene products of the members of Group C include BST1, Caspase 10 and DAPK-interacting protein 1. Finally, genes from Group D showed a gradual increase in expression from *in vitro* to intraocular tumour and a further increase from intraocular tumour to metastasis.

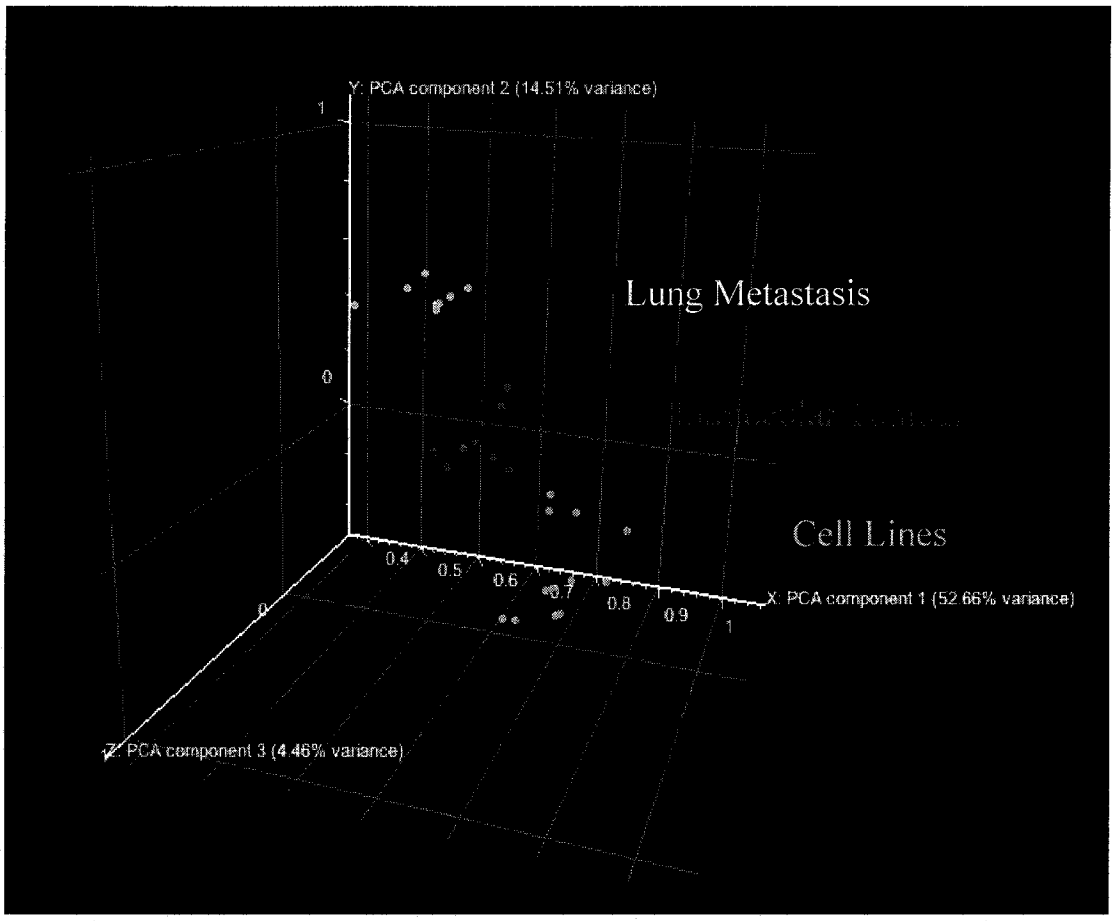

Figure 4.20) Principal Components Analysis of the Microarrays

Principal Components Analysis showed a clear segregation of the microarrays hybridized from cell lines (blue), the intraocular tumours (red) and the metastases (yellow). This clear separation indicates that there is a difference in transcriptional profile from each of the three locations.

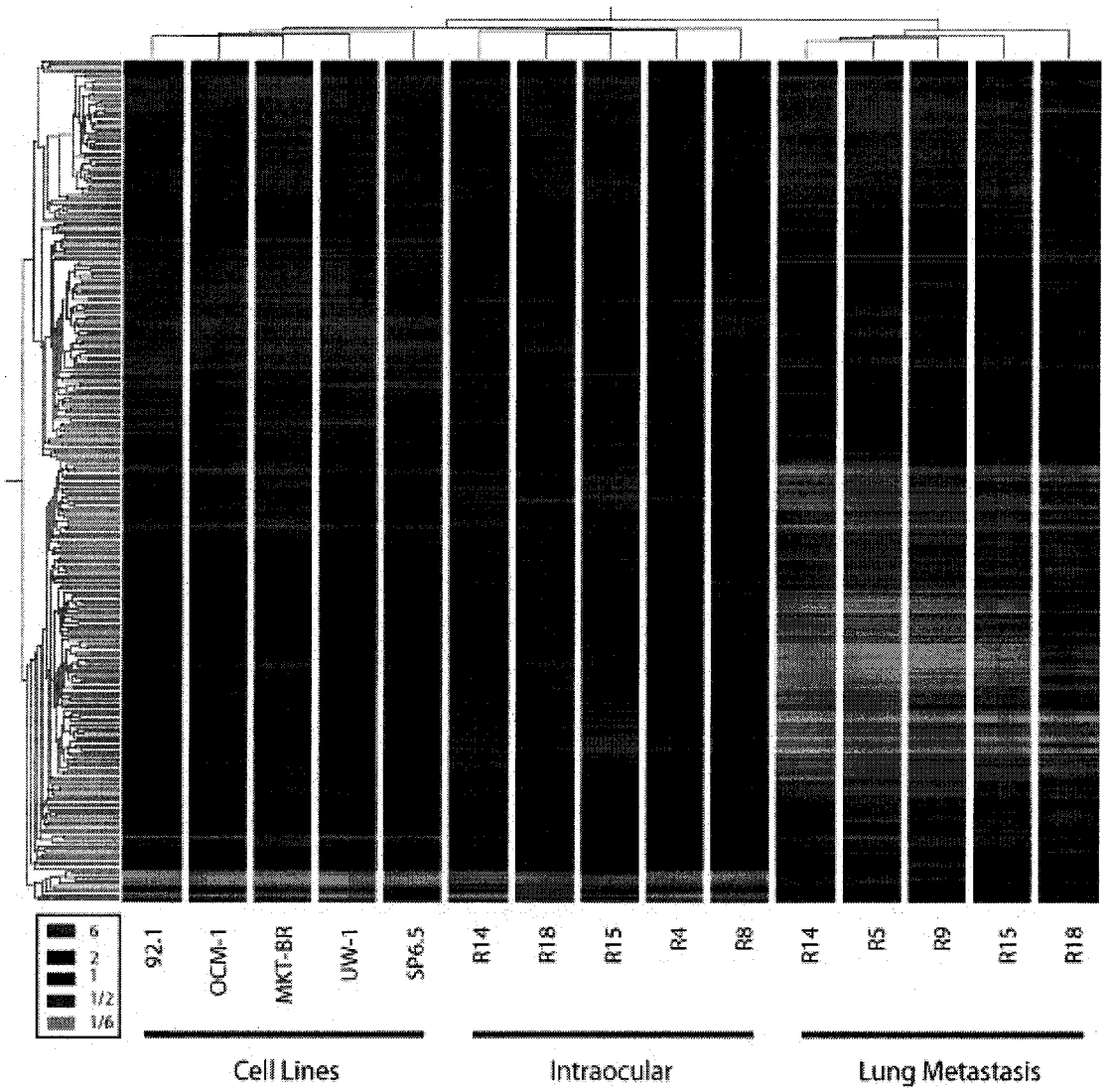

Figure 4.21) Transcriptional Profile of the Uveal Melanoma Cell Lines, Intraocular Tumours and Metastases.

The Figure shows the transcriptional profiling of the relationship from cell line to the intraocular tumour to metastasis samples from five different rabbits. Two dimensional hierarchical clustering of 314 genes with statistically significant changes in transcript abundance between *in vitro* cell lines, intraocular uveal melanomas and the lung metastatic tumours. Each gene is represented on the Y-axis while each cell line or solid tumour is on the X-axis. The average and normalized fluorescence ratio between the sample RNA and the Universal RNA are represented as a green to red colour scale.

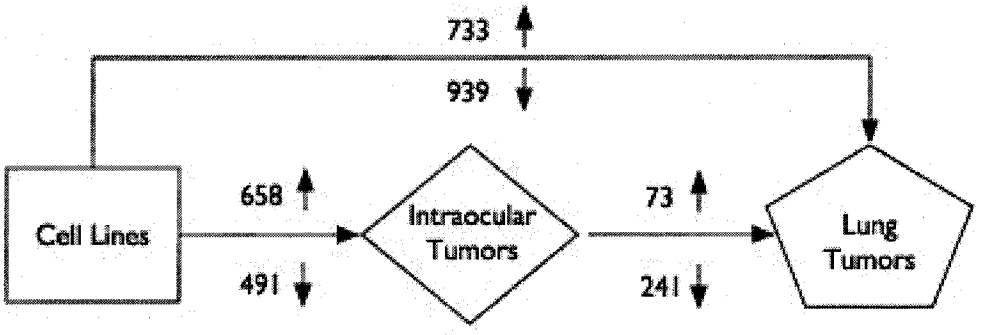

Figure 4.22) The Number of Significantly Modulated Transcripts Between Each Location.

Number of significantly modulated transcripts between uveal melanoma cell lines, primary uveal tumours and the lung metastatic lesions. Transcriptional profiles from each pair of samples were compared using the Welch t-test and an FDR of less than 0.05. Arrows indicate the number of transcripts with an increase or a decrease in abundance between the samples on the left and the ones on the right.

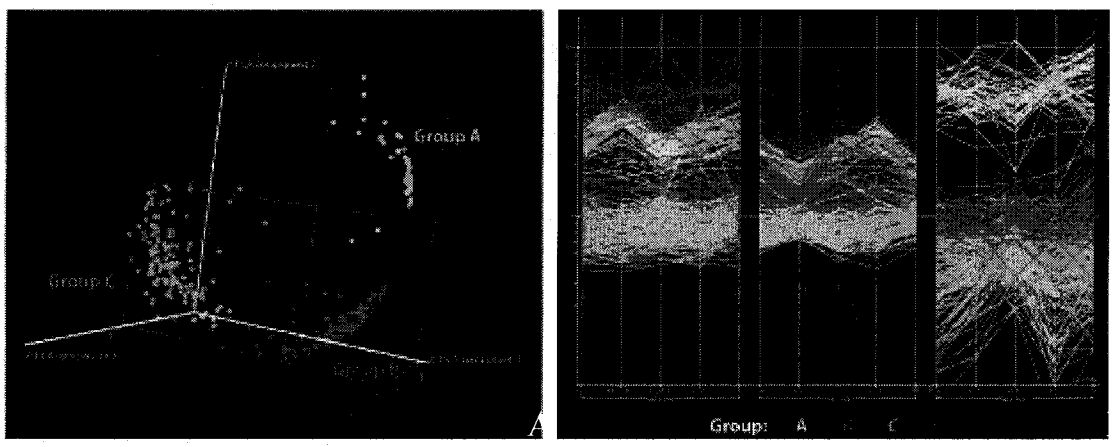

Figure 4.23) The Separation of the Significant Transcripts into Four Groups

A) The 314 transcripts that best differentiate the separate locations from one another were classified into four separate groups based on Principal Components Analysis. B) The log increase or decrease of these transcripts is shown plotted across each sample.

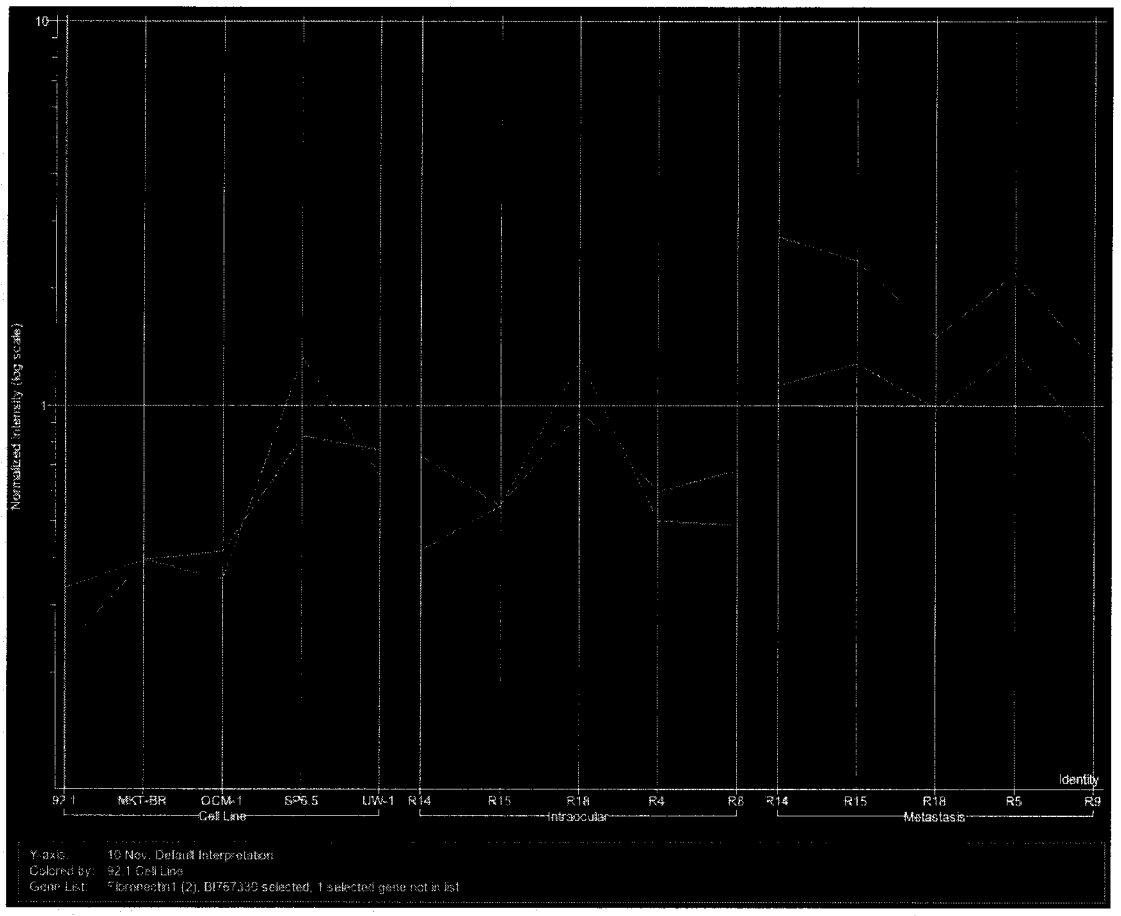

Figure 4.24) The Relative Abundance of mRNA for Fibronectin 1

The figure shows the increase in the transcriptional abundance of Fibronectin 1 as we go from the five uveal melanoma cell lines to intraocular to metastatic tissues.

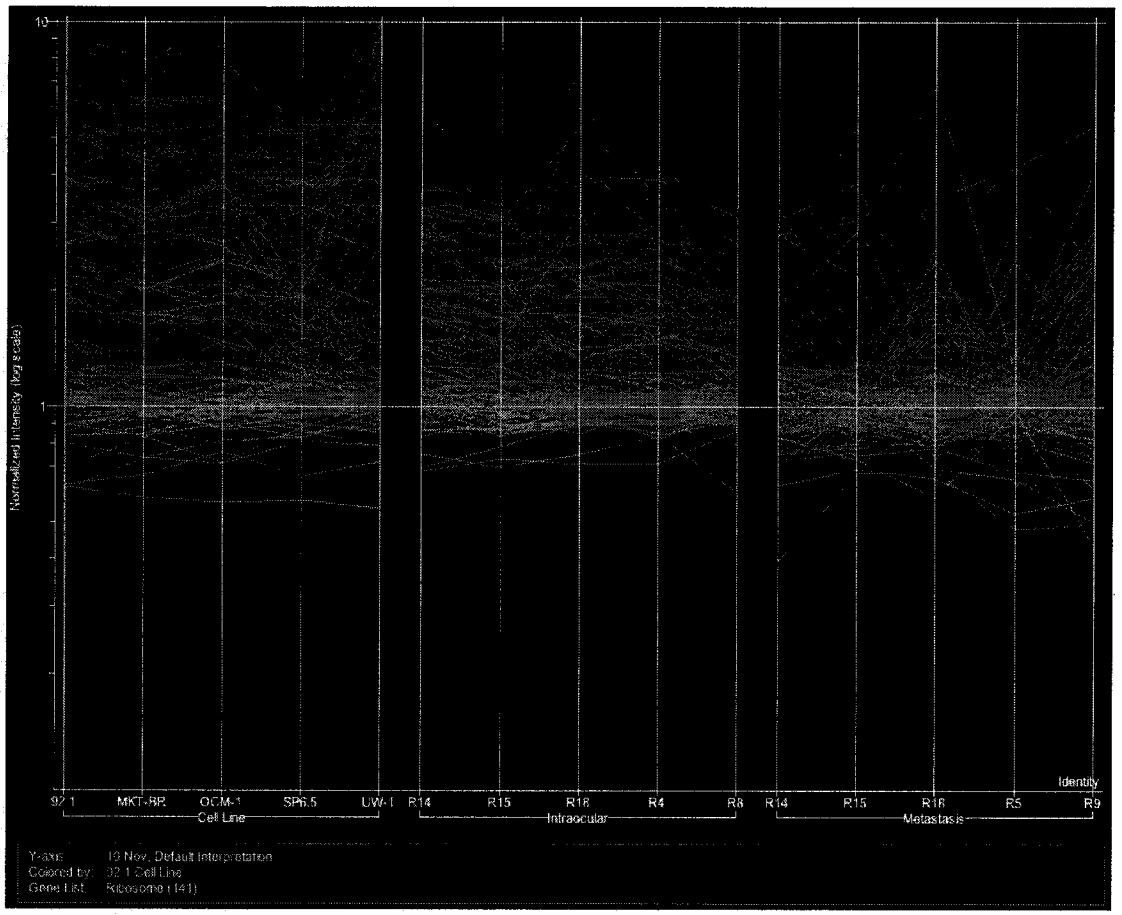

Figure 4.25) Relative Transcriptional Abundance of Ribosomal Proteins

This figure depicts the relative transcriptional abundance of ribosomal proteins for the different locations including the five human uveal melanoma cell lines, the intraocular tumour tissue samples and the metastatic lung nodules from the five rabbits. The general trend for the ribosomal proteins is a decrease in abundance with progression from cell line to intraocular to metastatic tissue.

4.2.4 Transcriptional Profiling of Circulating Malignant Cells and Re-Cultured Cells

At the time of sacrifice, circulating malignant cells (CMCs) were isolated from the peripheral blood of the rabbits using the Ficoll-Paque Plus method as previously described. At the same time, cells were isolated from the intraocular tumour and metastatic lesions and grown in culture under the same conditions as the original 92.1 cell line. RNA was then extracted from four cultures of re-cultured cells from each location, namely intraocular, CMCs and metastasis, and analyzed with DNA microarrays using the same methods as for the tissue samples.

We were worried that the process of re-culturing these cells after isolation from the rabbits would lead to a reversion of cells to the same transcriptional profile as seen in the original 92.1 cell line. To this end we compared the re-cultured data directly to the original cell lines, which revealed 207 significant changes that were at least two fold different from the 92.1 cell line as seen in Figure 4.27.

The resulting transcriptional profiles from the re-cultured cells are illustrated in Figure 4.26. No statistically significant changes were seen between the CMCs when compared to the intraocular or metastatic re-cultured cells alone. A total of 61 gene transcripts were discovered to be statistically different between the intraocular and metastatic re-cultured cells. Profiling data suggest that some of the CMC lines represent an intermediate step between these two other stages. A direct comparison with the cell line data is shown in Figure 4.29 to demonstrate

that the profiles of 61 genes did not change during the significant adaptation between *in vitro* culture and solid tumours but rather in the primary to secondary metastasis transition. Among the transcripts substantially up-regulated in the progression of re-cultured cells from intraocular, to CMC to metastasis were: Interleukin 1 Receptor, Insulin Receptor Substrate 2, Septin 7, Matrix metalloproteinase 2, Hemecentin, Glypican 3, Clusterin, and Cholecystokinin. A group of four modulators of small GTPases were also seen to increase: Rabphilin 3A, Syntaxin, Ral GPS2 and IQGAP2. Finally, transcripts that were substantially decreased in cells cultured from intraocular to CMC to metastasis included the melanoma specific markers Melan A, CD63 and SILVer. In addition, Alpha Kinase 3, Neuregulin, Thrombospondin 1, Dystonin and tissue inhibitor of metalloproteinase 1 decreased in expression.

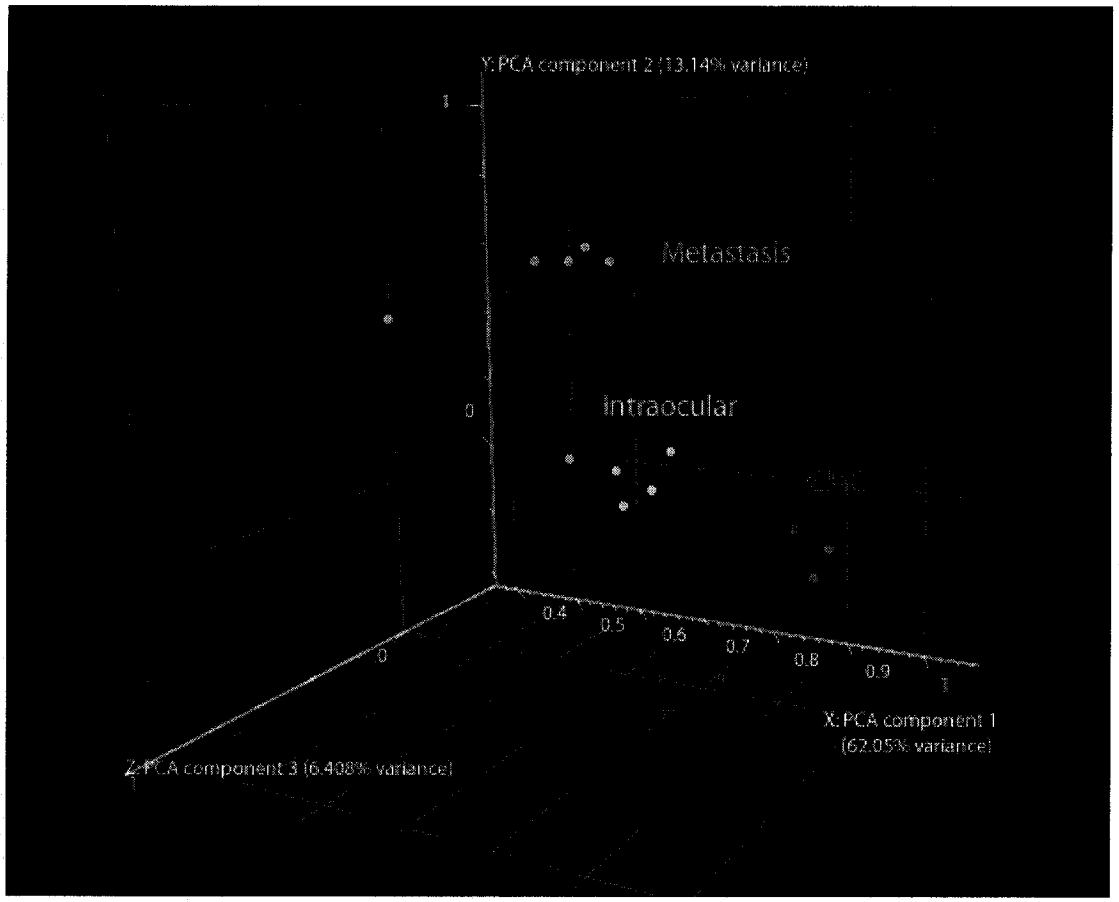

Figure 4.26) Principal Components Analysis for the Re-Cultured Data

A Principal Components Analysis was done for the re-cultured data. As seen, the CMC data clusters by itself, independent of the original 92.1 uveal melanoma cell line and separate from the intraocular or metastasis re-cultured cell data.

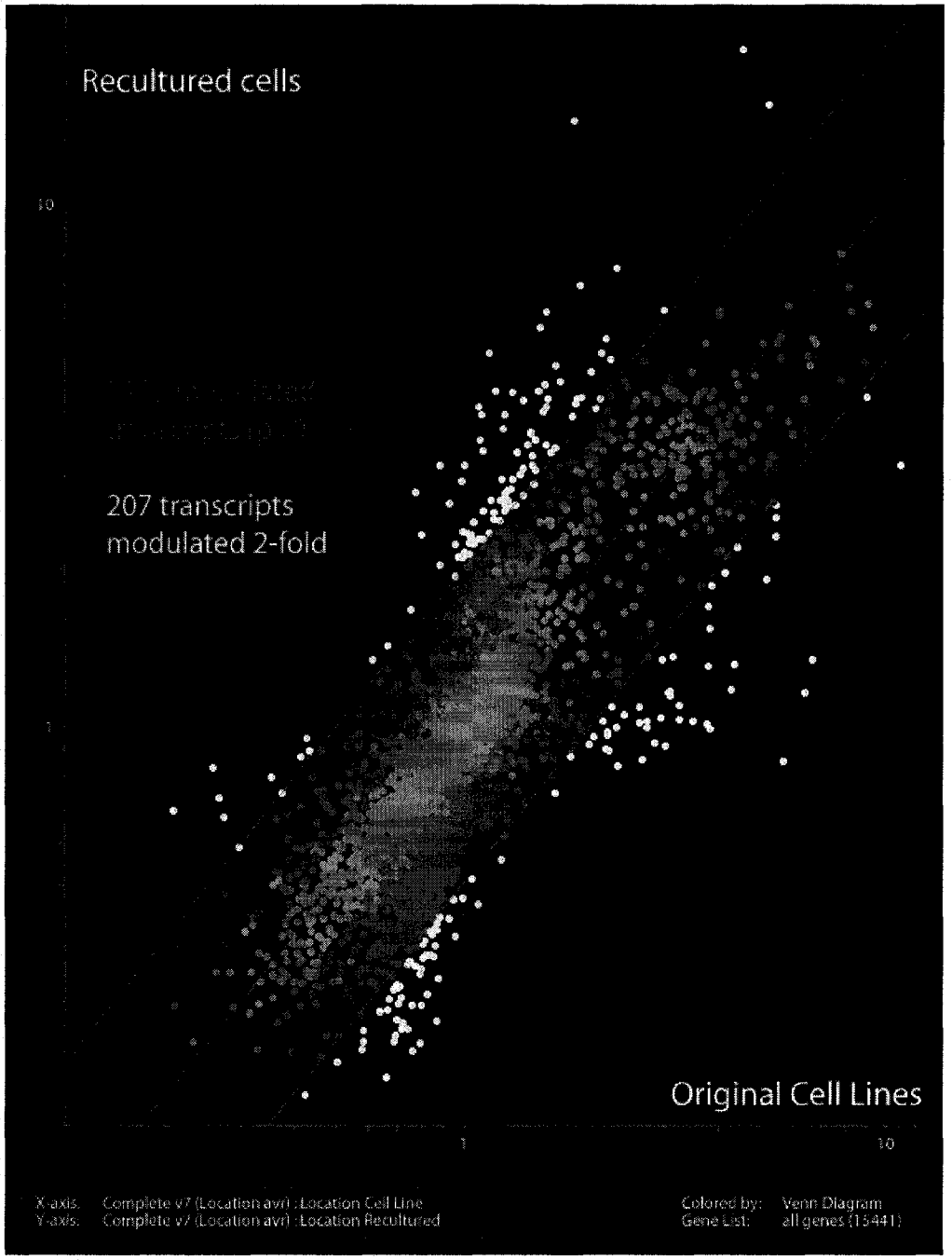

Figure 4.27) Scatter Plot of the Re-Cultured Cells Versus the Original Cell Lines

A scatter plot was used to demonstrate the changes that the re-cultured CMCs had maintained in culture as compared to the original 92.1 cell line. There were 3123 transcripts found to be significantly different than the original cell line, with 207 of these having at least a twofold difference.

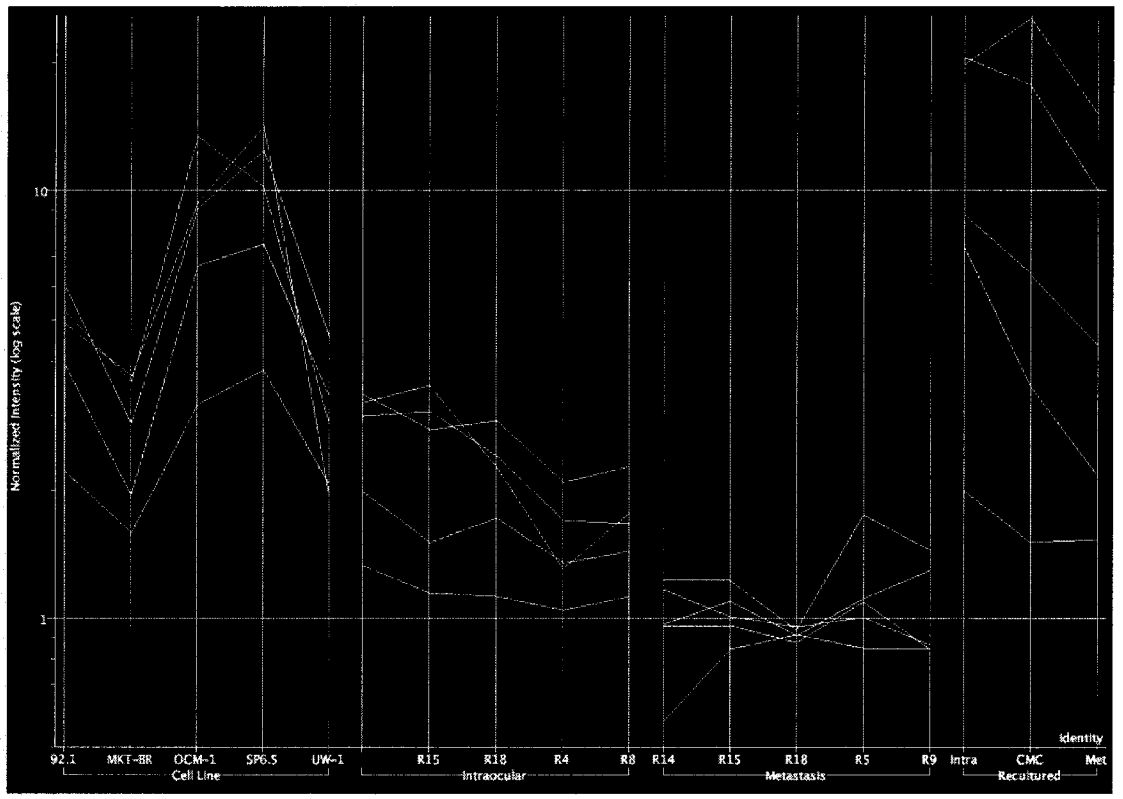

Figure 4.28) The Transcriptional Abundance of Melanoma Specific Markers

The decrease in melanoma specific markers (Melan A, CD63, SILVer) can be seen in this figure. The first area shows the relative expression of these markers in the five human uveal melanoma cell lines. The next shows the expression in the intraocular tumour tissues. The third shows the expression from the metastatic tissue. The fourth area shows the expression from the re-cultured cells isolated from the intraocular tumours, CMCs and metastases, which follows the same trend as the expression in the tissue.

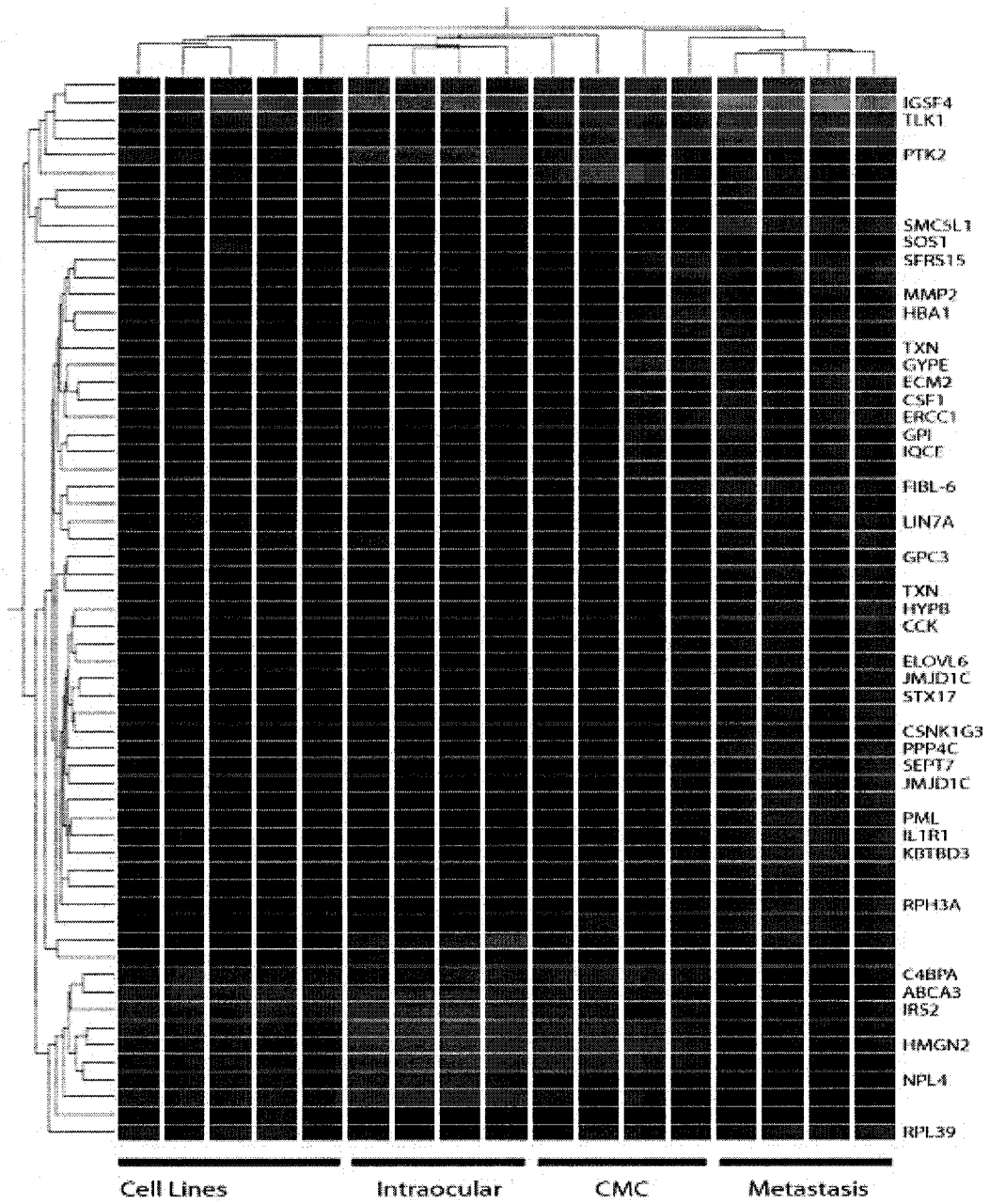

Figure 4.29) Transcriptional Profile of Re-Cultured Cells from Each Location Compared to the Original Cell Lines

Transcriptional profiles of the re-cultured cells as compared to the original cultured uveal melanoma cell lines. The hierarchical clustering of the profiles from 61 gene transcripts from the original cell lines or from re-cultured cells isolated from intraocular tumours, circulating malignant cells or lung metastasis are shown.

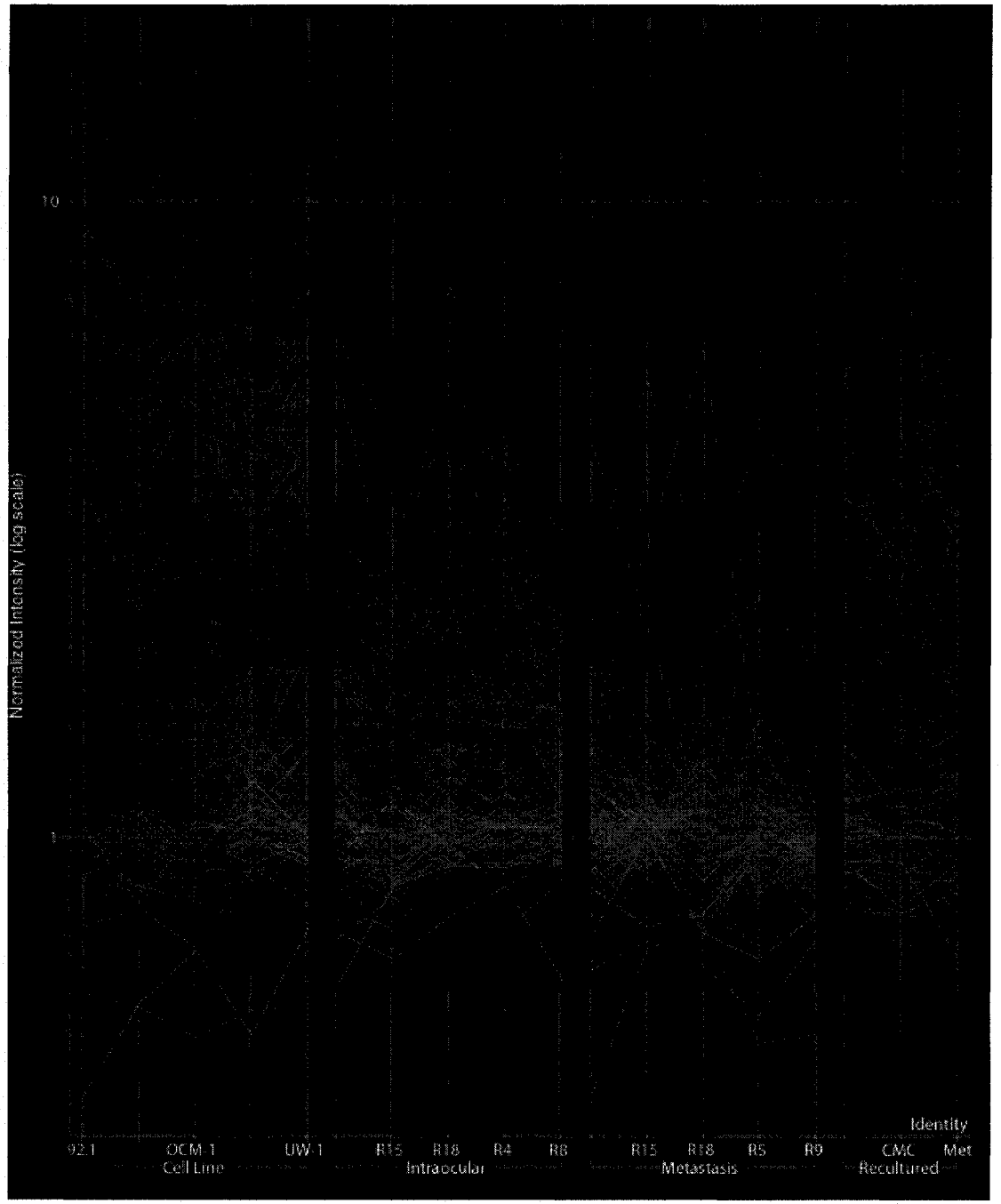

Figure 4.30) Relative Abundance of Ribosomal Proteins

The transcriptional abundance of ribosomal proteins was plotted and compared to the original intraocular and metastatic tissue as described previously. The re-cultured cells maintained the same pattern of ribosomal protein expression as seen in the isolated tissue, with a decrease in abundance as they went from intraocular to CMC, to metastasis.

4.2.5 Quantitative Real Time PCR Validation

Real-time PCR analysis of the mRNA confirmed the microarray results for six selected genes. The levels of ALPK3, IRS-2, Fibronectin 1 and Septin 7 increased from cell culture to primary tumour, to metastasis, thereby confirming their classification into Group A as shown in Figure 4.31. The levels of Melana A, as shown in Figure 4.32, decreased from cell culture to primary tumour, to metastasis, thereby confirming the classification of this gene into Group B. The mRNA levels for ATF4 are shown in the same figure, however, these revealed an increase in expression from cell line to intraocular, with a subsequent decrease in expression from intraocular to metastasis. This decrease in expression from intraocular to metastasis still allows for its classification into Group B.

Melting curve analysis of each of the products from the quantitative real time PCR revealed the formation of a single product, indicating good specificity and limited contamination of our samples as shown in Figure 4.33. Non-specific amplification would have revealed several different products through the melting curve analysis, each with a different denaturation temperature.

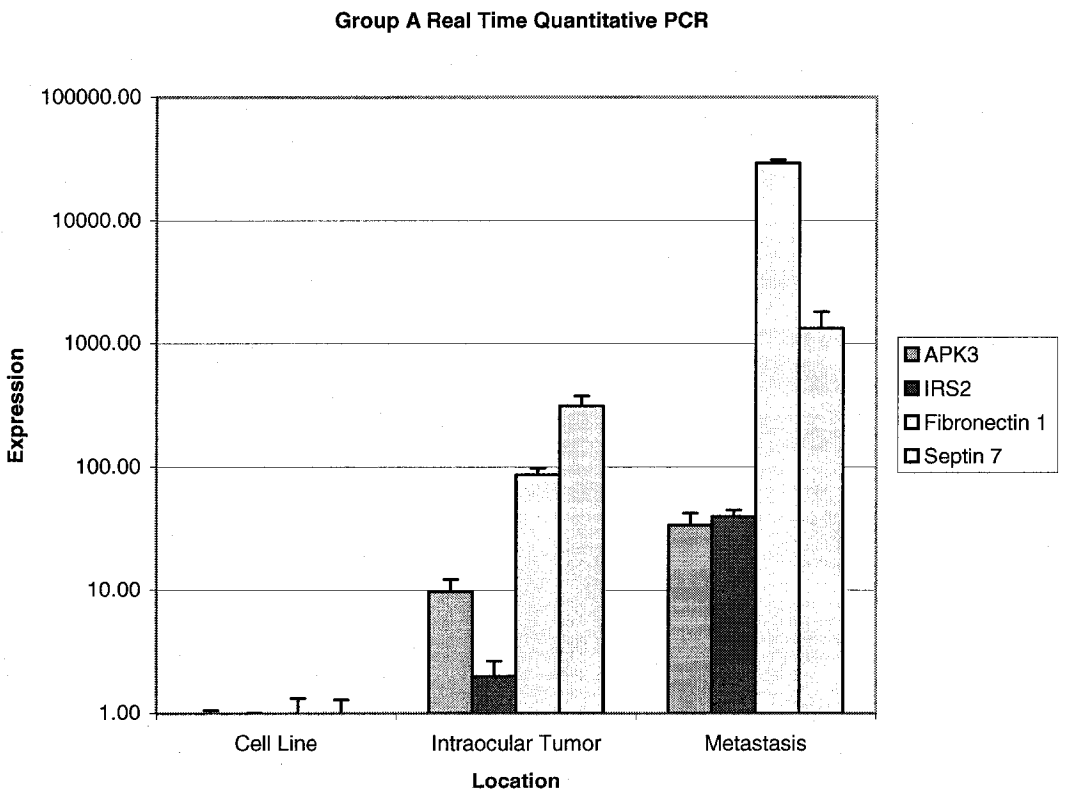

Figure 4.31) Quantitative Real Time PCR Data from Group A Genes

Real Time PCR data showing the expression levels of selected Group A genes, alpha kinase 3 (APK3), insulin receptor subunit 2 (IRS-2), Fibronectin 1 and Septin 7 from the cell line, intraocular tumours and metastatic lesion samples.

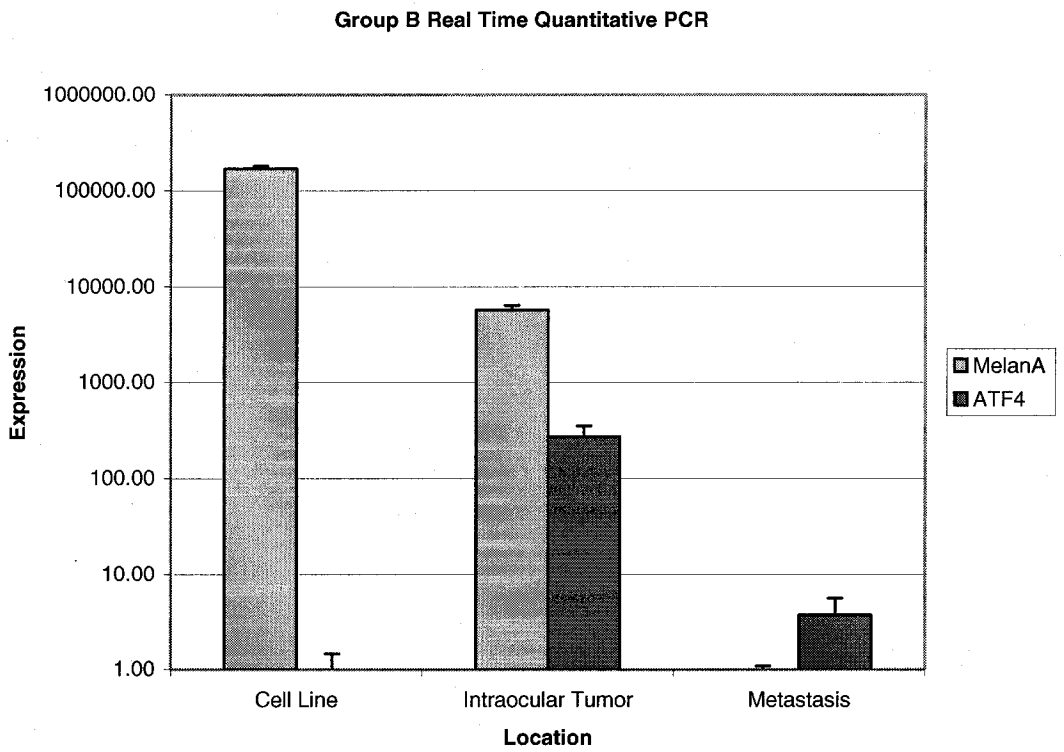

Figure 4.32) Quantitative Real Time PCR Data from Group B Genes

Real Time PCR data showing the expression levels of selected Group B genes, Melan A and ATF4 from the cell line, intraocular tumours and metastatic lesions of the samples.

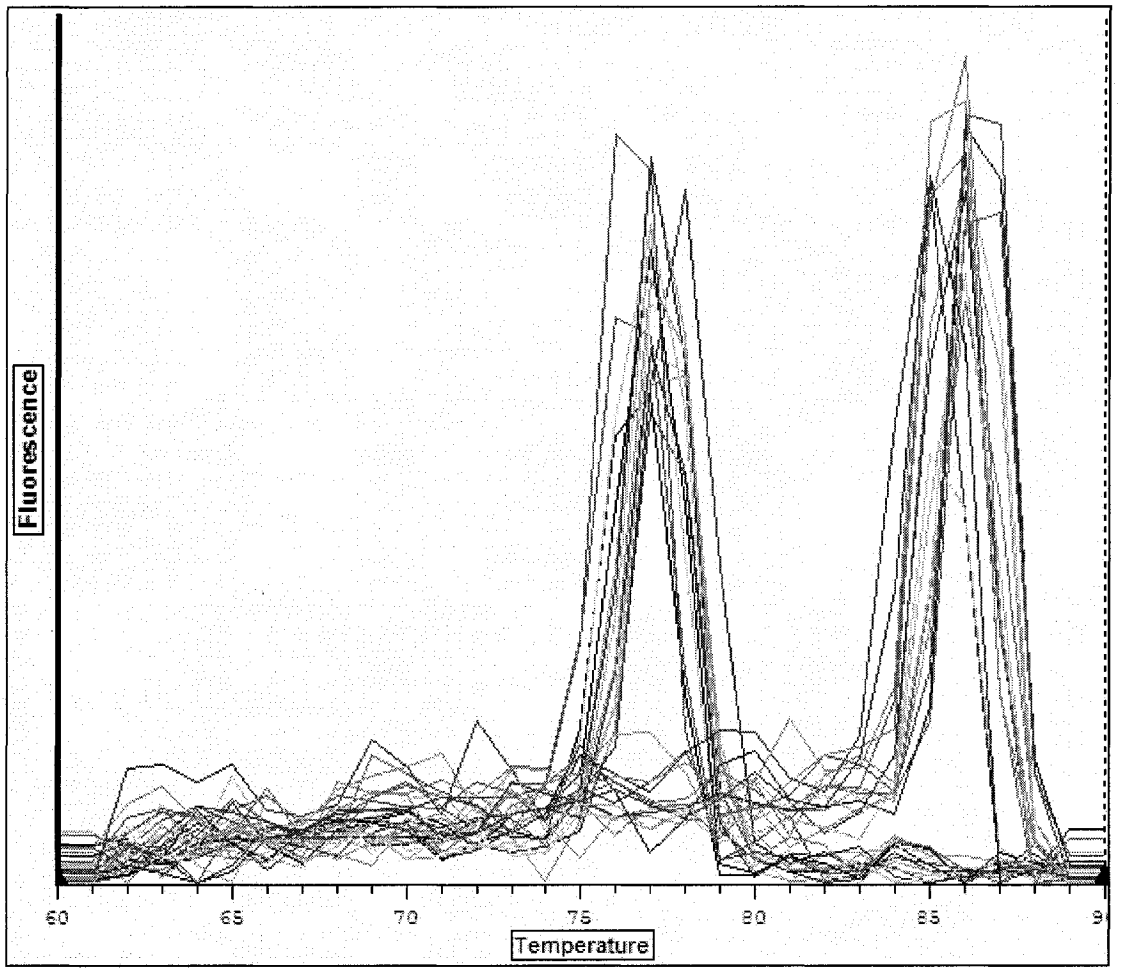

Figure 4.33) Melting Curve Analysis of Quantitative Real Time PCR Results

These melting curve analysis results are from the intraocular tumour samples with Melan A primer pair. The first set of peaks at approximately 77°C represents the Melan A products. The second set of peaks at approximately 85°C represents products of Beta Actin primer, which was used as the housekeeper gene for purposes of normalization.

4.2.6 Proliferation Assay

Ribosomal proteins clustered together in Group B, which decreased in abundance from intraocular to metastasis. Ribosomal proteins are considered a good indicator of the proliferation rates of cells in the samples. We performed an established proliferation assay to see if the re-cultured cells from the original 92.1 cell line, intraocular tumour, CMC and metastasis showed a similar decrease in proliferation rates over two time points (48 and 72 hours) as shown in Figure 4.34. The re-cultured cells isolated from the intraocular tumour showed a significant increase in proliferation from the original cell line ($p < 0.001$). The cultured CMCs showed a subsequent significant decrease in proliferation from the re-cultured intraocular cells, with the re-cultured metastatic cells showing a further decrease in proliferation ($p < 0.001$). The CMCs showed no significant change as compared to the original 92.1 cell line ($p = 0.48$). The re-cultured metastatic cells showed a significant decrease in proliferation as compared to the original 92.1 cell line ($p < 0.05$).

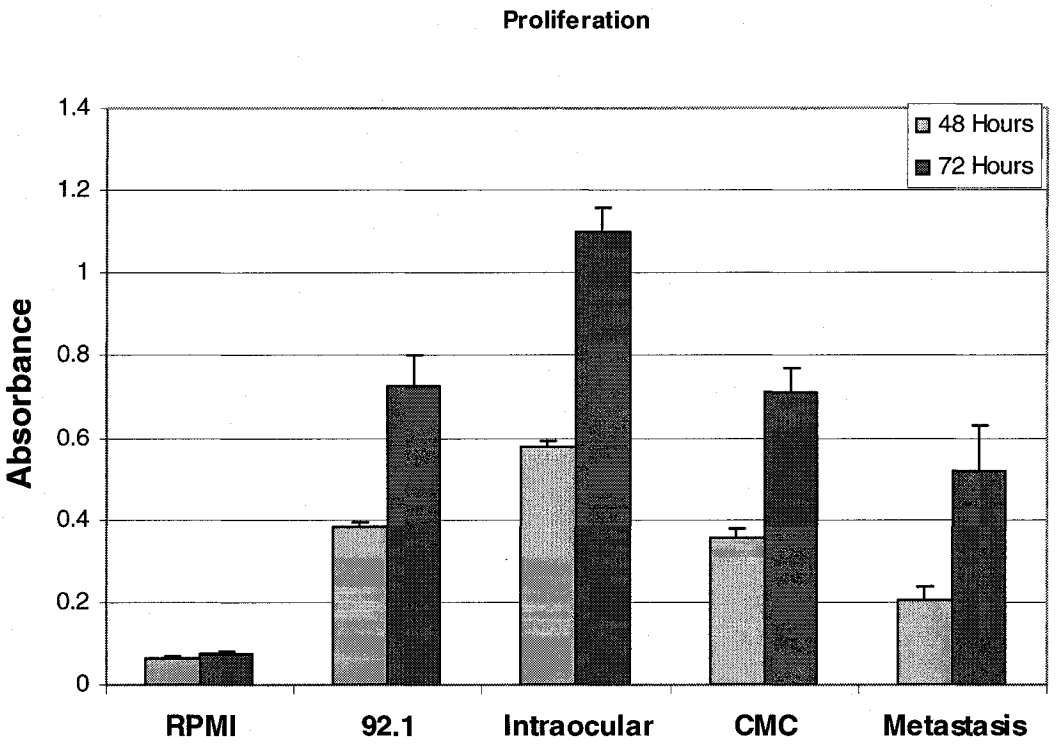

Figure 4.34) Proliferation Results for 48 and 72 Hours

Proliferation assay results from the original cell line, re-cultured intraocular, CMCs and re-cultured metastasis cells. There is a general decrease in proliferative ability as the cells go from intraocular to CMC, to metastasis.

4.2.7 Invasion Assay

The invasion assays were carried out with the re-cultured cells for 48 and 72-hour time points. These experiments investigated the ability of our cells to invade through an artificial basement membrane, Matrigel, towards a specific chemoattractant (VEGF) as shown in figure 4.35.

There was no significant change between the re-cultured intraocular tumour cell invasive ability as compared to the original 92.1 cell line in response to VEGF and 10 percent FBS. A significant increase in invasive ability as compared to the original cell line was seen for the CMCs after 72 hours of incubation ($p < 0.05$). An even more significant increase in proliferation ability was seen in the re-cultured metastatic cells during both 48 hour incubation ($p < 0.01$) and 72 hours ($p < 0.001$).

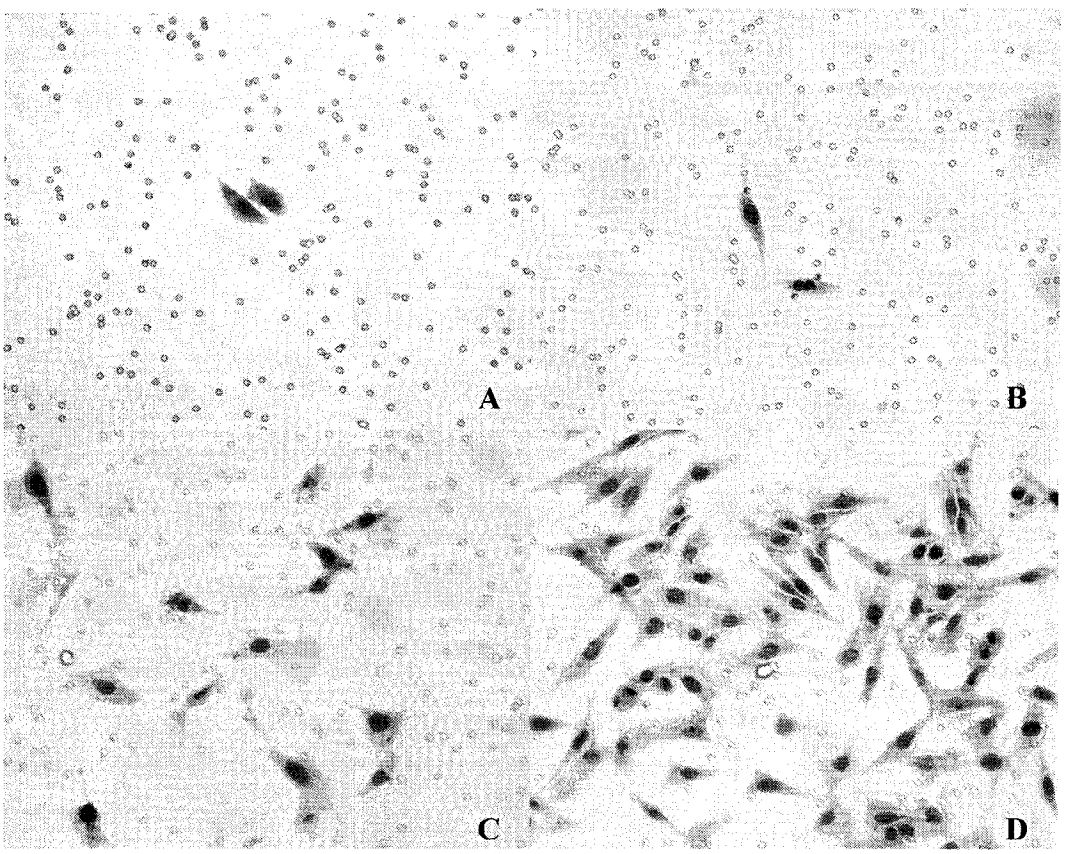

Figure 4.35) Invasion Assay Results

Photomicrographs (20X) of the cells that invaded into the Matrigel invasion assay a) the original 92.1 cell line b) re-cultured intraocular cells c) circulating malignant cells d) re-cultured metastatic cells.

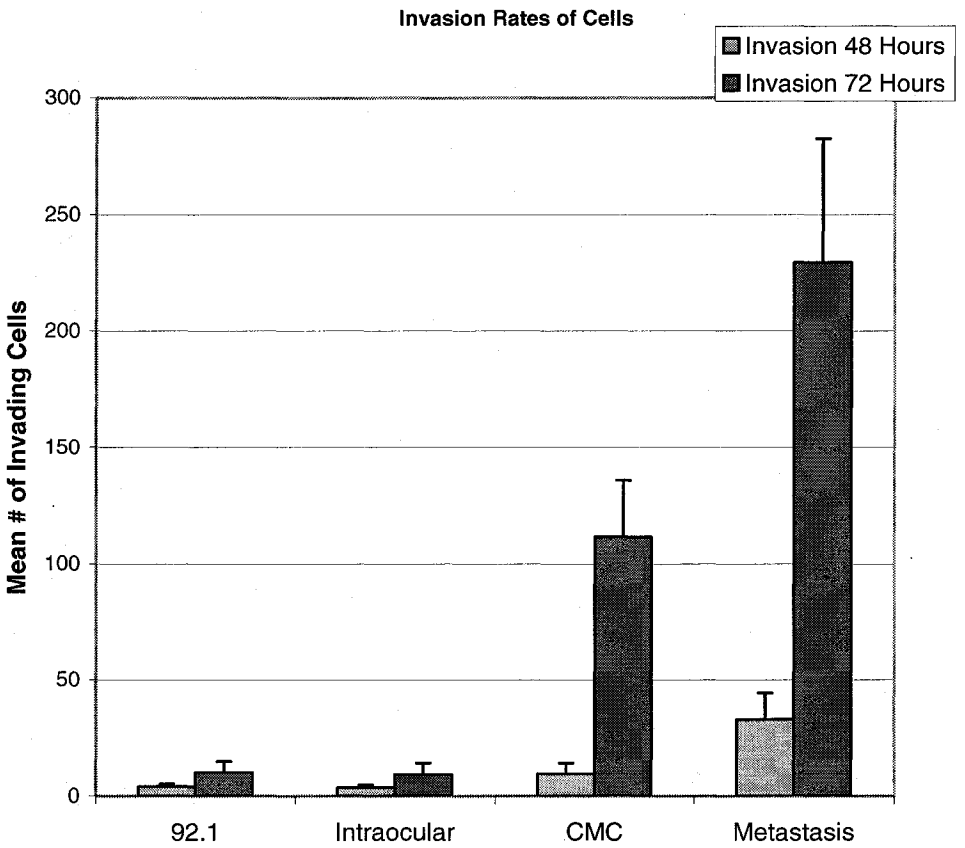

Figure 4.36) Invasive Ability of Re-Cultured Cells

The invasive ability of the re-cultured cells and the original 92.1 cell line with VEGF and 10 percent FBS as a chemoattractant is shown. The CMCs have a significant increase in invasive ability during the 72 hour time point, with the re-cultured metastatic cells having a significant increase in invasive ability for both time points.

4.2.8 Fibronectin Adhesion

The ability of the five human uveal melanoma cell lines to bind to fibronectin was measured using a colourimetric fibronectin adhesion assay. Based on these results we were able to divide the five cell lines into two groups, high and low adhesion (Figure 4.37). Three of the cell lines had a high adhesive ability (MKT-BR, OCM-1, UW-1) while the other two had low adhesive ability (92.1, SP6.5). These two groups correlated well with previously described metastatic potential and invasive ability of the cells [70].

We then compared the ability of these re-cultured cells to adhere to fibronectin back to the original 92.1 cell line as shown in figure 4.38. Even though 92.1 has a low ability to bind to fibronectin, the re-cultured cells from the intraocular tumours had a significantly decreased ability to bind to fibronectin ($p < 0.01$). The CMCs had a significantly increased ability to adhere to fibronectin compared to the re-cultured intraocular cells ($p < 0.001$) and the original 92.1 cell line ($p < 0.05$). This increase was maintained by those cells re-cultured from the metastasis; there was no significant difference between the CMCs and re-cultured metastatic cells ($p = 0.34$).

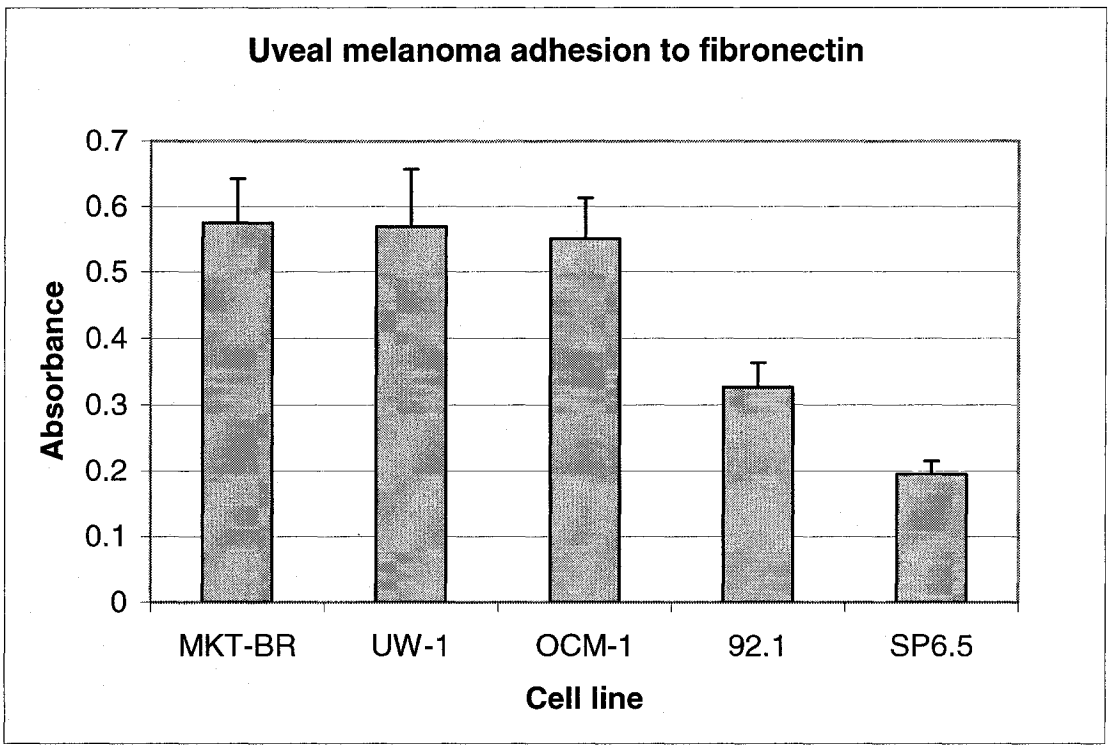

Figure 4.37) Fibronectin Adhesion Assay Results for the Five Cell Lines

The averaged adhesive ability of the five uveal melanoma cell lines to bind to fibronectin is shown. Three of the cell lines had a high adhesive ability (MKT-BR, OCM-1, UW-1) and two had a low adhesive ability (92.1, SP6.5).

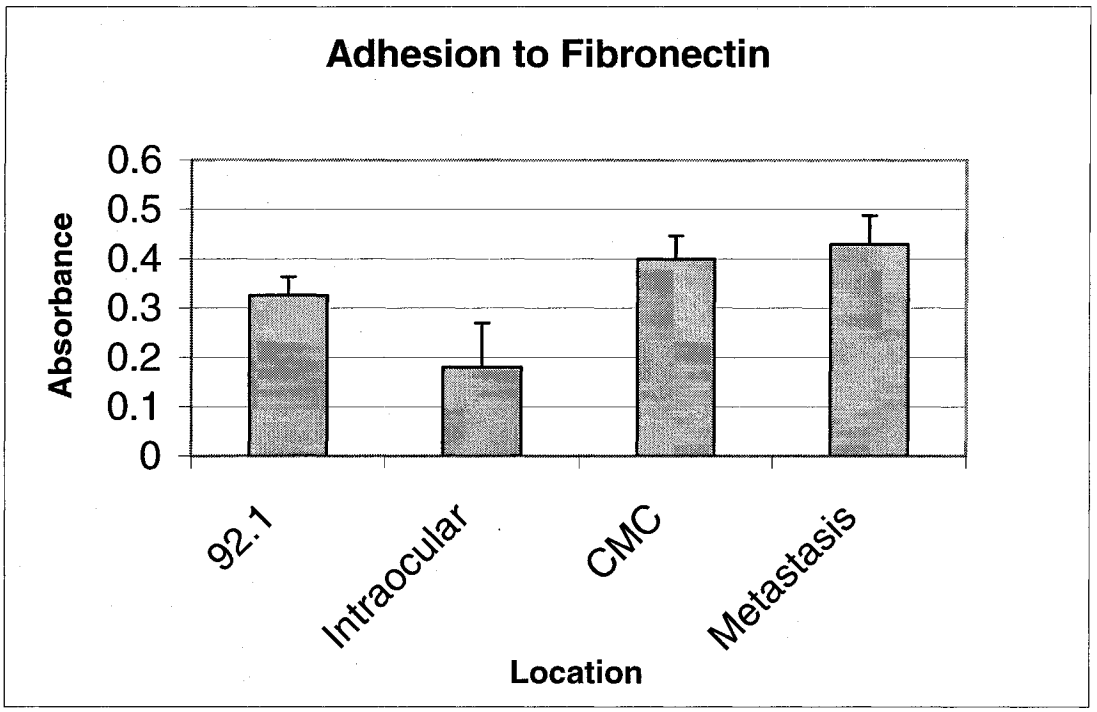

Figure 4.38) Fibronectin Adhesion Assay Results for Re-Cultured Cells

The ability of the re-cultured cells to adhere to fibronectin was compared to the original 92.1 cell line. The re-cultured cells from the intraocular tumours had a significantly decreased adhesive ability, while the CMCs and re-cultured metastasis cells had an increased binding ability.

4.3 Array Comparative Genomic Hybridization

4.3.1 Genomic DNA Quantification and Validation

Three different methods for extracting genomic DNA from the paraffin-embedded intraocular tumour sections were compared. The extracted DNA from each of these methods was compared using UV spectrophotometry and NanoDrop analysis (Table 4.1 and Table 4.2). The intraocular tumour sections, before and after LCM as well as the cap, were imaged and are shown in Figure 4.39.

The least amount of usable genomic DNA was isolated using the Laser Capture Microdisection technique with an average yield of approximately 1 ng/ul with no detectable DNA yield from one of the three samples. The LCM also yielded the worst purity ratios compared to the other two methods. The Pin Point Isolation system yielded better DNA quantity, ranging from 1.64 to 8.18 ng/ul and purity ratios ranging from 1 to 2.72. The macroscopic extraction method led to the best yield of DNA from the paraffin-embedded tissue, ranging from 10.3 to 55.61 ng/ul. The purity ratios were best from this method as well, ranging from 1.84 to 2. This method therefore gave the best genomic DNA yield and purity ratios from the three tested methods as shown in Table 4.1 and Table 4.2.

The extracted DNA was then run on an agarose electrophoresis DNA gel to view the extent of degradation. All samples displayed degradation to at least a minor extent, with typical band smearing showing on the agarose gels as shown in figure 4.40. The greatest amount of degradation was seen in the LCM samples, with the macroscopic extraction method yielding the least degradation in the samples.

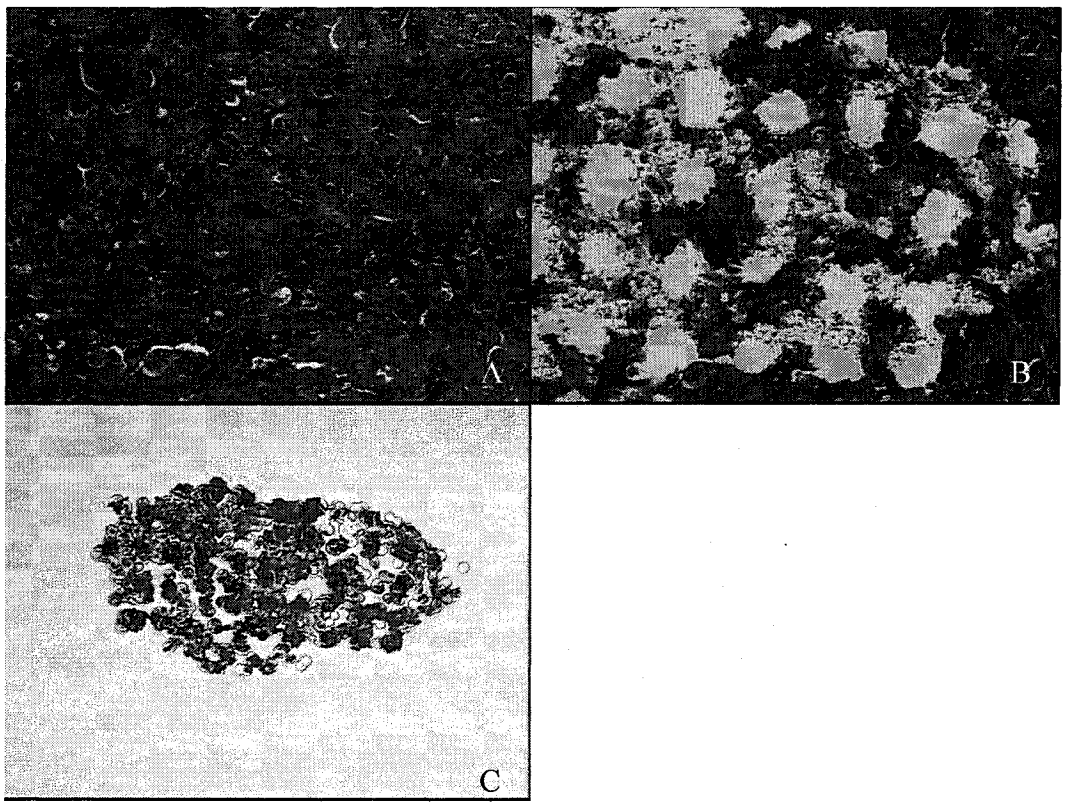

Figure 4.39) Laser Capture Microdisection of Intraocular Tumour Specimen

a) Section of the H & E stained intraocular tumour prior to LCM. The laser indicator is shown as the bright dot in the middle of the image. b) The intraocular tumour section after LCM. c) the LCM cap containing the isolated intraocular tumour cells.

DNA Quantity ng/ul	LCM	Pin Point Isolation	Macroscopic Extraction
R21	1.00	2.27	16.95
R26	-	1.64	10.30
R28	1.10	8.18	55.61

Table 4.1) Quantity of DNA Extracted from Paraffin

The quantity of extracted DNA from the paraffin embedded intraocular tissue is shown. The results are listed in ng/µl concentrations, with the macroscopic extraction yielding the highest levels of DNA.

DNA Ratio 260/280	LCM	Pin Point Isolation	Macroscopic Extraction
R21	1.25	2.72	1.84
R26	-	1.00	1.96
R28	1.278	1.40	2.00

Table 4.2) Quality of DNA Extracted from Paraffin

The 260 to 280 nm ratio of extracted DNA from the paraffin-embedded intraocular tissue is shown. The quality of the extracted DNA from paraffin embedded tissues is shown, with the macroscopic extraction technique yielding the best ratios.

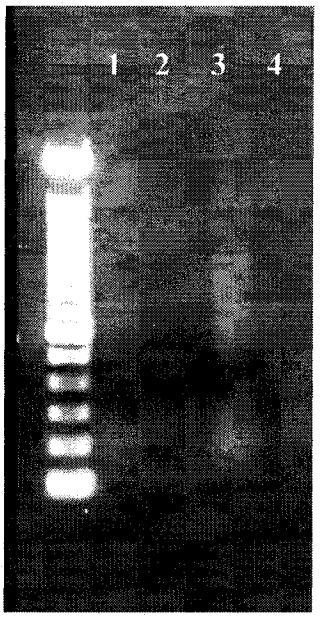

Figure 4.40) Picture of the Agarose DNA Gel Electrophoresis from LCM DNA

The agarose gel from the DNA extracted using the LCM method. Lane one contains the DNA ladder. Lane two is from the R21 sample, lane three from R28 and lane three from R26. The typical smearing of degraded DNA is seen for both lanes containing DNA, while lane 2 appears to be empty, verifying the Nano Drop results from R28.

4.3.2 Array Comparative Genomic Hybridization

Based on the quantity of genomic DNA that was isolated as well as the quality of the DNA, seven different samples were labelled for comparative genomic hybridization on the arrays (figure 4.41). The reference DNA was from a normal adult female with no known genetic abnormalities and our 92.1 cell line was isolated from a male patient. Therefore we expected that the X chromosome would be picked up as a deletion. Figure 4.42 shows the results for all seven hybridized chips and the control DNA. The two arrays that were used for hybridizing the LCM extracted DNA failed to detect the loss of the X chromosome. The two arrays that were used for hybridizing the DNA with the Pin Point system showed only partial areas of deletion of the X Chromosome. The three arrays that were hybridized with DNA from the macroscopic isolation technique showed almost entire loss of the X Chromosome.

Due to the amplification that was necessary with the LCM samples to increase the total amount of DNA to use with the aCGH, there was a significant amount of noise in these samples. The signal to noise ratio was below the acceptable limits according to the CGH analytics software and this noisy data can be seen in all of the results from the two arrays that were used with this extracted DNA. The DNA that was extracted using the Pin Point isolation system had to be purified twice before it was acceptable for use with the CGH arrays. Even with this double purification, the hybridized DNA yielded a signal to noise ratio that was marginal. This ratio was just at the acceptable limit according to the CGH analytics software and the hybridized DNA yielded data that had a significant

amount of noise as well, although less than the data from the LCM DNA. The DNA extracted using our macroscopic technique yielded the best signal to noise ratio, passing the quality control of the software.

These three arrays showed consistent results for each chromosome, while the other arrays failed to detect some of these changes or showed changes that were not detected by the three good arrays. Several deletions and amplifications were found to be consistent for all of the arrays through the genome. Of these, the largest was a sizeable amplification of chromosome 7 in the q arm (Figure 4.44). A smaller abnormality shown as a deletion in the chromosome 3, near q12.2 was observed in all of the arrays along with an amplification of the q28 region (Figure 4.43).

The amplification of the q arm of chromosome 7 is quite large, spanning the area of q21 to q35. This amplification contains several thousand genes, many of which are of unknown function. Among the known genes that are found in this area are Wnt2 and C-Met. These two genes are located close to one another at 7q31.2, which is located in the middle of the amplified area on this chromosome. Smaller deletions and amplifications can be seen throughout the genome. Of these the most significant ones were located on chromosomes 9, 11, 16 and 22.

A deletion from the high quality DNA was found for the majority of the q arm of chromosome 9, although this deletion was not seen with the DNA extracted using LCM or the Pin Point system. An area of amplification was seen on chromosome 11 in the p15 region from all of the DNA samples. A deletion was also seen on chromosome 11, in the q24 region, only from the DNA extracted

using the macroscopic extraction technique and not from the other two methods. A deletion was seen on chromosome 16, starting on p12.1 and continuing for the rest of the p arm, also from the DNA extracted using the macroscopic technique. A consistent area of amplification was seen on chromosome 22, in the q11 to q12.1 region in all DNA samples.

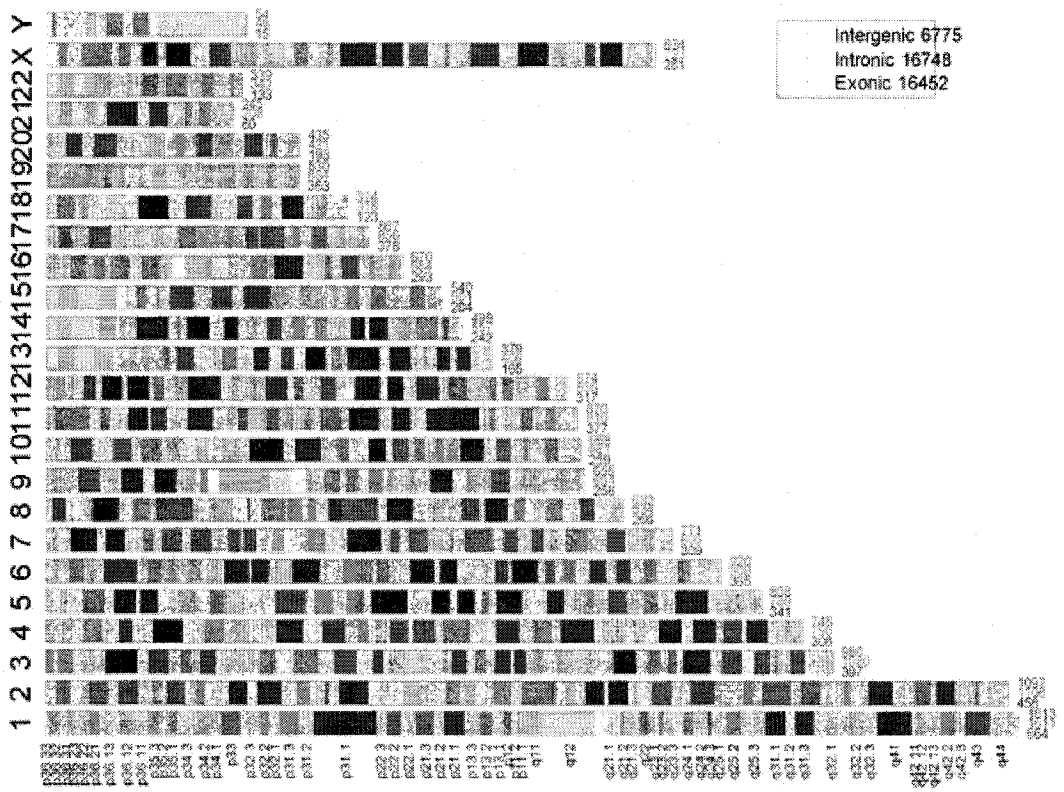

Figure 4.41) The Probe Spacing of the 44,000 Comparative Genomic Hybridization Arrays

The probe spacing from the 44,000 aCGH chips from Agilent, showing the 6,775 probes that are intergenic, the 16,748 probes that are intronic and the 16,452 probes that are exonic.

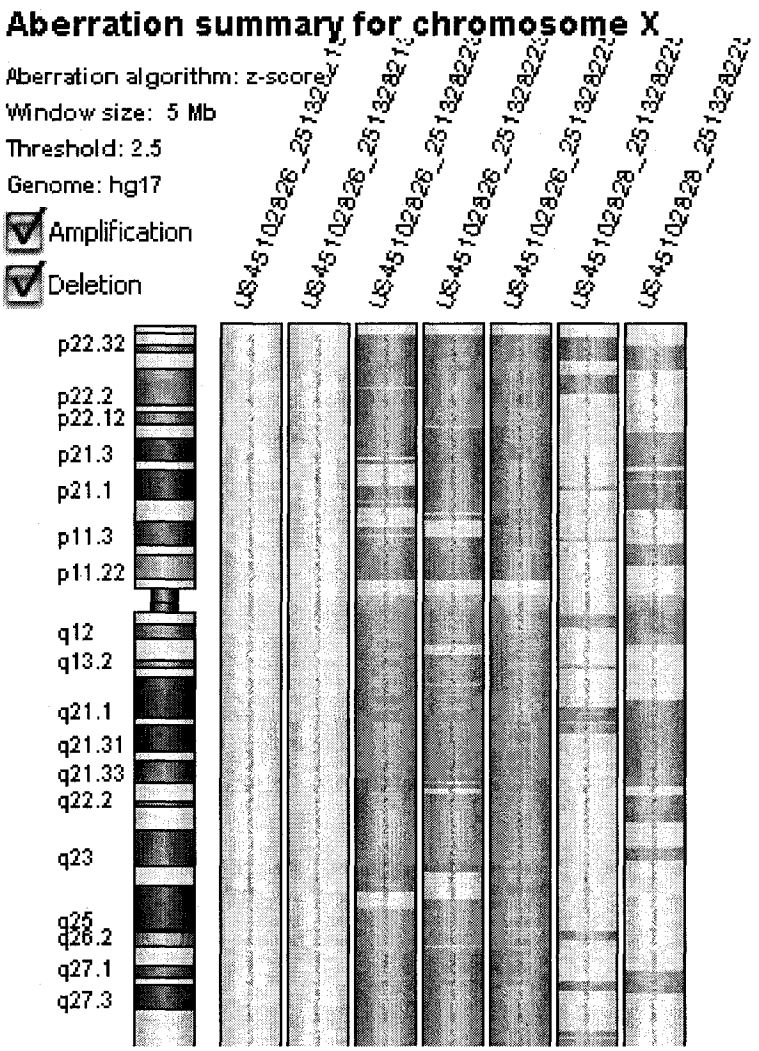

Figure 4.42) aCGH Analysis of the X Chromosome

The aCGH analysis of the X chromosome from the seven arrays that were hybridized from the genomic DNA extracted from the paraffin-embedded intraocular tissue. The control DNA is from a female adult; therefore, the X chromosome should be detected as a deletion. The first two arrays shown are from the LCM extracted DNA. The middle three are from the DNA extracted using the macroscopic technique. The last two arrays are from DNA extracted using the Pin Point system.

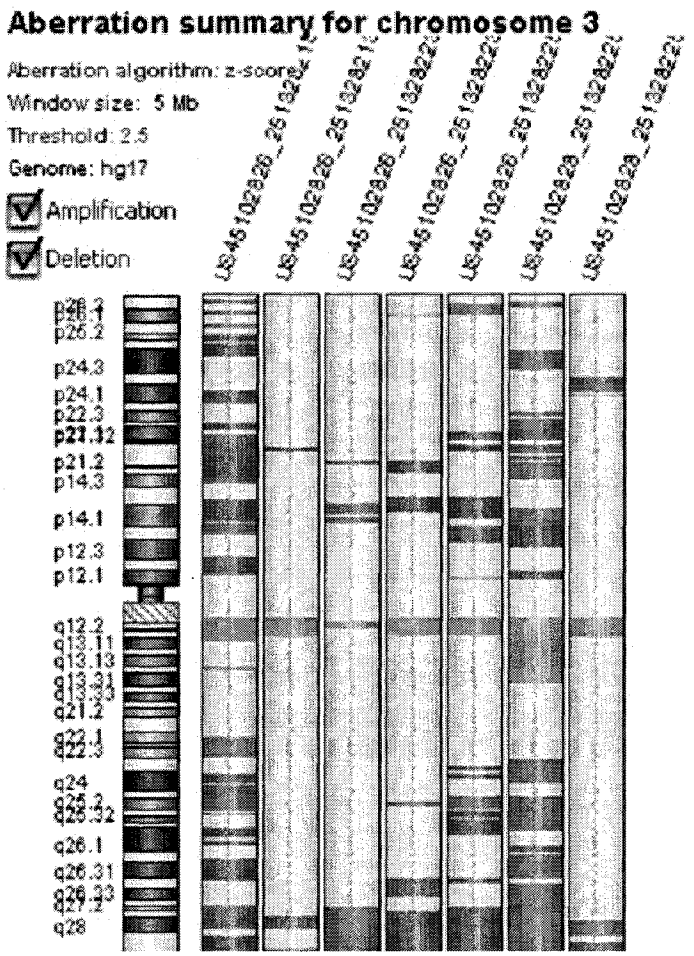

Figure 4.43) aCGH Analysis of Chromosome 3

The analysis of chromosome 3 showed a consistent deletion in the q12.2 region of chromosome 3 (in green), as well as an amplification of chromosome 3 in the q28 region (in red). The first two and last two arrays showed a considerable amount of noise that is not reproduced through the three arrays that were using the best quality DNA.

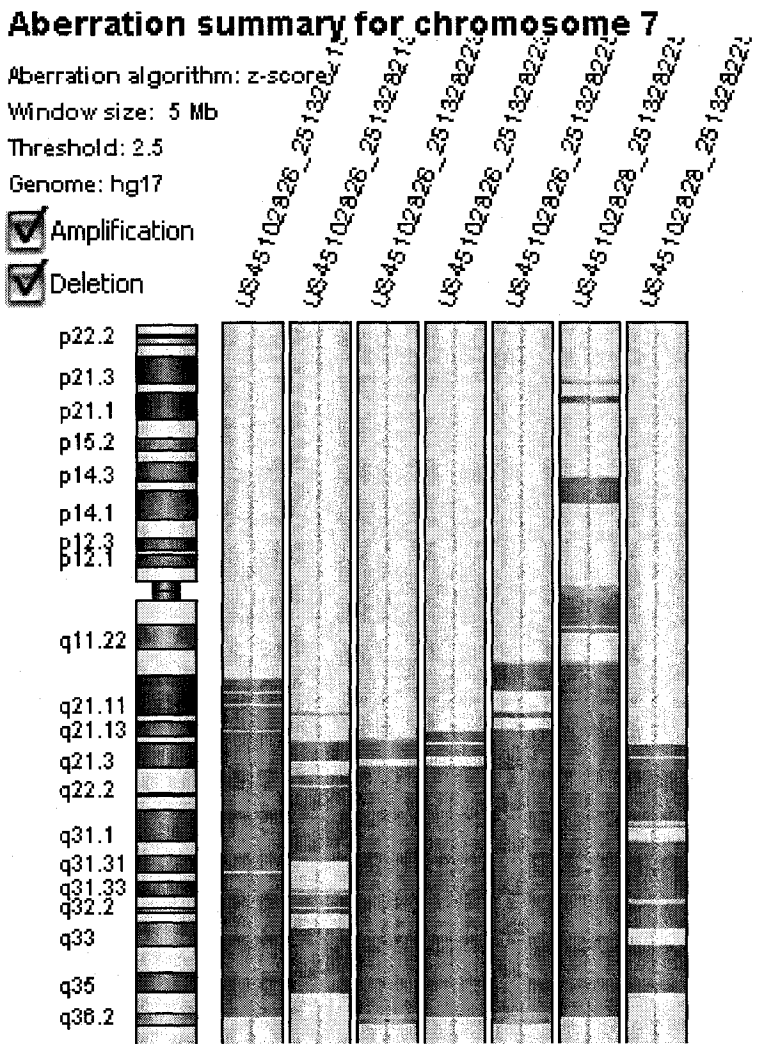

Figure 4.44) aCGH Analysis of Chromosome 7

A consistent amplification is seen on chromosome 7 in the q arm for all of the CGH arrays used.

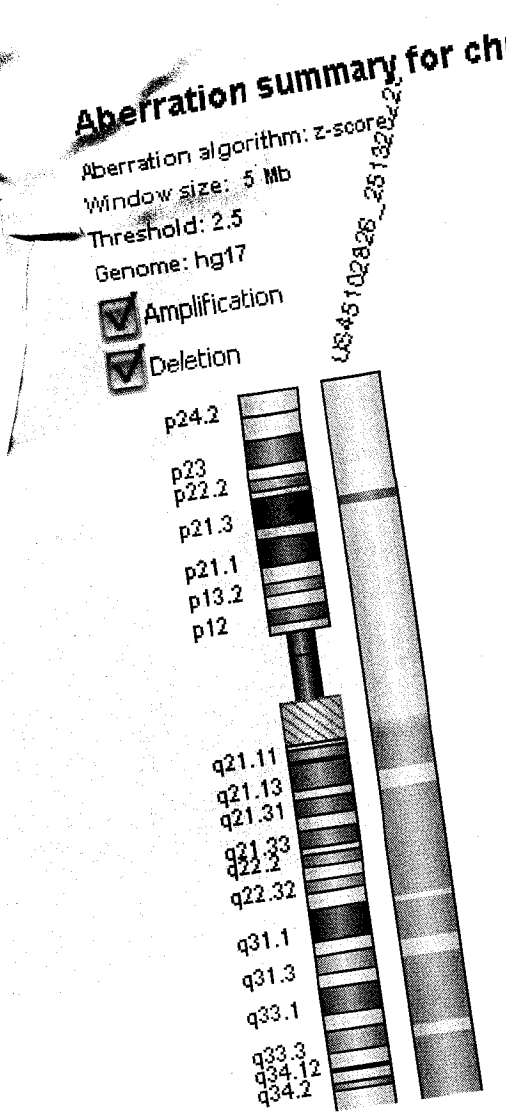

Figure 4.45) aCGH Analysis of Chromosome 9

Regions of amplification shown in chromosome 9 from the macroscopically isolated DNA, this amplification was not seen from the DNA isolated using any of the other methods.

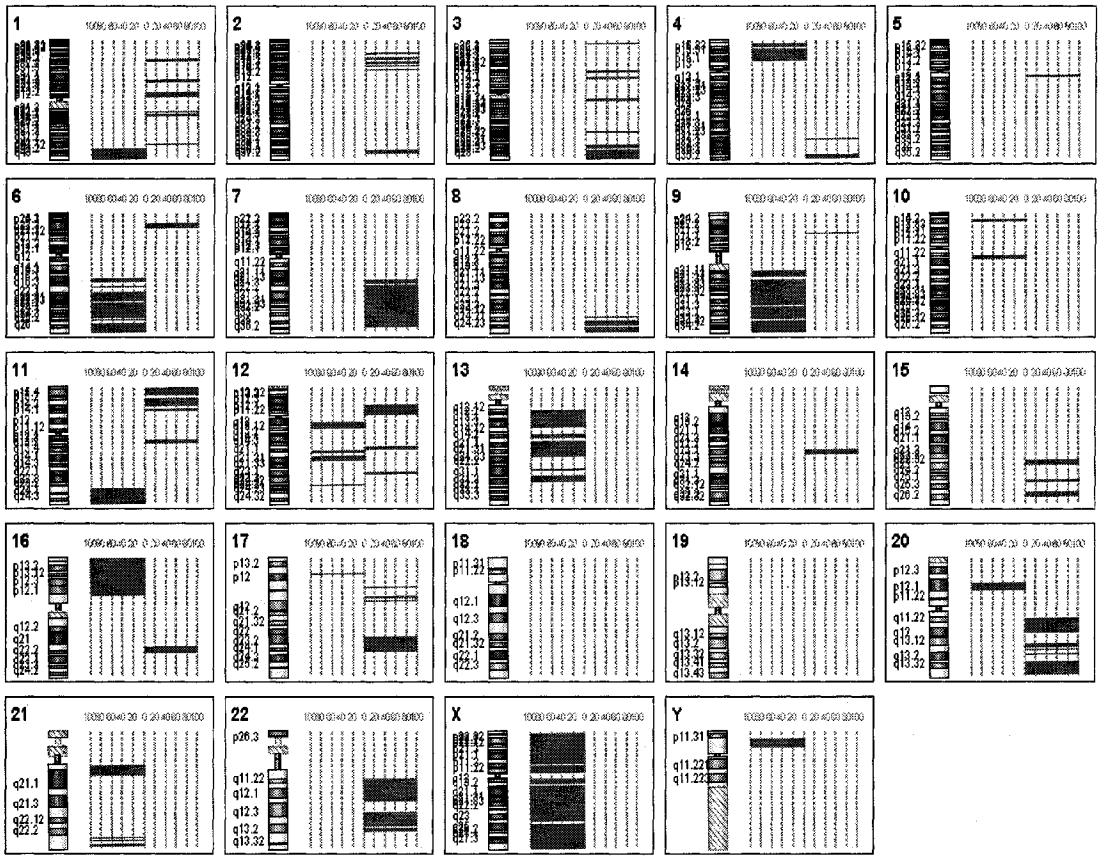

Figure 4.46) Genomic Aberrations from aCGH Analysis

A whole genome view of deletions and amplifications for each chromosome from the macroscopically extracted DNA from paraffin-embedded tissue.

Chapter 5

DISCUSSION

In this thesis I attempted to characterize the progression of uveal melanoma in an immunosuppressed animal model of the disease. This animal model allowed us to isolate tissue from the primary intraocular tumour and metastases and compare the transcriptional changes that occur as compared to the original cell lines. I was also able to re-culture cells from the intraocular tumours, circulating malignant cells and metastases, and use these cells to investigate the changes that circulating malignant cells undergo. Finally, I was then able to develop a method to isolate genomic DNA from paraffin embedded sections of the intraocular tumours. This DNA was then used for array comparative genomic hybridization to look for deletions and amplifications throughout the genome.

5.1 Animal Model of Uveal Melanoma

We were able to characterize the progression of uveal melanoma throughout this model by sacrificing one animal per week. This allowed us to document the progression of the intraocular tumour, circulating malignant cells and the presence of metastases.

5.1.1 Intraocular Tumours

The majority of animals had the development of intraocular tumours during the first five weeks of the experiment. The tumours displayed similarities to human uveal melanomas, including similar morphology, phenotype and

vascular loops. They were, however, more aggressive than the majority of human tumours with a high number of vascular loops present, high mitotic activity and large nucleoli. All histopathological indicators of poor prognosis were present in these intraocular tumours. This reflects the cell line that was used for this model, which has previously been characterized as being highly aggressive [92, 70]. This cell line was purposely chosen in order to give rise to ocular disease and subsequent metastases in three months, a series of events that can take 10 years or more to develop in our patients. The disease progression was considerably faster than in humans, with metastatic nodules present in the lungs of the animals by the seventh week, a desirable feature for a good animal model with metastatic disease.

Prior to sacrifice, we were able to detect the presence of intraocular tumours in the majority of the animals by fundoscopy. However, in 22 percent of the animals it was impossible to detect the presence of an intraocular tumour due to intraocular haemorrhage or retinal detachment. In these cases, ultrasound proved to be useful for overcoming the limitations of fundoscopy and allowed for a more accurate determination of tumour location, dimension and extraocular extensions [93].

5.1.2 Circulating Malignant Cells

This model marks the first time that CMCs have been isolated and cultured from the peripheral blood in an animal model of UM [93]. Staining with melanoma specific markers, such as Melan A and Tyrosinase, verified that these cells were indeed CMCs from the blood. The first CMCs were cultured at week 6

of the animal model. Since the life span of these cells in the blood is known to be short we believe that the isolated UM cells from the blood are the cells that escaped from the intraocular tumour, and not the result of mechanical injection at the time of surgery [125]. These cells were cultured for a short time and then stored in liquid nitrogen before RNA was extracted. Significant transcriptional changes were noticed as compared to the original cell line that was inoculated into the eye of the animals indicating that these cells were different than the original 92.1 cell line. This indicates that any changes or clonal selection that has occurred are maintained by these re-cultured intraocular, CMC and metastatic cells. These new cell lines open up a new avenue for *in vitro* techniques to characterize the changes that these cells have undergone.

The presence of CMCs in the blood of patients has been previously described [126, 127]. A recent publication from our laboratory showed that all uveal melanoma patients, regardless of the therapy that they receive, have the presence of these circulating malignant cells [124]. To date, no correlation between the presence of CMCs and patient outcome has been shown.

5.1.3 Animal Models of Uveal Melanoma

Until now, little progress has been made in the study and treatment of metastatic uveal melanoma, partially due to the lack of suitable animal models. Since this original characterization of the immunosuppresed rabbit model, the model has subsequently been used three more times [128, 129]. The model has proven to be highly reproducible, with intraocular tumour formation within the first several weeks and the presence of large metastatic nodules by the seventh

week. This high rate of metastasis enables for the systemic study of tumour dissemination and possible treatments using this model. Our model is ideal for the study of possible treatments, especially as results can be assessed histopathologically at the end of the experiment and during the model by detecting and characterizing the presence of CMCs.

5.1.4 Metastases

The primary site of metastasis in this model was the lung, with hepatic micrometastases being found in a smaller subset of animals at the end of the experiment. Although this is the first model to report the presence of liver metastases, it is not a perfect representation of the human disease. In our patients the liver is the primary site of metastases, with the lung being a secondary site in terms of patients who present with it as the first metastatic site [58]. It remains unclear why our UM cells first preferentially metastasize to the lung and then the liver in our animal model. This may provide a unique opportunity for the future study of potential tumour homing factors and the effects of the microenvironment on metastases.

5.1.5 Limitations of the Model

The main limitation of the model is the need for continuous immunosuppression to allow for the efficient development of the intraocular tumour and subsequent metastases [130]. The use of Cyclosporin A for this immunosuppression can result in severe toxicity that could limit the length of the experiment. We found that it was important to have animals of sufficient weight at the beginning of the experiment (> 3 kg) and a strict dosage regimen to

minimize these toxic side effects [91]. As a result, we were able to ensure the survival of many of the animals through the entire length of the 10-week experiment (17 animals). Two animals had to be sacrificed prematurely, one during the first week and the second during the eight-week, due to acute weight loss. The need for immunosuppression cannot be overcome with this model. A different model using nude mice would enable the use of human cells without the need for immunosuppression. However, this would create its own complications, as the size of the eye would make the implantation of cells into the eye for the formation of the intraocular tumour difficult.

5.1.6 Conclusion

The characterization of this model was the first to be reported in the literature and the first animal model of uveal melanoma to show the presence of liver metastases. Subsequent to the publication of this model, new animal models of metastatic disease in uveal melanoma using nude mice have been developed [131, 132]. None of these have demonstrated liver metastases or reproduced intraocular tumour growth. Our laboratory has sought to use nude mice to address the toxicity problems associated with the use of CsA [133]. This model showed the presence of cells in the liver of the mice using the 92.1 cell line that had been labelled with a green fluorescent protein marker, however no large nodules formed. This pilot project will be repeated over a longer time to study the formation of liver metastases. The cells are injected through the tail vein and therefore will only allow for the study of the last part of the metastatic cascade, including circulation, implantation at the site of metastases and metastatic growth.

Therefore the rabbit model of uveal melanoma will remain an important tool for the study of the intraocular tumour and CMC dissemination as well as the formation of metastases.

5.2 Transcriptional Profiling

After the establishment of the immunosuppressed albino rabbit model of uveal melanoma we then sought to compare the changes in transcriptional profiles that characterize an established cell line as it develops into intraocular tumours, circulating malignant cells and lung metastatic lesions. In addition, we were able to compare the expression profiles of five routinely used human uveal melanoma cell lines. This would have been impractical to carry out using patient samples, as metastases can take up to 10 years to develop in UM patients. Therefore finding matched fresh intraocular tumour samples as well as the corresponding metastases would have taken considerably longer than was available for these studies.

5.2.1 Cell Lines

We found that there was no significant transcriptional difference between the five human uveal melanoma cell lines when they were grown under normal culture conditions. This observation is interesting in light of the fact that one of the five cell lines (UW-1) has been documented as being established from transformed normal uveal melanocytes [122]. Therefore, this cell line may have undergone transformations *in vitro* that have effectively rendered it more similar to the true uveal melanoma cell lines. It may be that under different culture

conditions, stressors, or by chronic exposure to growth factors these five cell lines may begin to have significantly different transcriptional profiles.

Comparison of the transcriptional profiles from *in vitro* cultured cell lines with the solid tumours are of only limited interest because of the extreme differences in environmental conditions. Nevertheless, this data set has some value in identifying genes whose expression changed only during the transition from primary and secondary tumours.

5.2.2 Comparison of Tissue Samples and Re-Cultured Cells

Comparison of the intraocular tumours from individual rabbits showed few relative differences between the individual samples. Similarly, a comparison between the lung metastatic samples showed little variation as well. These results help to validate the human uveal melanoma immunosuppressed rabbit model, as it seems to produce relatively homogeneous tumours. If this was not the case we could expect to find transcriptional differences between the intraocular tumours and between the different metastatic nodules that were sampled. Since these tumours and metastases were considered to be virtually identical to one another, independent of the animal they were isolated from, we believe this helps to prove the homogeneity of the tumours produced in our model system.

Two different statistical tests identified 239 genes with a significant change in transcript abundance between the primary intraocular tumours and the metastatic lesions. It is interesting to note that among the changes that were observed was an increase in cytokeratin 18 and a corresponding decrease in vimentin transcript abundance in the metastatic lesions compared to the

intraocular tumours. This interconverted phenotype has previously been described as a marker of enhanced metastatic potential in uveal melanoma [52] and other cancer types such as breast cancer [134]. In our model we confirm that metastasizing cells undergo this switch in the expression of intermediate filaments.

We were also interested in analyzing the cells isolated from blood. These circulating malignant cells were present at very low concentrations in the blood of our animals and had to be re-cultured for a short time period in order to get a useable amount of RNA. For this reason we compared our re-cultured CMCs to re-cultured cells isolated from the intraocular and metastatic sites. As these were done subsequent to the tissue analysis, it was inappropriate to compare these results directly with the tissue analysis. Nevertheless, similar transcriptional changes were seen with many of the genes identified from the tumour samples that changed in the re-cultured data, including IRS-2, Septin 7, and all of the melanoma specific markers.

5.2.3 Validation of Genes of Interest

5.2.3.1 Quantitative Real-Time PCR

We validated the changes that were detected using quantitative real-time PCR and three different functional assays. We used the tRNA that had been extracted for transcriptional analysis for the quantitative real-time PCR verification of six separate gene products. Due to the limited amount of RNA that remained after the microarray analysis of the metastatic lesions, we were

restricted in how many transcripts we could validate with real-time PCR. After reviewing the literature we decided to validate four group A transcripts and two group B transcripts.

The quantitative real-time PCR analysis validated that APK-3, Septin7, Fibronectin 1 and Insulin Receptor Substrate-2 increased in expression from the cell line, to intraocular, to metastatic tissue. Fibronectin 1 and Septin 7 showed the greatest increase over the *in vitro* cell line, with a three and four fold increase in expression respectively. Of the four that we validated, IRS-2 showed the smallest increase in expression from cell line to intraocular, with a large increase happening from intraocular to metastases. The remaining validated gene of interest, APK-3, showed a one-fold increase over the cell line and then a small increase in expression from the intraocular to metastases.

The two group B gene products that we chose to validate were Melan-A and ATF4. Melan-A showed a substantial decrease in expression from the *in vitro* samples to the intraocular samples, with a more than five-fold decrease from the original cell lines to the samples from the metastatic lesions. In comparison, ATF4 showed a twofold increase in expression from the cell lines to the intraocular samples, followed by a corresponding twofold decrease from the intraocular to the metastatic lesions.

5.2.3.2 Functional Assays

We used three different functional assays to study changes in the re-cultured cells that were isolated from the intraocular tumours, blood and metastases. We tested two different time-points, in triplicate, for the proliferative

ability of these re-cultured cells as compared to the original 92.1 cell line. There was an increase in proliferation in the re-cultured intraocular cells, which then decreased in the CMCs and metastatic cells. This corresponded with the decrease in ribosomal proteins that we saw from the transcriptional analysis. The decrease in ribosomal proteins has been shown to correlate with the proliferation rate of cells [135]. The high level of ribosomal proteins and high proliferation rate of the re-cultured intraocular cells correspond to the histopathological indicators of high proliferation in the intraocular tumours such as many mitotic figures, high vascularization, areas of necroses and epithelioid cell type.

The invasive ability of the re-cultured cells appeared to be inverse to their proliferative ability. In comparison to the proliferation rate, the invasive ability of these cells increased from the original 92.1 cell line and intraocular tumour cells, to those cultured from blood to metastases. The re-cultured metastatic cells had the highest invasive ability, with nearly a doubling of the amount of cells that could invade through the matrigel in a 72 hour period as compared to the CMCs, which themselves were highly invasive compared to the intraocular tumour re-cultured cells. This increase in invasive ability of cells in a metastatic micro-environment has been previously shown [136]. We are unable to say if our increase in invasive ability and decrease in proliferation rate is due to the micro-environment, or if this is a clonal selection for those cells that are capable of escaping into the circulation from the intraocular tumour and forming metastases. Indeed, it is probably a combination of both of these factors that leads to these changes.

The final functional assay that we used was to assess the ability of our cell lines and re-cultured cells to adhere to fibronectin coated strips. We found that the cell lines with the highest proliferative and metastatic potential (92.1 and SP6.5) [70] had the lowest ability to bind to fibronectin. The re-cultured cells from the intraocular tumour had an even weaker binding ability to fibronectin. The CMCs and metastatic re-cultured cells each had an increase in ability to bind. This lack of binding to fibronectin by the intraocular tumour re-cultured cells correlates with the histopathological finding that epithilioid cells are only weakly attached to the extracellular matrix [137]. The epithilioid phenotype was correlated with the decreased expression of Alpha 5 Beta 1, the integrin that binds to fibronectin. Restoring the expression of this integrin in the SP6.5 cell line decreased the ability of this cell line to form tumours in a nude mouse xenograft model [138].

5.2.4 Fibronectin

A recent study by Kaplan et al. has shown that fibronectin expression may be necessary for the development of metastasis [139]. In addition, they showed that the arrival of melanoma cells to the sites of metastasis induced an additional up-regulation of fibronectin expression. Fibronectin was one of the transcripts that were highly up regulated in our metastatic samples, belonging to our Group A. This increase in expression was validated by real-time PCR data, which showed a greater than twofold increase in fibronectin expression between the intraocular tumour samples and the transition to metastasis. The original 92.1 cell line showed low expression of fibronectin, indicating that the expression of this

protein may be necessary for the formation of the lung metastasis and not for the growth of the primary tumour or cells in culture.

It may therefore be necessary for cells in the intraocular tumour to have low expression of fibronectin and its integrin in order to be able to escape into circulation. After the escape into circulation, the CMCs may then need to up-regulate their expression of fibronectin and its integrin to adhere to a distant site, invade and begin forming a metastatic nodule.

These results support work that has previously been published showing extracellular matrix proteins, including fibronectin, surrounding metastatic lesions from patients [140]. These results give further credence to the applicability of our model to the disease process in our patients.

5.2.5 Insulin Receptor Substrate 2

Insulin receptor substrate 2 (IRS-2) was also identified as a member of Group A transcripts and was validated by real-time PCR data, thus indicating that there was a large increase in IRS-2 expression by cells isolated from metastasic tumours. Two articles have recently demonstrated that the expression of the insulin-like growth factor 1 (IGF-1) receptor in uveal melanoma patients correlated with poor prognosis [47, 141]. In addition, the inhibition of the IGF-1 receptor by cyclolignan picropodophyllin was shown to inhibit growth, motility and invasion of uveal melanoma cells and cause tumour regression in a xenograft mouse model [47]. At least nine substrates to the insulin/IGF-1 receptors have been described [142]. It is believed that the phosphorylation of these diverse substrates may have different cellular effects depending on the substrate that is

activated. The insulin receptor substrate family members bear structural and functional similarities, however IRS-1 is believed to mediate mitogenic effects of the IGF-1 receptor, whereas IRS-2 is believed to play a role in metabolic and proliferative signals triggered by the insulin receptors [143]. It is also interesting to note that IRS-2 is the major effector of insulin signalling in the liver.

Among the downstream pathways that can be stimulated by IRS-2 is the phosphorylation of AKT via PI3K. Phosphorylated AKT has also been shown to be a prognostic indicator of increased metastasis in patients with uveal melanoma [48]. It is possible that this increased mortality rate may reflect the activation of AKT through the IGF-1 pathway. We hypothesize that due to the large increase in IRS-2 in samples from metastasis as compared to the intraocular tumour samples in this model, the cells may have overcome their need for IGF-1 stimulation in these metastatic nodules. This disregulation of the IGF-1 pathway should be studied further and fully characterized. Future studies will aim to use small interfering RNA to inhibit IRS-2 and study its effects on the IGF-1 pathway in uveal melanoma.

5.2.6 Alpha Kinase 3 and Septin 7

The remaining two group A transcripts that were validated with real-time PCR (alpha kinase 3, septin 7) have not been previously investigated in uveal melanoma. Alpha kinase 3 (ALPK3), also known as MIDORI, has been mapped to chromosome 15q. It belongs to a relatively new class of protein kinases that have a structure differing from that of the majority of other eukaryotic protein kinases [144]. Septin 7 belongs to a family of 13 known human septins that

contain a central GTP-binding domain whose function remains unknown [145, 146]. It is believed that the septin family of proteins can form a scaffold like arrangement in the cell, aiding in the arrangement of the cytoskeleton. As such, they may be involved in motility, cytokinesis and spatial orientation of cytoplasmic proteins [146]. To the best of our knowledge this is the first time that either of these proteins has been implicated in uveal melanoma and they may represent novel therapeutic targets. Further investigations into the roles of these proteins in the progression of melanoma cells from primary to metastatic tumours are warranted.

5.2.7 Activating Transcription Factor 4

We analyzed two genes of interest from our group B of transcripts. The first of these was Activating Transcription Factor 4 (ATF4), which is a member of the ATF/cyclic adenosine monophosphate-responsive element binding family of transcription factors. Evidence has shown that ATF4 can be induced by DNA damage, by either chemotherapy or UVA exposure [147, 148]. It is unclear why ATF4 expression is down-regulated in our metastatic samples compared to the intraocular samples.

5.2.8 Melan A

All of the melanoma specific markers (Melan A, SILVer, CD63) were grouped into Group B, indicating a substantial decrease in expression of these markers as the cells progressed towards metastasis. One of these markers, Melan A, is routinely used in immunohistochemical diagnosis of suspected melanomas and has been used as a marker for the detection of circulating malignant cells.

Melan A, also known as MART-1, is involved in melanosome maturation and has recently been shown to be required for the maturation of melanosomes from stage I to II [149]. SILVer has also been characterized as being correlated with the amount of melanin produced by melanocytes, implicating that it may function in the same pathway as Melan A. The down regulation of this transcript was verified by real-time PCR, which showed extensive loss of expression in the tumour samples as compared to the 92.1 cell line in culture. This loss of expression may indicate that the metastatic cells have dedifferentiated enough that they no longer express many of the currently used melanoma specific markers.

5.2.9 Re-Cultured Cells

As previously mentioned, many of the changes that were seen in the re-cultured cells were similar to those seen in tissue. In addition to these, we also saw several other genes that increased in transcript abundance including the Interleukin 1 receptor, matrix metalloproteinase 2 (MMP2) and four small GTPases: Rabphilin 3A, Syntaxin, Ral GPS2, IQGAP2. The presence of MMP2 has repeatedly been reported to be associated with worse prognosis in uveal melanoma patients [150]. The small GTPases may prove to be interesting future drug targets. Among those gene transcripts that were decreased in the re-cultured CMCs and metastatic cells was tissue inhibitor of metalloproteinase 1 (TIMP1) and melanoma specific markers. The decrease of expression of TIMP1, coupled with the increase in MMP2 expression, point towards increased invasive ability of these cells in circulation and metastasis as compared to the intraocular tumour

setting. This increase in invasive ability was shown in our invasion assays as described previously.

5.2.10 Conclusion

It is important to note that we are not able to say if these changes that we see are an active evolution of cells as they progress from cell culture to intraocular tumour to metastasis, or if we are simply selecting for sub-populations of cells from our cell line in each step. The cell line that was used in our xenograft model is one that has been maintained in culture for some time and has most likely undergone genetic changes during that time. To answer this question would require the design of an entirely new model and was ultimately beyond the scope of this animal model of uveal melanoma.

In addition, our metastatic samples were isolated from the lungs of rabbits, with only micrometastases in the livers. This is contrary to humans, where the major site of metastasis is the liver with a subset of patients presenting with metastasis to the lungs or other organs first. It is unclear why these differences occurred in our animal model; differences in secreted factors in the lungs of the animals compared to humans might play a role.

Our identification of a group of transcripts that are highly expressed in each of the separate locations may yield potential new markers that are not down-regulated as the cells progress towards metastasis. Elucidating the full function of these listed transcripts, including possible targets for potential immunotherapy, is the aim of future investigations.

5.3 Comparative Genomic Hybridization Array

To the best of our knowledge, this is the first time that genomic DNA has been extracted from paraffin-embedded, formalin fixed tissue of uveal melanoma and used for CGH array analysis. We compared three different methods for the extraction of the DNA from these samples. Using this as a guideline, future studies using archival material for these experiments will be undertaken.

5.3.1 Extraction of Genomic DNA

During the past year several different groups have studied the use of genomic DNA extracted from archival paraffin embedded formalin fixed tissue for use in CGH array analysis [120, 151, 119, 152, 121]. Each group has developed a custom in-house method for their DNA extraction and no set standard has been recognized in the literature. The majority of these have been used for breast or colorectal cancers, with only one previous report from a cutaneous melanoma [153]. We were therefore interested in seeing which methods would be useful for the isolation of the intraocular tumour from paraffin-embedded sections and subsequent DNA extraction. The new generation of CGH arrays is sensitive to degraded DNA therefore the genomic DNA that was extracted from our samples had to be of the highest quality possible.

Three different methods were tested for their ability to isolate and extract high quality genomic DNA from our intraocular tumour samples. The Laser Capture Microdissection (LCM) technique yielded the least DNA with the worst quality, followed by the Pin Point Isolation system. The macroscopic extraction method that we designed worked the best out of the three, yielding good quality

DNA that we were able to run on the CGH arrays. We chose to try LCM as our first method due to a paper that was published prior to the start of this study in which they used this technique to get DNA from a limited number of cells [154]. Our results were not as encouraging, resulting in a small yield and poor quality of DNA, and we therefore moved on to other methods. The second method was sold by Zymed laboratories and has been described as a good way to extract large amounts of DNA from paraffin-embedded tissue [155-157]. There was a definite improvement over the amount of DNA that was extracted using LCM, but we found it to still be of poor quality. Following this, we moved on to create our own protocol for the extraction of genomic DNA from paraffin-embedded tissue. This had the advantage of requiring basic tools that were already present in the laboratory, such as an incubator, scalpel and a stereoscopic microscope. The resulting scrapings of paraffin-embedded tissue were then digested and purified genomic DNA isolated with a commercially available kit from Gentra. This allowed for the extraction of two to 10 times as much DNA as the other two methods and of much better quality and purity.

We verified this in our samples by detecting the apparent loss of an X chromosome. The 92.1 cell line is from a male patient and the reference DNA is from a female patient. We would thus expect that our samples would demonstrate an apparent loss of the entire X chromosome when compared to the normal reference DNA. This was not the case in the arrays that were run using genomic DNA from LCM or the Pin Point isolation system. The results were too noisy for the software to determine if the entire chromosome had been lost. Instead, it

showed only regions of the chromosome to have been deleted in the DNA from the Pin Point isolation system, while no deletions at all were shown with the LCM samples. In comparison, our macroscopic technique showed deletion of nearly the entire X chromosome. There were still small bands remaining that did not show up as deletions. This was likely due to the small amount of degradation that even this DNA showed.

For the first time, we have established a method for the extraction of genomic DNA from archival material for human uveal melanoma. This method will enable us to do future genetic studies using archival patient samples. It is our hope that this will shed more light on the genetic aberrations, including monosomy of chromosome 3, that are currently being debated in uveal melanoma.

5.3.2 Chromosomal Abnormalities in the Intraocular Tumours

As described previously in the literature review section, there has been contradictory evidence regarding the role of monosomy 3 in uveal melanoma. We showed a small deletion of chromosome 3 in our study in the q12.2 region. This was accompanied by an area of amplification of the q28 region. A full loss of chromosome 3 has only been shown in one established cell line [158]. In fact, a previous study looked a 10 different uveal melanoma cell lines and found that none of them, including 92.1, had a loss of chromosome 3 [105]. Instead they found that the cell lines showed a much higher incidence of rearrangement of chromosome 3 using FISH, SKY and traditional CGH analysis. These results of course must be balanced with the fact that these cell lines have now been in

culture for nearly a decade. We made every effort to ensure that the 92.1 cell line remained, as close to the original cell line as possible, however there are almost certainly genetic changes that have occurred during the time it has spent in culture.

The most prominent chromosomal abnormality that was seen across all the extracted DNA samples was a large area of amplification of the q arm of chromosome 7. Polysomy of chromosome 7 has been previously reported in cutaneous melanoma [159] and breast cancer [160]. These studies showed a correlation between the extra copies of chromosome 7 and association with markers of worse prognosis. In comparison to these studies that showed the gain of an entire copy of chromosome 7, we showed an area of amplification. This area contained several hundred genes, including C-Met, Wnt2 and BRAF. This amplification was consistently seen in each of the DNA samples that we analysed using the CGH arrays.

C-Met is a plasma membrane receptor for hepatocyte growth factor (HGF). The activation of this tyrosine kinase has been shown to induce proliferation, motility, adhesion and invasion of tumour cells [71, 161, 162]. The activation of c-Met by HGF is thought to be one of the key events in tumour progression. There have been numerous reports showing the amplification and over-expression of c-Met in various cancers [163-165]. With regards to uveal melanoma, one study showed that the expression of c-Met correlated with a metastatic phenotype [166]. Interestingly, the co-expression of c-Met and IGF-1R was shown to be a strong indicator of increased mortality rate in uveal melanoma

patients [141]. This may link with our previous observation that IRS-2, a component of the IGF1-R cascade, is highly up-regulated in metastases.

The amplification of Wnt2 has been shown in a variety of other cancers, including colorectal and cutaneous melanoma [167, 168]. The use of an anti-Wnt2 monoclonal antibody led to an increase in apoptosis in cultured cutaneous melanoma cells and reduced tumour growth in a xenograft nude mouse model [169]. This is the first report showing the amplification of Wnt2 in uveal melanoma. Increased levels of Wnt2 led to the stabilization and accumulation of beta-catenin in the cytoplasm. It also causes the translocation of beta-catenin to the nucleus where it binds to T-cell transcription factor. This heterodimeric complex can lead to the activation of a variety of Wnt target genes, including c-myc and cyclin D1. Recent work has suggested a role for beta-catenin in the transformation of cells from a spindle cell type to the more aggressive epithelioid cell type in uveal melanoma [100, 170]. Previous studies have shown no mutations associated with beta-catenin in uveal melanoma [171]. We theorize that this increase in beta-catenin in the more aggressive uveal melanoma cell types may therefore reflect an increase in the expression of Wnt pathway proteins, such as Wnt2, that lead to a stabilization of beta-catenin and increased levels in the cell. Further studies using patient material are warranted to investigate the role of Wnt2 in this transformation from spindle to epithelioid cell type.

Alterations in the MAPK pathway have previously been described as being crucial in the development of cutaneous melanoma [172, 173]. This pathway contains the Ras oncoprotein that activates one of three isoforms of RAF,

a serine/threonine protein kinase. The isoform that is most commonly mutated in cutaneous melanomas is BRAF, with missense mutations having been described in up to 66 percent of cutaneous melanomas [173]. There has been contradictory evidence regarding the role of BRAF in uveal melanoma. One study has reported no evidence of BRAF mutations in their uveal melanoma patient samples [174], however the sample size was fairly low (n=6). In contrast, a recent report has shown the presence of a BRAF mutation in a uveal melanoma patient sample [175]. Another group showed that uveal melanoma cells were sensitive to inhibition of BRAF by siRNA and that this inhibition caused a significant decrease in cellular proliferation [176].

5.4 Conclusion

This thesis strove to describe an immunosuppressed rabbit model of human uveal melanoma and the transcriptional changes that occur as the cells go from culture to the intraocular tumour, to circulation and finally to the formation of metastases. In addition to this, we sought to use the latest generation of comparative genomic hybridization arrays to study the genetic changes from archival material of the intraocular tumours from this model.

For the first time in the literature we have described the transcriptional changes that occur at different steps in the metastatic cascade of UM. We were unable to conclude if these changes were due to the selection of a sub population of cells from the original culture or if the cells evolve as they progress towards the formation of metastases. It is possible that both mechanisms are responsible for

the changes in transcriptional abundance that we characterized. This detailed characterization of the changes that these cells undergo as they form metastases has already significantly increased our understanding of the metastases and revealed to us possible new therapeutic targets.

As far as we are aware, this was also the first time that genomic DNA was extracted from paraffin-embedded archival material of uveal melanoma and used for CGH array analysis. This will have significant implications for future studies using patient archival material or fine needle biopsy material.

Future directions will focus on the possible therapeutic targets that have been identified as being up-regulated in the metastasis from our animal model. It would also be ideal to verify these targets in patients, although the limited availability of metastatic tissue would make this a lengthy study. The exact function of these up or down regulated genes that I identified is unclear for many of them. The identification of their role in the progression of uveal melanoma from the eye to metastatic sites would be of great interest. The described method for extracting genomic DNA will also be used with patient material to analysis chromosomal abnormalities in archival patient material.

REFERENCES

1. Callender, G.R., *Malignant melanotic tumors of the eye: a study of histology in 111 cases.* Trans Am Acad Ophthalmol Otolaryngol, 1931. **36**: p. 131-142.
2. McLean IW, B.M., Zimmerman LE, Jakobiec FA, *Tumors of the Eye and Ocular Adnexa. Atlas of Tumor Pathology.* 3rd ed, ed. J. Rosai. Vol. 12. 1994: Armed Forces Institute of Pathology. 161-194.
3. Woll, E., A. Bedikian, and S.S. Legha, *Uveal melanoma: natural history and treatment options for metastatic disease.* Melanoma Res, 1999. **9**(6): p. 575-81.
4. Egan, K.M., J.M. Seddon, R.J. Glynn, E.S. Gragoudas, and D.M. Albert, *Epidemiologic aspects of uveal melanoma.* Surv Ophthalmol, 1988. **32**(4): p. 239-51.
5. Singh, A.D., L. Bergman, and S. Seregard, *Uveal melanoma: epidemiologic aspects.* Ophthalmol Clin North Am, 2005. **18**(1): p. 75-84, viii.
6. Hu, D.N., G.P. Yu, S.A. McCormick, S. Schneider, and P.T. Finger, *Population-based incidence of uveal melanoma in various races and ethnic groups.* Am J Ophthalmol, 2005. **140**(4): p. 612-7.
7. Saornil, M.A., *Iris colour and uveal melanoma.* Can J Ophthalmol, 2004. **39**(4): p. 448-52.
8. Barker-Griffith, A.E. and B.W. Streeten, *Familial uveal melanoma: a report of four cases in two families and literature review.* Can J Ophthalmol, 2004. **39**(4): p. 403-8.
9. Kodjikian, L., K. Nguyen, L. Lumbroso, M. Gauthier-Villars, P. Chauvel, H. Plauchu, et al., *Familial uveal melanoma: a report on two families and a review of the literature.* Acta Ophthalmol Scand, 2003. **81**(4): p. 389-95.
10. Krygier, G., K. Lombardo, C. Vargas, I. Alvez, R. Costa, M. Ros, et al., *Familial uveal melanoma: report on three sibling cases.* Br J Ophthalmol, 2001. **85**(8): p. 1007-8.
11. Singh, A.D., H. Demirci, C.L. Shields, J.A. Shields, and A.F. Smith, *Concurrent choroidal melanoma in son and father.* Am J Ophthalmol, 2000. **130**(5): p. 679-80.
12. Singh, A.D., J.A. Shields, R.C. Eagle, C.L. Shields, M. Marmor, and P. De Potter, *Iris melanoma in a ten-year-old boy with familial atypical mole-melanoma (FAM-M) syndrome.* Ophthalmic Genet, 1994. **15**(3-4): p. 145-9.
13. Young, L.H., K.M. Egan, S.M. Walsh, and E.S. Gragoudas, *Familial uveal melanoma.* Am J Ophthalmol, 1994. **117**(4): p. 516-20.
14. Singh, A.D., I.G. Rennie, S. Seregard, M. Giblin, and J. McKenzie, *Sunlight exposure and pathogenesis of uveal melanoma.* Surv Ophthalmol, 2004. **49**(4): p. 419-28.

15. Fernandes, B.F., J.C. Marshall, and M.N. Burnier, Jr., *Blue light exposure and uveal melanoma.* Ophthalmology, 2006. **113**(6): p. 1062 e1; author reply 1062.
16. Marshall, J.C., K.D. Gordon, C.S. McCauley, J.P. de Souza Filho, and M.N. Burnier, *The effect of blue light exposure and use of intraocular lenses on human uveal melanoma cell lines.* Melanoma Res, 2006. **16**(6): p. 537-41.
17. Netter, F.H., *Atlas of Human Anatomy.* 10 ed, ed. F.D. Arthur. 1997, East Hanover: Hoechstetter.
18. Grin, J.M., J.M. Grant-Kels, C.M. Grin, A. Berke, and B.D. Kels, *Ocular melanomas and melanocytic lesions of the eye.* J Am Acad Dermatol, 1998. **38**(5 Pt 1): p. 716-30.
19. McLean, I.W., *Uveal nevi and malignant melanoma*, in *Ophthalmic Pathology: an atlas and textbook*, W.H. Spencer, Editor. 1996, W.B. Saunders: Philadelphia. p. 2121-2217.
20. Shields, J.A. and C.L. Shields, *Melanocytic tumors of the iris stroma*, in *Intraocular tumors: a text and atlas*, J.A. Shields and C.L. Shields, Editors. 1992, Saunders: Philadelphia. p. 61-84.
21. Shields, J.A. and C.L. Shields, *Posterior uveal melanoma: clinical and pathologic features*, in *Intraocular tumors: a text and atlas*, J.A. Shields and C.L. Shields, Editors. 1992, Saunders: Philadelphia. p. 61-84.
22. McLean, I.W., M.N. Burnier Jr., L.E. Zimmerman, and F. Jakobiec, *Tumors of the uveal tract*, in *Tumors of the eye and ocular adnexa*, I.W. McLean, et al., Editors. 1994, Armed Forces Institute of Pathology: Washington DC. p. 155-214.
23. Affeldt, J.C., D.S. Minckler, S.P. Azen, and L. Yeh, *Prognosis in uveal melanoma with extrascleral extension.* Arch Ophthalmol, 1980. **98**(11): p. 1975-9.
24. Chang, M., L.E. Zimmerman, and I. McLean, *The persisting pseudomelanoma problem.* Arch Ophthalmol, 1984. **102**(5): p. 726-7.
25. *Accuracy of diagnosis of choroidal melanomas in the Collaborative Ocular Melanoma Study. COMS report no. 1.* Arch Ophthalmol, 1990. **108**(9): p. 1268-73.
26. Conway, R.M., T. Chew, P. Golchet, K. Desai, S. Lin, and J. O'Brien, *Ultrasound biomicroscopy: role in diagnosis and management in 130 consecutive patients evaluated for anterior segment tumours.* Br J Ophthalmol, 2005. **89**(8): p. 950-5.
27. Shields, C.L., J.A. Shields, P. De Potter, M. Quaranta, J. Freire, L.W. Brady, et al., *Plaque radiotherapy for the management of uveal metastasis.* Arch Ophthalmol, 1997. **115**(2): p. 203-9.
28. Diener-West, M., J.D. Earle, S.L. Fine, B.S. Hawkins, C.S. Moy, S.M. Reynolds, et al., *The COMS randomized trial of iodine 125 brachytherapy for choroidal melanoma, III: initial mortality findings. COMS Report No. 18.* Arch Ophthalmol, 2001. **119**(7): p. 969-82.
29. Singh, A.D. and A. Topham, *Survival rates with uveal melanoma in the United States: 1973-1997.* Ophthalmology, 2003. **110**(5): p. 962-5.

30. Diener-West, M., B.S. Hawkins, J.A. Markowitz, and A.P. Schachat, *A review of mortality from choroidal melanoma. II. A meta-analysis of 5-year mortality rates following enucleation, 1966 through 1988.* Arch Ophthalmol, 1992. **110**(2): p. 245-50.
31. McLean, I.W., K.S. Keefe, and M.N. Burnier, *Uveal melanoma. Comparison of the prognostic value of fibrovascular loops, mean of the ten largest nucleoli, cell type, and tumor size.* Ophthalmology, 1997. **104**(5): p. 777-80.
32. Gamel, J.W. and I.W. McLean, *Quantitative analysis of the Callender classification of uveal melanoma cells.* Arch Ophthalmol, 1977. **95**(4): p. 686-91.
33. McLean, I.W., W.D. Foster, L.E. Zimmerman, and J.W. Gamel, *Modifications of Callender's classification of uveal melanoma at the Armed Forces Institute of Pathology.* Am J Ophthalmol, 1983. **96**(4): p. 502-9.
34. McLean, I.W., W.D. Foster, and L.E. Zimmerman, *Uveal melanoma: location, size, cell type, and enucleation as risk factors in metastasis.* Hum Pathol, 1982. **13**(2): p. 123-32.
35. Lattman, J., S. Kroll, D.H. Char, S. Ghazvini, H. Frigillana, J.M. O'Brien, et al., *Cell cycling and prognosis in uveal melanoma.* Clin Cancer Res, 1995. **1**(1): p. 41-7.
36. Seregard, S., B. Spangberg, C. Juul, and M. Oskarsson, *Prognostic accuracy of the mean of the largest nucleoli, vascular patterns, and PC-10 in posterior uveal melanoma.* Ophthalmology, 1998. **105**(3): p. 485-91.
37. Whelchel, J.C., S.E. Farah, I.W. McLean, and M.N. Burnier, *Immunohistochemistry of infiltrating lymphocytes in uveal malignant melanoma.* Invest Ophthalmol Vis Sci, 1993. **34**(8): p. 2603-6.
38. Clemente, C.G., M.C. Mihm, Jr., R. Bufalino, S. Zurrida, P. Collini, and N. Cascinelli, *Prognostic value of tumor infiltrating lymphocytes in the vertical growth phase of primary cutaneous melanoma.* Cancer, 1996. **77**(7): p. 1303-10.
39. Kivela, T., T. Makitie, R.T. Al-Jamal, and P. Toivonen, *Microvascular loops and networks in uveal melanoma.* Can J Ophthalmol, 2004. **39**(4): p. 409-21.
40. Makitie, T., P. Summanen, A. Tarkkanen, and T. Kivela, *Microvascular loops and networks as prognostic indicators in choroidal and ciliary body melanomas.* J Natl Cancer Inst, 1999. **91**(4): p. 359-67.
41. Mueller, A.J., W.R. Freeman, U.C. Schaller, A. Kampik, and R. Folberg, *Complex microcirculation patterns detected by confocal indocyanine green angiography predict time to growth of small choroidal melanocytic tumors: MuSIC Report II.* Ophthalmology, 2002. **109**(12): p. 2207-14.
42. Folberg, R., X. Chen, H.C. Boldt, J. Pe'er, C.K. Brown, R.F. Woolson, et al., *Microcirculation patterns other than loops and networks in choroidal and ciliary body melanomas.* Ophthalmology, 2001. **108**(5): p. 996-1001.
43. Folberg, R., V. Rummelt, R. Parys-Van Ginderdeuren, T. Hwang, R.F. Woolson, J. Pe'er, et al., *The prognostic value of tumor blood vessel*

morphology in primary uveal melanoma. Ophthalmology, 1993. **100**(9): p. 1389-98.
44. Anastassiou, G., S.E. Coupland, A. Stang, R. Boeloeni, H. Schilling, and N. Bornfeld, *Expression of Fas and Fas ligand in uveal melanoma: biological implication and prognostic value.* J Pathol, 2001. **194**(4): p. 466-72.
45. Pereira, P.R., A.N. Odashiro, J.C. Marshall, Z.M. Correa, R. Belfort, Jr., and M.N. Burnier, Jr., *The role of c-kit and imatinib mesylate in uveal melanoma.* J Carcinog, 2005. **4**(1): p. 19.
46. All-Ericsson, C., L. Girnita, S. Seregard, A. Bartolazzi, M.J. Jager, and O. Larsson, *Insulin-like growth factor-1 receptor in uveal melanoma: a predictor for metastatic disease and a potential therapeutic target.* Invest Ophthalmol Vis Sci, 2002. **43**(1): p. 1-8.
47. Girnita, A., C. All-Ericsson, M.A. Economou, K. Astrom, M. Axelson, S. Seregard, et al., *The insulin-like growth factor-I receptor inhibitor picropodophyllin causes tumor regression and attenuates mechanisms involved in invasion of uveal melanoma cells.* Clin Cancer Res, 2006. **12**(4): p. 1383-91.
48. Saraiva, V.S., A.L. Caissie, L. Segal, C. Edelstein, and M.N. Burnier, Jr., *Immunohistochemical expression of phospho-Akt in uveal melanoma.* Melanoma Res, 2005. **15**(4): p. 245-50.
49. Figueiredo, A., A.L. Caissie, S.A. Callejo, I.W. McLean, P. Gold, and M.N. Burnier, Jr., *Cyclooxygenase-2 expression in uveal melanoma: novel classification of mixed-cell-type tumours.* Can J Ophthalmol, 2003. **38**(5): p. 352-6.
50. Marshall, J.C., A.L. Caissie, S.R. Cruess, J. Cools-Lartigue, V. Saraiva, and M.N. Burnier Jr, *The effects of a cyclooxygenase-2 (COX-2) expression and inhibition on human uveal melanoma cell lines and macrophage nitric oxide production.* Opthalmic Research, 2007. **In Press**.
51. Burnier Jr, M.N., J.C. Marshall, F. Gregoire, S. Di Cesare, P. Logan, and A.-K. A., *The Effect of a COX-2 Inhibitor on an Ocular Melanoma Animal Model.* IOVS E-Abstract 2218, 2006.
52. Hendrix, M.J., E.A. Seftor, R.E. Seftor, L.M. Gardner, H.C. Boldt, M. Meyer, et al., *Biologic determinants of uveal melanoma metastatic phenotype: role of intermediate filaments as predictive markers.* Lab Invest, 1998. **78**(2): p. 153-63.
53. Fuchs, U., T. Kivela, P. Summanen, I. Immonen, and A. Tarkkanen, *An immunohistochemical and prognostic analysis of cytokeratin expression in malignant uveal melanoma.* Am J Pathol, 1992. **141**(1): p. 169-81.
54. El-Shabrawi, Y., N. Ardjomand, and H. Radner, *MMP-9 is predominantly expressed in epithelioid and not spindle cell uveal melanoma.* J Pathol, 2001. **194**(2): p. 201-6.
55. Coupland, S.E., G. Anastassiou, A. Stang, H. Schilling, I. Anagnostopoulos, N. Bornfeld, et al., *The prognostic value of cyclin D1, p53, and MDM2 protein expression in uveal melanoma.* J Pathol, 2000. **191**(2): p. 120-6.

56. Karlsson, M., B. Boeryd, J. Carstensen, B. Franlund, B. Gustafsson, B. Kagedal, et al., *Correlations of Ki-67 and PCNA to DNA ploidy, S-phase fraction and survival in uveal melanoma.* Eur J Cancer, 1996. **32A**(2): p. 357-62.
57. Seregard, S., M. Oskarsson, and B. Spangberg, *PC-10 as a predictor of prognosis after antigen retrieval in posterior uveal melanoma.* Invest Ophthalmol Vis Sci, 1996. **37**(7): p. 1451-8.
58. Rietschel, P., K.S. Panageas, C. Hanlon, A. Patel, D.H. Abramson, and P.B. Chapman, *Variates of survival in metastatic uveal melanoma.* J Clin Oncol, 2005. **23**(31): p. 8076-80.
59. Gombos, D.S., K.R. Van Quill, M. Uusitalo, and J.M. O'Brien, *Geographic disparities in diagnostic screening for metastatic uveal melanoma.* Ophthalmology, 2004. **111**(12): p. 2254-8.
60. Diener-West, M., S.M. Reynolds, D.J. Agugliaro, R. Caldwell, K. Cumming, J.D. Earle, et al., *Screening for metastasis from choroidal melanoma: the Collaborative Ocular Melanoma Study Group Report 23.* J Clin Oncol, 2004. **22**(12): p. 2438-44.
61. Kodjikian, L., J.D. Grange, S. Baldo, S. Baillif, J.G. Garweg, and M. Rivoire, *Prognostic factors of liver metastases from uveal melanoma.* Graefes Arch Clin Exp Ophthalmol, 2005. **243**(10): p. 985-93.
62. Kodjikian, L., J.D. Grange, and M. Rivoire, *Prolonged survival after resection of liver metastases from uveal melanoma and intra-arterial chemotherapy.* Graefes Arch Clin Exp Ophthalmol, 2005. **243**(6): p. 622-4.
63. Aoyama, T., M.J. Mastrangelo, D. Berd, F.E. Nathan, C.L. Shields, J.A. Shields, et al., *Protracted survival after resection of metastatic uveal melanoma.* Cancer, 2000. **89**(7): p. 1561-8.
64. Rivoire, M., L. Kodjikian, S. Baldo, P. Kaemmerlen, S. Negrier, and J.D. Grange, *Treatment of liver metastases from uveal melanoma.* Ann Surg Oncol, 2005. **12**(6): p. 422-8.
65. Marshall, J.A., Pardo, M., Caissie, AL., Callejo, SA., Burnier, MN., *Cell proliferation Profile of Five Human Uveal Melanoma Cell Lines of Different Metastatic Potential.* Invest. Ophthalmol. Vis. Sci. 43, 2002. **43**: p. 1127.
66. Nio, Y., K. Tamura, N. Kan, T. Inamoto, K. Ohgaki, and H. Kodama, *In vitro DNA synthesis in freshly separated human breast cancer cells assessed by tritiated thymidine incorporation assay: relationship to the long-term outcome of patients.* Br J Surg, 1999. **86**(11): p. 1463-9.
67. Soulieres, D., A. Rousseau, M. Tardif, M. Larochelle, M. Tremblay, L. Vaillancourt, et al., *The radiosensitivity of uveal melanoma cells and the cell survival curve.* Graefes Arch Clin Exp Ophthalmol, 1995. **233**(2): p. 85-9.
68. Skehan, P., R. Storeng, D. Scudiero, A. Monks, J. McMahon, D. Vistica, et al., *New colourimetric cytotoxicity assay for anticancer-drug screening.* J Natl Cancer Inst, 1990. **82**(13): p. 1107-12.

69. Saraiva, V.S., J.C. Marshall, J. Cools-Lartigue, and M.N. Burnier, Jr., *Cytotoxic effects of violacein in human uveal melanoma cell lines.* Melanoma Res, 2004. **14**(5): p. 421-424.
70. Marshall, J.C., A.L. Caissie, S.A. Callejo, E. Antecka, and M.N. Burnier Jr, *Cell proliferation profile of five human uveal melanoma cell lines of different metastatic potential.* Pathobiology, 2004. **71**(5): p. 241-5.
71. Woodward, J.K., S.R. Elshaw, A.K. Murray, C.E. Nichols, N. Cross, D. Laws, et al., *Stimulation and inhibition of uveal melanoma invasion by HGF, GRO, IL-1alpha and TGF-beta.* Invest Ophthalmol Vis Sci, 2002. **43**(10): p. 3144-52.
72. Callejo, S.A., J.C. Marshall, J. Cools-Lartigue, V.S. Saraiva, and M.N. Burnier, Jr., *Macrophage-derived soluble factor enhances melanoma inhibitory activity expression by uveal melanoma cells in vitro.* Melanoma Res, 2004. **14**(2): p. 91-5.
73. Pereira, P.R., A.N. Odashiro, J.C. Marshall, Z.M. Correa, R. Belfort, Jr., and M.N. Burnier, Jr., *The role of c-kit and imatinib mesylate in uveal melanoma.* J Carcinog, 2005. **4**: p. 19.
74. Marshall, J.C., A.L. Caissie, J. Cools-Lartigue, S.A. Callejo, and M.N. Burnier, *The Invasive Properties of Uveal Melanoma Cell Lines and Their Response to Interleukin-6 (IL-6) and Vascular Endothelial Growth Factor (VEGF).* IOVS E Abstract 1562, 2003.
75. Cools-Lartigue, J., J.C. Marshall, A.L. Caissie, V.S. Saraiva, and M.N. Burnier, Jr., *Secretion of hepatocyte growth factor and vascular endothelial growth factor during uveal melanoma-monocyte in vitro interactions.* Melanoma Res, 2005. **15**(3): p. 141-5.
76. Cools-Lartigue, J., J.C. Marshall, A.L. Caissie, V.S. Saraiva, and M.N. Burnier, Jr., *Secretion of interleukin-6 and prostaglandin E2 during uveal melanoma-monocyte in vitro interactions.* Exp Eye Res, 2004. **79**(4): p. 451-4.
77. Dithmar, S., D.M. Albert, and H.E. Grossniklaus, *Animal models of uveal melanoma.* Melanoma Res, 2000. **10**(3): p. 195-211.
78. Diters, R.W., R.R. Dubielzig, G.D. Aguirre, and G.M. Acland, *Primary ocular melanoma in dogs.* Vet Pathol, 1983. **20**(4): p. 379-95.
79. Acland, G.M., I.W. McLean, G.D. Aguirre, and R. Trucksa, *Diffuse iris melanoma in cats.* J Am Vet Med Assoc, 1980. **176**(1): p. 52-6.
80. Albert, D.M., J.A. Shadduck, J.L. Craft, and J.Y. Niederkorn, *Feline uveal melanoma model induced with feline sarcoma virus.* Invest Ophthalmol Vis Sci, 1981. **20**(5): p. 606-24.
81. Benson, W.R., *Intraocular tumor after ethionine and N-2-fluorenylacetamide.* Arch Pathol, 1962. **73**: p. 404-6.
82. Albert, D.M., J.A. Shadduck, H.S. Liu, F.W. Sunderman, Jr., M.D. Wagoner, H.G. Dohlman, et al., *Animal models for the study of uveal melanoma.* Int Ophthalmol Clin, 1980. **20**(2): p. 143-60.
83. Kramer, T.R., M.B. Powell, M.M. Wilson, J. Salvatore, and H.E. Grossniklaus, *Pigmented uveal tumours in a transgenic mouse model.* Br J Ophthalmol, 1998. **82**(8): p. 953-60.

84. Tolleson, W.H., J.C. Doss, J. Latendresse, A.R. Warbritton, W.B. Melchior, Jr., L. Chin, et al., *Spontaneous uveal amelanotic melanoma in transgenic Tyr-RAS+ Ink4a/Arf-/- mice.* Arch Ophthalmol, 2005. **123**(8): p. 1088-94.
85. Greene, H.S., *A spontaneous melanoma in the hamster with a propensity for amelanotic alteration and sarcomatous transformation during transplantation.* Cancer Res, 1958. **18**(4): p. 422-5.
86. Greene, H.S. and E.K. Harvey, *The growth and metastasis of amelanotic melanomas in heterologous hosts.* Cancer Res, 1966. **26**(4): p. 706-14.
87. Krohn, D.L., R. Brandt, D.A. Morris, and A.S. Keston, *Subchoroidal transplantation of experimental malignant melanoma.* Am J Ophthalmol, 1970. **70**(5): p. 753-6.
88. Green, E.L., *Handbook of genetically standardized JAX Mice*. 1962: Bar Harbor.
89. Grossniklaus, H.E., M.W. Wilson, B.C. Barron, and M.J. Lynn, *Anterior vs posterior intraocular melanoma. Metastatic differences in a murine model.* Arch Ophthalmol, 1996. **114**(9): p. 1116-20.
90. Grossniklaus, H.E., B.C. Barron, and M.W. Wilson, *Murine model of anterior and posterior ocular melanoma.* Curr Eye Res, 1995. **14**(5): p. 399-404.
91. Blanco, G., A.M. Saornil, E. Domingo, Y. Diebold, R. Lopez, G. Rabano, et al., *Uveal melanoma model with metastasis in rabbits: effects of different doses of cyclosporine A.* Curr Eye Res, 2000. **21**(3): p. 740-7.
92. Lopez-Velasco, R., A. Morilla-Grasa, M.A. Saornil-Alvarez, J.L. Ordonez, G. Blanco, G. Rabano, et al., *Efficacy of five human melanocytic cell lines in experimental rabbit choroidal melanoma.* Melanoma Res, 2005. **15**(1): p. 29-37.
93. Blanco, P.L., J.C. Marshall, E. Antecka, S.A. Callejo, J.P. Souza Filho, V. Saraiva, et al., *Characterization of ocular and metastatic uveal melanoma in an animal model.* Invest Ophthalmol Vis Sci, 2005. **46**(12): p. 4376-82.
94. Seykora, J.T., D. Jih, R. Elenitsas, W.H. Horng, and D.E. Elder, *Gene expression profiling of melanocytic lesions.* Am J Dermatopathol, 2003. **25**(1): p. 6-11.
95. Pollock, P.M. and J.M. Trent, *The genetics of cutaneous melanoma.* Clin Lab Med, 2000. **20**(4): p. 667-90.
96. Bittner, M., P. Meltzer, Y. Chen, Y. Jiang, E. Seftor, M. Hendrix, et al., *Molecular classification of cutaneous malignant melanoma by gene expression profiling.* Nature, 2000. **406**(6795): p. 536-40.
97. Talantov, D., A. Mazumder, J.X. Yu, T. Briggs, Y. Jiang, J. Backus, et al., *Novel genes associated with malignant melanoma but not benign melanocytic lesions.* Clin Cancer Res, 2005. **11**(20): p. 7234-42.
98. Hoek, K., D.L. Rimm, K.R. Williams, H. Zhao, S. Ariyan, A. Lin, et al., *Expression profiling reveals novel pathways in the transformation of melanocytes to melanomas.* Cancer Res, 2004. **64**(15): p. 5270-82.

99. Onken, M.D., L.A. Worley, J.P. Ehlers, and J.W. Harbour, *Gene expression profiling in uveal melanoma reveals two molecular classes and predicts metastatic death.* Cancer Res, 2004. **64**(20): p. 7205-9.
100. Onken, M.D., J.P. Ehlers, L.A. Worley, J. Makita, Y. Yokota, and J.W. Harbour, *Functional gene expression analysis uncovers phenotypic switch in aggressive uveal melanomas.* Cancer Res, 2006. **66**(9): p. 4602-9.
101. Sisley, K., M.A. Parsons, J. Garnham, A.M. Potter, D. Curtis, R.C. Rees, et al., *Association of specific chromosome alterations with tumour phenotype in posterior uveal melanoma.* Br J Cancer, 2000. **82**(2): p. 330-8.
102. Naus, N.C., A.C. Verhoeven, E. van Drunen, R. Slater, C.M. Mooy, D.A. Paridaens, et al., *Detection of genetic prognostic markers in uveal melanoma biopsies using fluorescence in situ hybridization.* Clin Cancer Res, 2002. **8**(2): p. 534-9.
103. Glatz-Krieger, K., M. Pache, C. Tapia, A. Fuchs, S. Savic, D. Glatz, et al., *Anatomic site-specific patterns of gene copy number gains in skin, mucosal, and uveal melanomas detected by fluorescence in situ hybridization.* Virchows Arch, 2006. **449**(3): p. 328-33.
104. Loercher, A.E. and J.W. Harbour, *Molecular genetics of uveal melanoma.* Curr Eye Res, 2003. **27**(2): p. 69-74.
105. White, J.S., R.L. Becker, I.W. McLean, A.E. Director-Myska, and J. Nath, *Molecular cytogenetic evaluation of 10 uveal melanoma cell lines.* Cancer Genet Cytogenet, 2006. **168**(1): p. 11-21.
106. Naus, N.C., E. van Drunen, A. de Klein, G.P. Luyten, D.A. Paridaens, J.C. Alers, et al., *Characterization of complex chromosomal abnormalities in uveal melanoma by fluorescence in situ hybridization, spectral karyotyping, and comparative genomic hybridization.* Genes Chromosomes Cancer, 2001. **30**(3): p. 267-73.
107. Hughes, S., B.E. Damato, I. Giddings, P.S. Hiscott, J. Humphreys, and R.S. Houlston, *Microarray comparative genomic hybridisation analysis of intraocular uveal melanomas identifies distinctive imbalances associated with loss of chromosome 3.* Br J Cancer, 2005. **93**(10): p. 1191-6.
108. Barrett, M.T., A. Scheffer, A. Ben-Dor, N. Sampas, D. Lipson, R. Kincaid, et al., *Comparative genomic hybridization using oligonucleotide microarrays and total genomic DNA.* Proc Natl Acad Sci U S A, 2004. **101**(51): p. 17765-70.
109. Kilic, E., W. van Gils, E. Lodder, H.B. Beverloo, M.E. van Til, C.M. Mooy, et al., *Clinical and cytogenetic analyses in uveal melanoma.* Invest Ophthalmol Vis Sci, 2006. **47**(9): p. 3703-7.
110. Sisley, K., I.G. Rennie, M.A. Parsons, R. Jacques, D.W. Hammond, S.M. Bell, et al., *Abnormalities of chromosomes 3 and 8 in posterior uveal melanoma correlate with prognosis.* Genes Chromosomes Cancer, 1997. **19**(1): p. 22-8.
111. White, J.S., I.W. McLean, R.L. Becker, A.E. Director-Myska, and J. Nath, *Correlation of comparative genomic hybridization results of 100 archival*

uveal melanomas with patient survival. Cancer Genet Cytogenet, 2006. **170**(1): p. 29-39.
112. Scholes, A.G., B.E. Damato, J. Nunn, P. Hiscott, I. Grierson, and J.K. Field, *Monosomy 3 in uveal melanoma: correlation with clinical and histologic predictors of survival.* Invest Ophthalmol Vis Sci, 2003. **44**(3): p. 1008-11.
113. Patel, K.A., N.D. Edmondson, F. Talbot, M.A. Parsons, I.G. Rennie, and K. Sisley, *Prediction of prognosis in patients with uveal melanoma using fluorescence in situ hybridisation.* Br J Ophthalmol, 2001. **85**(12): p. 1440-4.
114. White, V.A., J.D. Chambers, P.D. Courtright, W.Y. Chang, and D.E. Horsman, *Correlation of cytogenetic abnormalities with the outcome of patients with uveal melanoma.* Cancer, 1998. **83**(2): p. 354-9.
115. Ehlers, J.P., L. Worley, M.D. Onken, and J.W. Harbour, *DDEF1 is located in an amplified region of chromosome 8q and is overexpressed in uveal melanoma.* Clin Cancer Res, 2005. **11**(10): p. 3609-13.
116. Aalto, Y., L. Eriksson, S. Seregard, O. Larsson, and S. Knuutila, *Concomitant loss of chromosome 3 and whole arm losses and gains of chromosome 1, 6, or 8 in metastasizing primary uveal melanoma.* Invest Ophthalmol Vis Sci, 2001. **42**(2): p. 313-7.
117. Sisley, K., N. Tattersall, M. Dyson, K. Smith, H.S. Mudhar, and I.G. Rennie, *Multiplex fluorescence in situ hybridization identifies novel rearrangements of chromosomes 6, 15, and 18 in primary uveal melanoma.* Exp Eye Res, 2006. **83**(3): p. 554-9.
118. Gordon, K.B., C.T. Thompson, D.H. Char, J.M. O'Brien, S. Kroll, S. Ghazvini, et al., *Comparative genomic hybridization in the detection of DNA copy number abnormalities in uveal melanoma.* Cancer Res, 1994. **54**(17): p. 4764-8.
119. Lassmann, S., R. Weis, F. Makowiec, J. Roth, M. Danciu, U. Hopt, et al., *Array CGH identifies distinct DNA copy number profiles of oncogenes and tumor suppressor genes in chromosomal- and microsatellite-unstable sporadic colourectal carcinomas.* J Mol Med, 2006.
120. Aviel-Ronen, S., C.Q. Zhu, B.P. Coe, N. Liu, S.K. Watson, W.L. Lam, et al., *Large fragment Bst DNA polymerase for whole genome amplification of DNA from formalin-fixed paraffin-embedded tissues.* BMC Genomics, 2006. **7**(1): p. 312.
121. Devries, S., S. Nyante, J. Korkola, R. Segraves, K. Nakao, D. Moore, et al., *Array-based comparative genomic hybridization from formalin-fixed, paraffin-embedded breast tumors.* J Mol Diagn, 2005. **7**(1): p. 65-71.
122. Diebold, Y., G. Blanco, M.A. Saornil, N. Fernandez, and M.C. Lazaro, *Morphologic and immunocytochemical characterization of four human uveal cell lines (melanoma- and melanocytes-derived).* Curr Eye Res, 1997. **16**(5): p. 487-95.
123. De Waard-Siebinga, I., D.J. Blom, M. Griffioen, P.I. Schrier, E. Hoogendoorn, G. Beverstock, et al., *Establishment and characterization of an uveal-melanoma cell line.* Int J Cancer, 1995. **62**(2): p. 155-61.

124. Callejo, S.A., E. Antecka, P.L. Blanco, C. Edelstein, and M.N. Burnier, *Identification of circulating malignant cells and its correlation with prognostic factors and treatment in uveal melanoma. A prospective longitudinal study.* Eye, 2006.
125. Chambers, A.F., A.C. Groom, and I.C. MacDonald, *Dissemination and growth of cancer cells in metastatic sites.* Nat Rev Cancer, 2002. **2**(8): p. 563-72.
126. Keilholz, U., P. Goldin-Lang, N.E. Bechrakis, N. Max, A. Letsch, A. Schmittel, et al., *Quantitative detection of circulating tumor cells in cutaneous and ocular melanoma and quality assessment by real-time reverse transcriptase-polymerase chain reaction.* Clin Cancer Res, 2004. **10**(5): p. 1605-12.
127. Tobal, K., L.S. Sherman, A.J. Foss, and S.L. Lightman, *Detection of melanocytes from uveal melanoma in peripheral blood using the polymerase chain reaction.* Invest Ophthalmol Vis Sci, 1993. **34**(9): p. 2622-5.
128. Burnier, J., M. N., J.C. Marshall, F.J. Gregoire, S. Di Cesare, P. Logan, and A. Al-Kandari, *The Effect of a COX-2 Inhibitor on an Ocular Melanoma Animal Model.* IOVS E Abstract 2218, 2006.
129. Odashiro, A.N., P.L. Blanco, J.C. Marshall, J.P. Souza Filho, V. Saraiva, and M.N. Burnier Jr, *Intraocular Inoculation of Cutaneous Melanoma Cells in an Uveal Melanoma Animal Model.* IOVS E Abstract 4243, 2005.
130. Ordonez, J.L., M.A. Saornil, E. Domingo, G. Blanco, Y. Diebold, A. Morilla-Grasa, et al., *The need for continuous immunosuppression with cyclosporin A to maintain an experimental model of uveal melanoma.* Melanoma Res, 2002. **12**(5): p. 441-7.
131. Notting, I.C., J.T. Buijs, I. Que, R.E. Mintardjo, G. van der Horst, M. Karperien, et al., *Whole-body bioluminescent imaging of human uveal melanoma in a new mouse model of local tumor growth and metastasis.* Invest Ophthalmol Vis Sci, 2005. **46**(5): p. 1581-7.
132. Heegaard, S., M. Spang-Thomsen, and J.U. Prause, *Establishment and characterization of human uveal malignant melanoma xenografts in nude mice.* Melanoma Res, 2003. **13**(3): p. 247-51.
133. Logan, P., J.C. Marshall, B.F. Fernandes, S. Maloney, V. Saraiva, and M.N. Burnier Jr, *In Vivo Imaging of Flourescently Labeled Human Uveal Melanoma Cells in Nude Mice.* IOVS E Abstract 2230, 2006.
134. Thomas, P.A., D.A. Kirschmann, J.R. Cerhan, R. Folberg, E.A. Seftor, T.A. Sellers, et al., *Association between keratin and vimentin expression, malignant phenotype, and survival in postmenopausal breast cancer patients.* Clin Cancer Res, 1999. **5**(10): p. 2698-703.
135. Rosenwald, I.B., *The role of translation in neoplastic transformation from a pathologist's point of view.* Oncogene, 2004. **23**(18): p. 3230-47.
136. Seftor, E.A., K.M. Brown, L. Chin, D.A. Kirschmann, W.W. Wheaton, A. Protopopov, et al., *Epigenetic transdifferentiation of normal melanocytes by a metastatic melanoma microenvironment.* Cancer Res, 2005. **65**(22): p. 10164-9.

137. Beliveau, A., M. Berube, A. Rousseau, G. Pelletier, and S.L. Guerin, *Expression of integrin alpha5beta1 and MMPs associated with epithelioid morphology and malignancy of uveal melanoma.* Invest Ophthalmol Vis Sci, 2000. **41**(8): p. 2363-72.
138. Beliveau, A., M. Berube, P. Carrier, C. Mercier, and S.L. Guerin, *Tumorigenicity of the mixed spindle-epithelioid SP6.5 and epithelioid TP17 uveal melanoma cell lines is differentially related to alpha5beta1 integrin expression.* Invest Ophthalmol Vis Sci, 2001. **42**(12): p. 3058-65.
139. Kaplan, R.N., R.D. Riba, S. Zacharoulis, A.H. Bramley, L. Vincent, C. Costa, et al., *VEGFR1-positive haematopoietic bone marrow progenitors initiate the pre-metastatic niche.* Nature, 2005. **438**(7069): p. 820-7.
140. Berube, M., M. Talbot, C. Collin, C. Paquet-Bouchard, L. Germain, S.L. Guerin, et al., *Role of the extracellular matrix proteins in the resistance of SP6.5 uveal melanoma cells toward cisplatin.* Int J Oncol, 2005. **26**(2): p. 405-13.
141. Economou, M.A., C. All-Ericsson, V. Bykov, L. Girnita, A. Bartolazzi, O. Larsson, et al., *Receptors for the liver synthesized growth factors IGF-1 and HGF/SF in uveal melanoma: intercorrelation and prognostic implications.* Invest Ophthalmol Vis Sci, 2005. **46**(12): p. 4372-5.
142. Saltiel, A.R. and C.R. Kahn, *Insulin signalling and the regulation of glucose and lipid metabolism.* Nature, 2001. **414**(6865): p. 799-806.
143. Boissan, M., E. Beurel, D. Wendum, C. Rey, Y. Lecluse, C. Housset, et al., *Overexpression of insulin receptor substrate-2 in human and murine hepatocellular carcinoma.* Am J Pathol, 2005. **167**(3): p. 869-77.
144. Ryazanov, A.G., K.S. Pavur, and M.V. Dorovkov, *Alpha-kinases: a new class of protein kinases with a novel catalytic domain.* Curr Biol, 1999. **9**(2): p. R43-5.
145. Versele, M. and J. Thorner, *Some assembly required: yeast septins provide the instruction manual.* Trends Cell Biol, 2005. **15**(8): p. 414-24.
146. Spiliotis, E.T., M. Kinoshita, and W.J. Nelson, *A mitotic septin scaffold required for Mammalian chromosome congression and segregation.* Science, 2005. **307**(5716): p. 1781-5.
147. Torigoe, T., H. Izumi, H. Ishiguchi, Y. Yoshida, M. Tanabe, T. Yoshida, et al., *Cisplatin resistance and transcription factors.* Curr Med Chem Anticancer Agents, 2005. **5**(1): p. 15-27.
148. Jean, S., C. Bideau, L. Bellon, G. Halimi, M. De Meo, T. Orsiere, et al., *The expression of genes induced in melanocytes by exposure to 365-nm UVA: study by cDNA arrays and real-time quantitative RT-PCR.* Biochim Biophys Acta, 2001. **1522**(2): p. 89-96.
149. Hoashi, T., H. Watabe, J. Muller, Y. Yamaguchi, W.D. Vieira, and V.J. Hearing, *MART-1 is required for the function of the melanosomal matrix protein PMEL17/GP100 and the maturation of melanosomes.* J Biol Chem, 2005. **280**(14): p. 14006-16.
150. Vaisanen, A., M. Kallioinen, K. von Dickhoff, L. Laatikainen, M. Hoyhtya, and T. Turpeenniemi-Hujanen, *Matrix metalloproteinase-2*

(MMP-2) immunoreactive protein--a new prognostic marker in uveal melanoma? J Pathol, 1999. **188**(1): p. 56-62.
151. Johnson, N.A., R.A. Hamoudi, K. Ichimura, L. Liu, D.M. Pearson, V.P. Collins, et al., *Application of array CGH on archival formalin-fixed paraffin-embedded tissues including small numbers of microdissected cells.* Lab Invest, 2006. **86**(9): p. 968-78.
152. van Beers, E.H., S.A. Joosse, M.J. Ligtenberg, R. Fles, F.B. Hogervorst, S. Verhoef, et al., *A multiplex PCR predictor for aCGH success of FFPE samples.* Br J Cancer, 2006. **94**(2): p. 333-7.
153. Harvell, J.D., S. Kohler, S. Zhu, T. Hernandez-Boussard, J.R. Pollack, and M. van de Rijn, *High-resolution array-based comparative genomic hybridization for distinguishing paraffin-embedded Spitz nevi and melanomas.* Diagn Mol Pathol, 2004. **13**(1): p. 22-5.
154. Cardoso, J., L. Molenaar, R.X. de Menezes, C. Rosenberg, H. Morreau, G. Moslein, et al., *Genomic profiling by DNA amplification of laser capture microdissected tissues and array CGH.* Nucleic Acids Res, 2004. **32**(19): p. e146.
155. Takeuchi, T., S.B. Liang, N. Matsuyoshi, S. Zhou, Y. Miyachi, H. Sonobe, et al., *Loss of T-cadherin (CDH13, H-cadherin) expression in cutaneous squamous cell carcinoma.* Lab Invest, 2002. **82**(8): p. 1023-9.
156. Shirasaki, F., M. Takata, N. Hatta, and K. Takehara, *Loss of expression of the metastasis suppressor gene KiSS1 during melanoma progression and its association with LOH of chromosome 6q16.3-q23.* Cancer Res, 2001. **61**(20): p. 7422-5.
157. Burton, M.P., B.G. Schneider, R. Brown, N. Escamilla-Ponce, and M.L. Gulley, *Comparison of histologic stains for use in PCR analysis of microdissected, paraffin-embedded tissues.* Biotechniques, 1998. **24**(1): p. 86-92.
158. Nareyeck, G., M. Zeschnigk, G. Prescher, D.R. Lohmann, and G. Anastassiou, *Establishment and characterization of two uveal melanoma cell lines derived from tumors with loss of one chromosome 3.* Exp Eye Res, 2006. **83**(4): p. 858-64.
159. Udart, M., J. Utikal, G.M. Krahn, and R.U. Peter, *Chromosome 7 aneusomy. A marker for metastatic melanoma? Expression of the epidermal growth factor receptor gene and chromosome 7 aneusomy in nevi, primary malignant melanomas and metastases.* Neoplasia, 2001. **3**(3): p. 245-54.
160. Kapranos, N., S. Kounelis, H. Karantasis, and E. Kouri, *Numerical aberrations of chromosomes 1 and 7 by fluorescent in situ hybridization and DNA ploidy analysis in breast cancer.* Breast Journal, 2005. **11**(6): p. 448-53.
161. Halaban, R., B. Fan, J. Ahn, Y. Funasaka, H. Gitay-Goren, and G. Neufeld, *Growth factors, receptor kinases, and protein tyrosine phosphatases in normal and malignant melanocytes.* J Immunother, 1992. **12**(3): p. 154-61.

162. Halaban, R., *Growth factors and tyrosine protein kinases in normal and malignant melanocytes.* Cancer Metastasis Rev, 1991. **10**(2): p. 129-40.
163. Lengyel, E., D. Prechtel, J.H. Resau, K. Gauger, A. Welk, K. Lindemann, et al., *C-Met overexpression in node-positive breast cancer identifies patients with poor clinical outcome independent of Her2/neu.* Int J Cancer, 2005. **113**(4): p. 678-82.
164. Zeng, Z., M.R. Weiser, M. D'Alessio, A. Grace, J. Shia, and P.B. Paty, *Immunoblot analysis of c-Met expression in human colourectal cancer: overexpression is associated with advanced stage cancer.* Clin Exp Metastasis, 2004. **21**(5): p. 409-17.
165. Elia, G., Y. Ren, P. Lorenzoni, R. Zarnegar, M.M. Burger, and D. Rusciano, *Mechanisms regulating c-met overexpression in liver-metastatic B16-LS9 melanoma cells.* J Cell Biochem, 2001. **81**(3): p. 477-87.
166. Hendrix, M.J., E.A. Seftor, R.E. Seftor, D.A. Kirschmann, L.M. Gardner, H.C. Boldt, et al., *Regulation of uveal melanoma interconverted phenotype by hepatocyte growth factor/scatter factor (HGF/SF).* Am J Pathol, 1998. **152**(4): p. 855-63.
167. Pham, K., T. Milovanovic, R.J. Barr, T. Truong, and R.F. Holcombe, *Wnt ligand expression in malignant melanoma: pilot study indicating correlation with histopathological features.* Mol Pathol, 2003. **56**(5): p. 280-5.
168. Katoh, M., *Differential regulation of WNT2 and WNT2B expression in human cancer.* Int J Mol Med, 2001. **8**(6): p. 657-60.
169. You, L., B. He, Z. Xu, K. Uematsu, J. Mazieres, N. Fujii, et al., *An anti-Wnt-2 monoclonal antibody induces apoptosis in malignant melanoma cells and inhibits tumor growth.* Cancer Res, 2004. **64**(15): p. 5385-9.
170. Conway, R.M., C. Cursiefen, J. Behrens, G.O. Naumann, and L.M. Holbach, *Biomolecular markers of malignancy in human uveal melanoma: the role of the cadherin-catenin complex and gene expression profiling.* Ophthalmologica, 2003. **217**(1): p. 68-75.
171. Edmunds, S.C., D.P. Kelsell, J.L. Hungerford, and I.A. Cree, *Mutational analysis of selected genes in the TGFbeta, Wnt, pRb, and p53 pathways in primary uveal melanoma.* Invest Ophthalmol Vis Sci, 2002. **43**(9): p. 2845-51.
172. Takata, M. and T. Saida, *Genetic alterations in melanocytic tumors.* J Dermatol Sci, 2006. **43**(1): p. 1-10.
173. Davies, H., G.R. Bignell, C. Cox, P. Stephens, S. Edkins, S. Clegg, et al., *Mutations of the BRAF gene in human cancer.* Nature, 2002. **417**(6892): p. 949-54.
174. Wong, C.W., Y.S. Fan, T.L. Chan, A.S. Chan, L.C. Ho, T.K. Ma, et al., *BRAF and NRAS mutations are uncommon in melanomas arising in diverse internal organs.* J Clin Pathol, 2005. **58**(6): p. 640-4.
175. Malaponte, G., M. Libra, P. Gangemi, V. Bevelacqua, K. Mangano, F. D'Amico, et al., *Detection of BRAF gene mutation in primary choroidal melanoma tissue.* Cancer Biol Ther, 2006. **5**(2): p. 225-7.

176. Calipel, A., F. Mouriaux, A.L. Glotin, F. Malecaze, A.M. Faussat, and F. Mascarelli, *Extracellular signal-regulated kinase-dependent proliferation is mediated through the protein kinase A/B-Raf pathway in human uveal melanoma cells.* J Biol Chem, 2006. **281**(14): p. 9238-50.

Appendix